

Recent developments in polymers/polymer nanocomposites for additive manufacturing



H. Wu^a, W.P. Fahy^{a,b}, S. Kim^{a,b}, H. Kim^{a,b}, N. Zhao^b, L. Pilato^a, A. Kafi^c, S. Bateman^c, J.H. Koo^{a,b,*}

^a KAI, LLC, Austin, TX 78739, USA

^b Department of Mechanical Engineering, Cockrell School of Engineering, The University of Texas at Austin, Austin, TX 78712, USA

^c Centre for Additive Manufacturing, School of Engineering, Royal Melbourne Institute of Technology University, Melbourne, Victoria 3001, Australia

ARTICLE INFO

Keywords:

Additive Manufacturing (AM)
Fused Filament Fabrication (FFF)
Selective Laser Sintering (SLS)
Multi Jet Fusion (MJF)
Stereolithography (SLA)
Polymer nanocomposites

ABSTRACT

In recent years, there have been significant advances on materials development for additive manufacturing (AM) applications. However, the use of composites or nanocomposite materials for improved performance and multifunctionality are still limited. This review paper attempts to provide a comprehensive review of both commercially available materials as well as research activities related to recent progress on high-performance polymer nanocomposites that are being used in various AM techniques. Four AM techniques including Fused Filament Fabrication (FFF), Selective Laser Sintering (SLS), Multi Jet Fusion (MJF), and Stereolithography (SLA) are discussed. The development of printable polymer composites especially polymer nanocomposites is rapidly expanding the AM materials portfolio, which makes the production of multifunctional parts with complex structures possible.

1. Introduction

Additive Manufacturing (AM), also known generically as 3D printing, is a key enabling technology relevant to many industrial sectors [1] including aerospace [2], biomedical [3,4], automotive [5], and turbomachinery [6]. AM is also relevant in manufacturing and manufacturing aides, such as tooling, jigs, and fixtures [7,8].

From its origins for prototyping new designs, AM now holds the potential to increase a manufacturer's agility, reduce the innovation cycle time, and open-up new design paradigms by providing a technique to directly produce physical outputs from digital inputs without the need for conventional tooling [9].

According to ISO/ASTM 52900-15, AM is defined as the "process of joining materials to make parts from 3D model data, usually layer upon layer, as opposed to subtractive manufacturing and formative manufacturing methodologies." Some historical terms for AM include "additive fabrication, additive processes, additive techniques, additive layer manufacturing, layer manufacturing, solid freeform fabrication, and freeform fabrication" [10]. ASTM Technical Committee F42 (Additive Manufacturing) has classified the range of AM processes into seven distinct categories [10]. These categories include (i) material jetting, (ii) binder jetting, (iii) material extrusion, (iv) powder bed fusion, (v) direct energy deposition, (vi) sheet lamination, and (vii) vat photopolymerisation. It is noted that in many publications, the authors tend to use terms, such as AM or 3D printing, and Fused Deposition Modeling (FDM) or Fused Filament Fabrication (FFF) interchangeably.

* Corresponding author.

E-mail address: jkoo@mail.utexas.edu (J.H. Koo).

Nomenclature	
ABS	Acrylonitrile butadiene styrene
AM	Additive Manufacturing
BNNP	Boron nitride nanoplatelets
BAAM	Big Area Additive Manufacturing
BT	barium titanate
CB	carbon black
CNF	Carbon nanofiber
CFF	Continuous Filament Fabrication
CNC	Crystalline nanocellulose
CNT	Carbon nanotube
DED	Direct Energy Deposition
DLP	Digital Light Processing
DLS	Digital Light Synthesis
FDM	Fused Deposition Modeling
FFF	Fused Filament Fabrication
FRP	fiber-reinforced polymer
GO	Graphene oxide
GnP/GNP	Graphene nanoplatelets
rGO	reduced Graphene Oxide
HIPS	High impact polystyrene
HRC	Heat Release Capacity
HRR	Heat Release Rate
JF3D	Jet Fusion 3D Printing
LCP	Liquid crystal polymers
LFS	Low Force Stereolithography
LIRF	Locally Induced RF
L-CNC	Lignin coated crystalline nanocellulose
MCC	Microscale Combustion Calorimetry
ME3DP	Material Extrusion 3D Printing
MJF	Multi Jet Fusion
MWCNT	multi-walled carbon nanotube
MSL	Microstereolithography
OTB	Oxyacetylene Test Bed
PA	Polyamide or Nylon
PNCs	Polymer Nanocomposites
PBS	Polybutylene succinate
PBT	Polybutylene terephthalate
PC	Polycarbonate
pDSC	Photo Differential Scanning Calorimetry
PE	Polyethylene
PEI	Polyethylenimine
PEEK	Polyether ether ketone
PEKK	Polyether ketone ketone
PET	Polyethylene terephthalate
PLA	Polylactic acid
PMMA	Poly (methyl methacrylate)
PP	Polypropylene
PPS	Polyphenylene sulfide
PPSF	Polyphenylsulfone
PS	Polystyrene
PU	Polyurethane
PVC	Polyvinyl chloride
SEM	Scanning Electron Microscopy
SLS	Selective Laser Sintering
SLA	Stereolithography
SLM	Selective Laser Melting
SLGO	Single-layer graphene oxide
TEM	Transmission Electron Microscopy
T _g	Glass Transition Temperature
TGA	Thermogravimetric Analysis
TPS	Thermal Protection Systems
TPU	Thermoplastic polyurethane
UTS	Ultimate tensile strength
VGCF	vapor grown carbon fiber
λ	thermal conductivity

Although many AM techniques have been developed since the 1980s, there have been limited breakthroughs in commercialization until recently [11]. Fig. 1 shows the number of publications in the field of AM and 3D printing since 2008. Significant momentum in academic research interest started to accelerate since 2013. In 2016, the AM market in materials and services reached \$6.1 billion

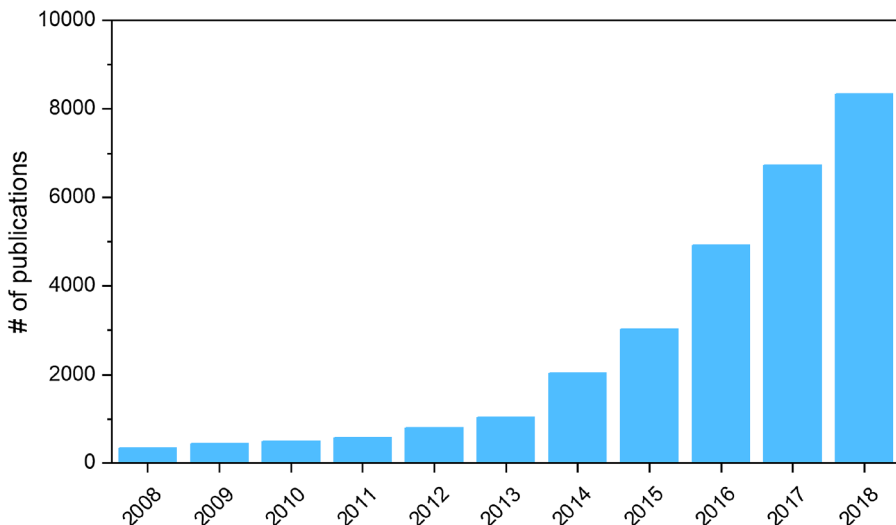


Fig. 1. Total number of publications in the field of Additive Manufacturing/3D printing since 2008 (data from Web of Science, 2018).

[12] and it is forecast that by 2035 the market could exceed \$350 billion [13].

Fig. 2 shows some of the applications enabled by AM which include customized sport and musical instruments, lightweight prosthetic leg, dental splints, and molds for injection molding and composite layup, etc. AM has great potential in industrial applications, such as flexible electronics, sensors and antennas [12]. AM also enables rapid tooling of complex parts. It is anticipated that aerospace, medical, and automotive are three industries can be significantly changed by the AM revolution [13]. Some of these applications are discussed in more detail in section 4 where the polymer nanocomposites are developed of specific applications.

AM could assist aerospace manufacturers in producing complex parts with lightweight structures, which is critical to reduce fuel cost. In the medical industry, AM allows for customization of medical devices tailored to the individual patient that is both fast and cost-effective. This is especially true for hearing aids, orthopedics and prosthetics, and surgical guides and models [13]. For the automotive industry, AM could save cost and improve lead time for manufacturing of small batch customized parts. Novel high-performance polymers are under development. Many chemical companies and research institutes have already started to develop AM specific materials. For example, Gantenbein et al. recently developed printable hierarchical liquid-crystal-polymer structures with superior mechanical performance [14]. AM equipment companies have also invested heavily in technological innovations. One such innovation is the printing of multiple materials concurrently using multiple printing heads [15,16].

AM distinguishes itself from other manufacturing processes by its layer-by-layer fabrication approach. This approach theoretically enables the creation of complex previously un-manufacturable parts including those which are (i) topologically optimized, (ii) integrated, and (iii) functional [17,18].

Even so, AM is typically slower than conventional manufacturing processes like injection molding. In addition, the feedstock material for AM is often expensive. This is because high quality filament or powders are needed for satisfactory print results. Further, the interrelationships between design – materials – process parameters and the ultimate properties of the AM part are not always predictable using modeling techniques as the ultimate part properties vary widely based on the process settings. Such challenges necessitate technical staff having new capabilities with the design of suitable training programs for AM remaining an ongoing industry challenge [19].

Notwithstanding its potential, key limitations and barriers still exist particularly for industrial application. For example, bodies, such as the ASTM [20] are continuing to develop standards surrounding nomenclature, design rules, file formats, materials, and processes. Grand challenges that still remain include the following: development of rapid certification protocols for unique AM parts, minimization of secondary processing steps to finish near net shape forms, and part reproducibility and metrology relative to input files [21–26]. On the other hand, AM is also drawing attention from the legal community with reference to intellectual property rights, copyright infringement, and its use for the production of counterfeits [27,28].

It is worth mentioning that one of the major limitations for AM is still the lack of a robust materials selection portfolio. The majority of the materials used for AM are thermoplastics without any modification meaning the printed parts cannot be used for high-performance applications or when multifunctionality is desired. The nature of the various AM techniques also limits the choice of

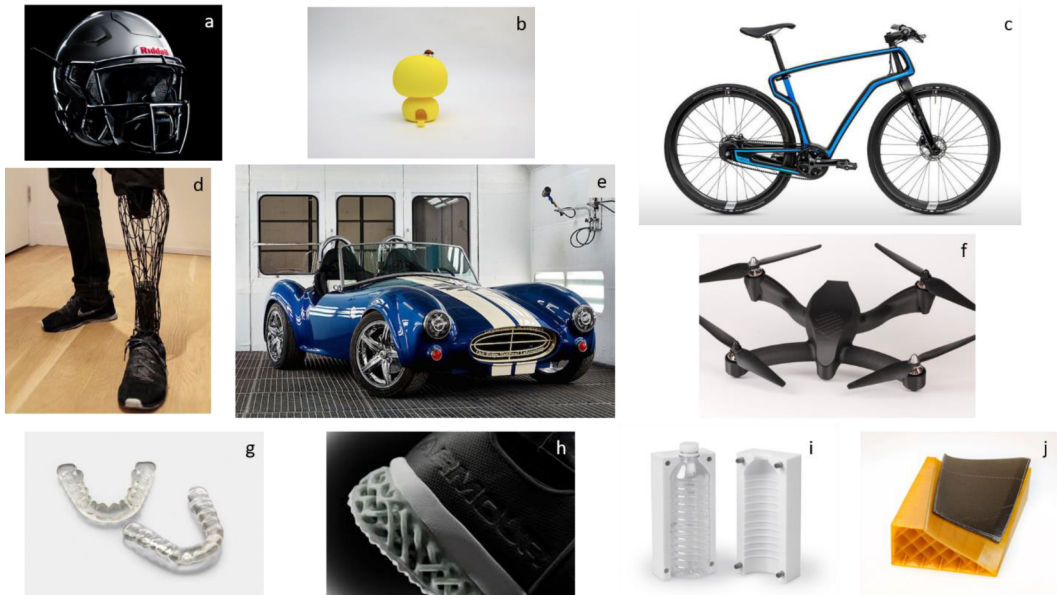


Fig. 2. (a) Football helmet liner made by Carbon's Digital Light Synthesis (DLS). (Carbon and Riddell); (b) 3D printed habitats for insects (by Angelo Renna from designboom.com); (c) carbon fiber reinforced bike frame made by Direct Energy Deposition (DED) (Arevo); (d) prototype prosthetic leg (by William Root); (e) full size Shelby Cobra made by Big Area Additive Manufacturing (BAAM) (Oak Ridge National Labs (ORNL)); (f) 3D printed drone made by continuous filament fabrication (CFF) (Markforged); (g) dental splints made by Low Force Stereolithography(LFs) a form of SLA (Formlabs), (h) 3D printed midsoles made by Selective Laser Sintering (SLS) (Under Armour and EOS); (i) and (j) 3D printed injection mold and mold for composite manufacturing made by FDM (Stratasys).

materials. For instance, ABS and PLA are the predominant materials for FFF, and PA11 and PA12 have been the only options for SLS for a very long time.

While AM of metal materials have attracted tremendous research efforts [29–33], this review will only focus on polymeric materials. The goal of this review is to summarize commercially available polymer materials as well as recent development in polymer nanocomposites for the four distinctive AM techniques: Fused Filament Fabrication (FFF), Selective Laser Sintering (SLS), Stereolithography (SLA), and Multi Jet Fusion (MJF).

2. AM techniques

There currently exists multiple polymer AM techniques for rapid prototyping within the industry. In general, ASTM classifies the current AM techniques into seven main categories: 1. materials extrusion, 2. powder bed fusion, 3. vat photopolymerization, 4. binder jetting, 5. material jetting, 6. directed energy deposition, and 7. sheet lamination. A common theme among these AM methods is that they all form 3D physical parts by bonding layer after layer of the material in use. This review will mainly be focusing on the first three techniques and their relevant work in polymer nanocomposites. While FFF uses filament as feed material, SLS and MJF uses powder materials in the size of 20–150 µm. SLA uses liquid resins. For powder-based AM techniques, support materials are not necessary since the unsintered powders serve such purpose nicely. The feedstock powders can be recycled for SLS and MJF process, although the part quality may degrade due to change in particle size distribution from the original powders. A comparison of each AM technology in this review is given in Table 1. Fig. 3 compares the technical capabilities of the several different AM techniques.

To accompany these AM techniques, a plethora of materials have been developed for each method. Although a variety of materials exist for each technology, only a few materials are widely used for each method. Therefore, the need for more robust material properties continues to drive the research and development of new materials that are compatible with the different AM techniques. This review will introduce the previously mentioned AM techniques and discuss properties and applications of commercially available polymers/polymer nanocomposites in AM.

2.1. Fused Filament Fabrication (FFF)

The first form of AM technologies that is discussed is FFF also known as material extrusion 3D printing (ME3DP). Based on FDM which is a form of material extrusion first developed by Scott Crump (Stratasys) in the late 1980s [34,35]. FFF involves melt depositing polymers or polymer composites by filament extrusion according to the input design requirements [36]. It is the most widely used form of AM and accounted for 96% of global 3D printer sales in 2016 [37]. This widespread use of FFF machines is partially due to an open source movement to allow anyone to use this AM technology [38].

FFF machines generally consist of a filament spool which is fed through a system of rollers and gears to the extruder head where the heated head melts the thermoplastic and deposits it onto the build platform as shown in Fig. 4. Some FFF machines have one extruder head while others have two. Dual extruder machines are typically used with one head depositing the thermoplastic build material while the second head deposits rafts or other support material. Support materials (which can later be dissolved, melted, or broken away from the printed article) are used to provide the physical scaffolding required to print hollow/porous articles or achieve overhang structures [39].

To print, FFF parts are initially designed in a computer aided drawing (CAD) software package and saved as a STL file. Next, the STL file is imported into a slicer program that automatically slices the data, calculates the support structure, and creates tool paths. Slicer programs also offer a selection of process parameters, such as nozzle temperature and extrusion rate. The tool path dictates where along the X and Y axis the extruder must traverse. This enables the extruder to deposit material in complex shapes or precise designs anywhere on the build platform. The build platform is generally made with a thermally conductive material, such as metal or glass. The platform acts as the foundation for the first layer of the 3D print. When a layer is completed, the build platform moves downward (Z axis) in a specified increment so that the subsequent layer can be deposited and bonded to the previous layer. The distance that the build platform moves down is referred to as the layer height, which typically ranges from 100 to 300 µm. However, advanced FFF machines are now available that can create finer layers by decreasing the layer height to less than 25 µm. Numerous studies have been carried out to determine the effect of production parameters on the mechanical properties of 3D printed parts using open source slicer packages [40–45] with this area continuing to be an active area of research and development.

For printed parts to achieve high strength, bonding between adjacent filament beads through intermolecular polymer chain

Table 1
Comparison of different AM techniques covered in this review.

Technology	SLS	FFF	MJF	SLA
Category	Powder bed fusion	Materials extrusion	Powder bed fusion	Vat photopolymerization
Feed Stock	Powder	Filament	Powder	Liquid resin
Materials	Metals, thermoplastics, glass, ceramics	Large variety of thermoplastics	Nylon 11 and 12, TPU	Photopolymers
Resolution (microns)	60–150	50–500	21	25
Support (for complex printing)	Not required	Required	Not required	Required
Recyclability	Manual	N/A	Automatic	N/A
Machine Price (USD)	> 250,000	> 200	> 300,000	> 3500

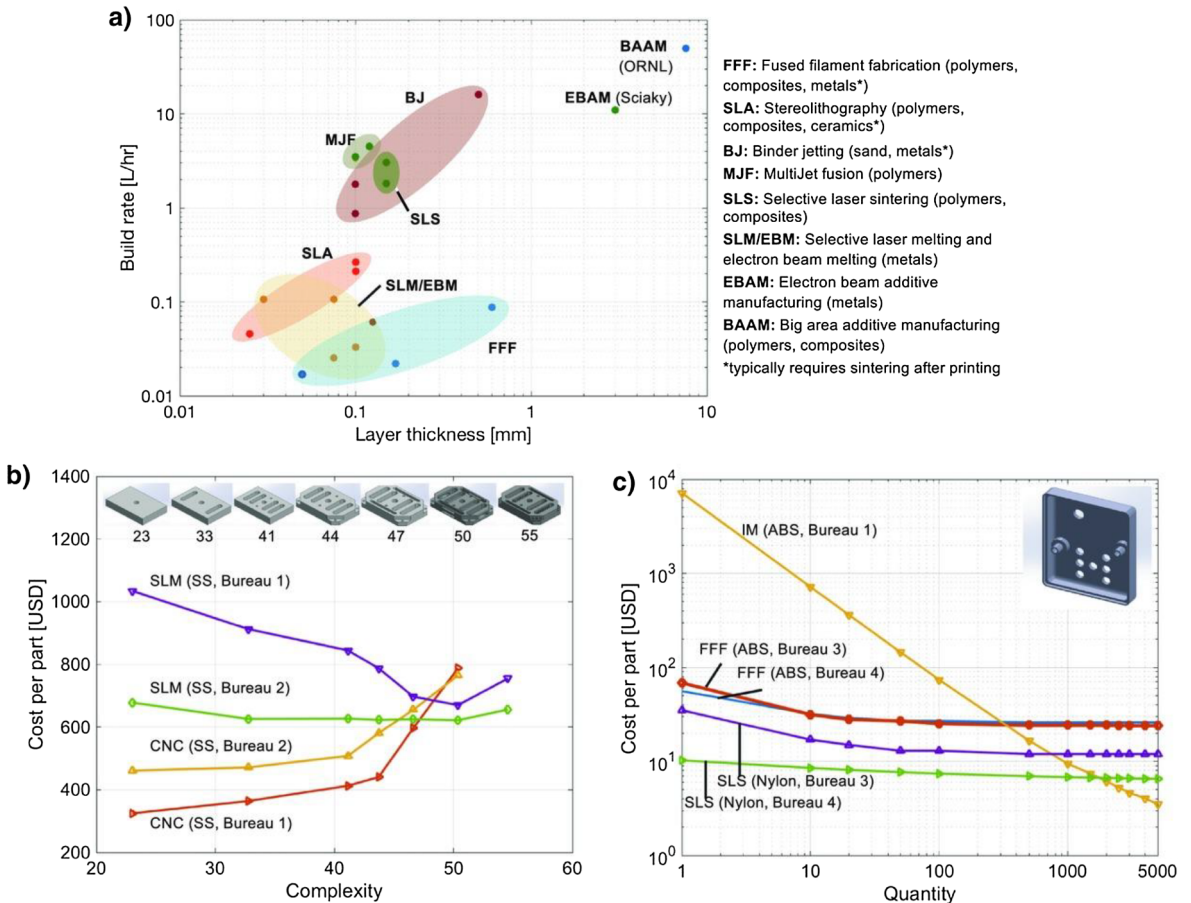


Fig. 3. Technical capabilities and cost of AM processes compared to conventional forming. (a) Comparison of build rate and layer thickness (a measure of resolution) of mainstream AM processes, drawn from specifications of industrial equipment; (b) cost versus complexity for a series of parts with identical bounding box dimensions, evaluated by price quotes from service bureaus, for a single part made of 316L stainless steel; and (c) cost versus quantity for an exemplary polymer component, comparing injection molding (IM), fused filament fabrication (FFF), and selective laser sintering (SLS). ABS = acrylonitrile butadiene styrene; L/hr = liters per hour; mm = millimeters; SS = stainless steel; USD = U.S. dollars [12]. Copyright 2017, John Wiley and Sons.

entanglement need to be formed. Upon heating, the initial contact forms a neck during which diffusion of the polymer chains occur as shown in Fig. 5. A number of parameters including viscosity, thermal conductivity, heat capacity, and the cooling rate play a role in this process. For example, higher temperature helps with the interlayer fusion process by reducing the melt viscosity [47]. Due to the lack of z-direction strength, delamination often occurs under shear stress [48].

Popescu et al. [50] categorized all the process parameters for FFF into three categories: slicing, building orientation, and temperature conditions (Fig. 6). Several key parameters that affect the part's mechanical performance include raster-to-raster air gap, raster angle, layer thickness, infill density, and build orientation. In addition, the effect of support structures on mechanical properties of the printed parts has also been studied [39,51]. Goh et al. [43] compiled all the mechanical property results of FFF printed neat polymers and discussed the effect of different parameters on mechanical performance in detail (Fig. 7). For hydroscopic materials, such as nylons, moisture within the filament can lead to high porosity of the printed parts thus significantly lowering mechanical properties [52].

The main advantage of FFF is that it is available at an inexpensive price and software innovations have allowed easier user interaction with the machines as well as tool path optimizations. Furthermore, polylactic acid (PLA) and acrylonitrile butadiene styrene (ABS), the most commonly used materials on FFF machines, are also commercially available at very low prices.

Whilst the advantages of FFF as discussed above are well known, the mechanical properties of FFF printed parts are generally inferior to injection molded parts due to part anisotropy [3,37,53], and often greater porosity [52]. Anisotropy in AM part mechanical properties originates from the level of interfacial adhesion between discrete layers, tool (extrusion or print head) paths compared to the inherent properties of the polymer in plane. This effect can be probed by investigating the ultimate tensile strength of tensile bars printed in various orientations (e.g., zx, xz, and xy) with interlayer adhesion (or deficiencies thereof) leading to brittle failure and reduced mechanical properties when built and tested in the (zx) direction [54,55]. Process parameters like raster angle, part design, air gap, build orientation, and post-processing can assist with research to overcome anisotropy [37,56]. Anisotropy

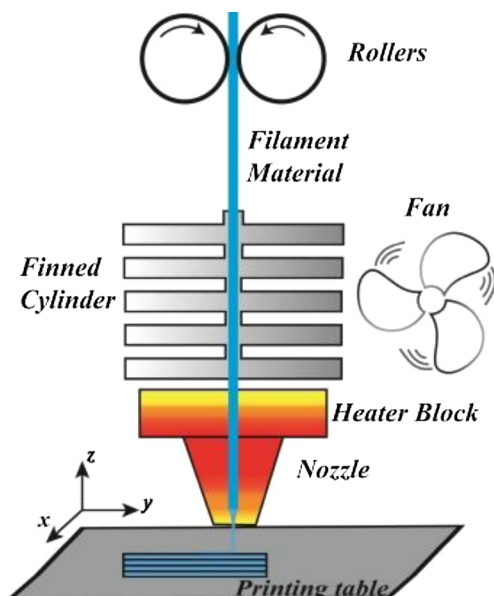


Fig. 4. Schematic showing how a typical FFF machine operates [46]. Copyright 2017, Elsevier.

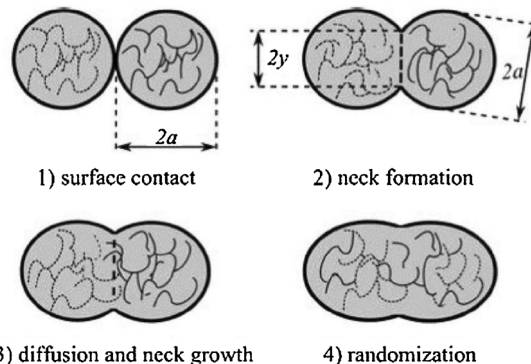


Fig. 5. Schematic overview of the polymer fusion process [49]. Copyright 2014, Emerald Group Publishing Limited.

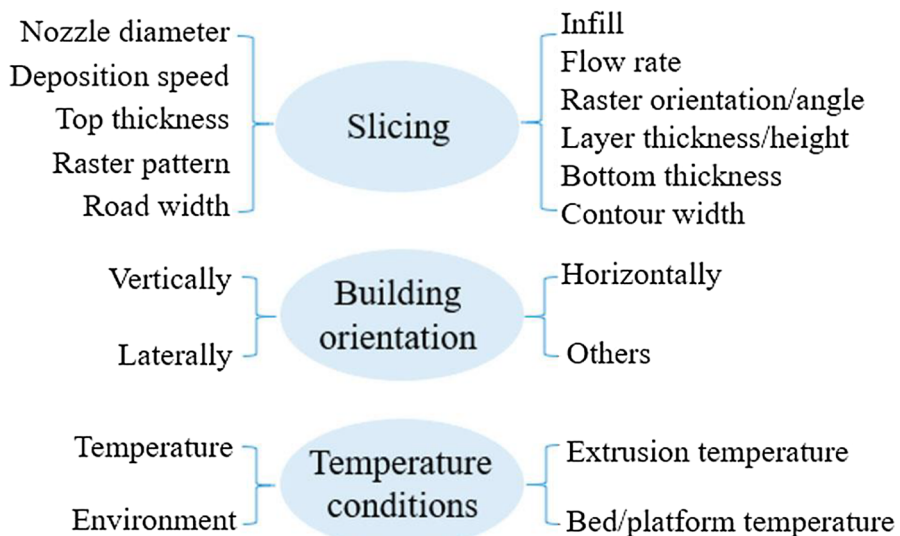


Fig. 6. Process parameters for FFF [50,51]. Copyright 2018, Elsevier. Copyright 2019, Taylor & Francis.

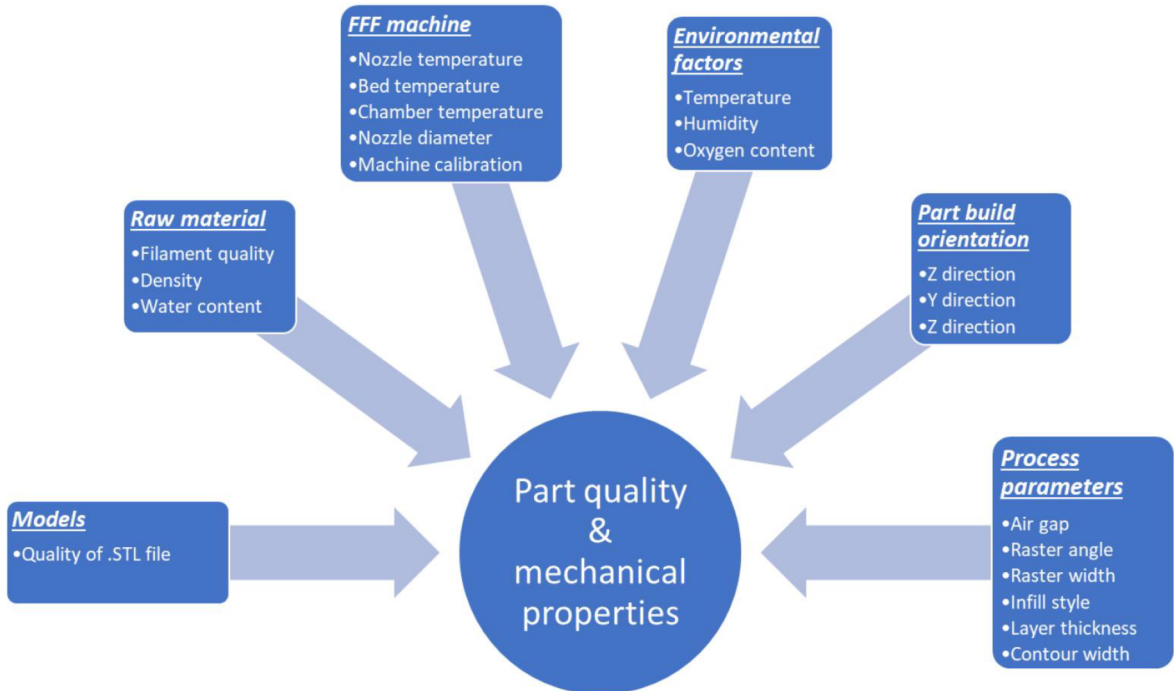


Fig. 7. Factors affecting the part quality and mechanical properties of the FFF-fabricated thermoplastic parts [43]. Copyright 2019, Taylor & Francis.

continues to be an active research challenge.

Whilst the resolution of FFF is not as fine as material jetting technologies (Z layer thickness $\sim 120 \mu\text{m}$ compared with $< 25 \mu\text{m}$) [57] a key advantage is that commercially produced and notionally well understood amorphous and semicrystalline thermoplastic polymers can be used as build materials. This contrasts to materials jetting and vat photo-polymerisation techniques, like SLA, which both require the use of photo-curable build materials. Photo-curable materials are typically based on acrylate chemistries which can lead to ambiguity in material (cross-link) structure over time and changes in physical properties with environmental aging [58]. The search for new materials for photo-polymerisation based additive manufacturing application is on-going [59] as is the research into thermoplastic filament formulation [60].

2.2. Selective Laser Sintering (SLS)

SLS is a powder-based additive manufacturing technique that allows freeform fabrication of complex 3D parts by solidifying powder materials layer by layer successively. Solidification is achieved by selectively fused or sintered defined areas in each layer

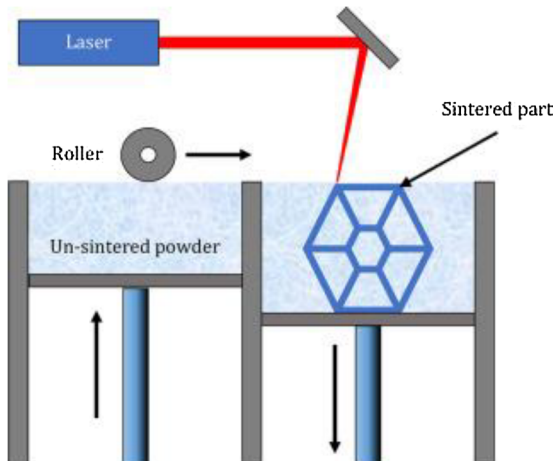


Fig. 8. Schematic showing how a typical SLS machine operates [3]. Copyright 2016, Elsevier.

using thermal energy from a focused laser radiation system [61,62]. First, a layer of powder is deposited into the build chamber. A laser beam then sinters or melts selective areas according to the cross-sectional data of the 3D CAD model on the powder bed to form a solid layer. Once the initial layer is completed, the build platform is lowered by 100–200 μm and a new layer of powder is applied on top [63]. The new layer is sintered by the laser and simultaneously bonded to the previous layer [64]. This process repeats until the final 3D physical part is produced. Fig. 8 shows the schematic by describing a typical SLS machine operation.

SLS can be distinguished from Selective Laser Melting (SLM) process by the different solidification processes in terms of bonding mechanisms. SLM involves full melting of the powdered material to the liquid phase, which results in a fully-dense part after solidification. However, SLS initiates the bonding via partially liquefying the surface of the particles or forming solid-state necking between particles through laser radiation. Nowadays, these two terms are often used mutually due to high similarity of the process. In terms of the layer to layer bonding, the new layer of powders is deposited on top of the previous layer and laser radiation initiates new powders to wet, coalescence, and then bond to form multiple layers [65].

Commonly used lasers in SLS include continuous CO₂ lasers, Q-switched Nd:YAG lasers, short-pulse Cu-vapor lasers, and fiber lasers [66–69]. The choice of a proper laser for SLS mainly depends upon the processing material since the absorptivity varies significantly for different materials. For example, CO₂ lasers with 10.6 μm wavelength are commonly used for sintering polymers and oxide ceramics, which require high absorption in the far infrared or long wavelength region. Nd:YAG lasers with wavelength of 1064 nm or 532 nm are well suited for metals and carbide ceramics based on absorptivity [70].

SLS process is capable of producing parts made from a wide variety of materials, including polymers, glasses, ceramics, and metals for rapid prototyping, and even rapid manufacturing of final products [71–73]. The most commonly used polymer for SLS is polyamide (PA) [63]. Compared to SLA and FFF, SLS process does not require supporting materials because the sintered layers are surrounded and supported by the residual powder at all times, which allows the construction of parts with high geometric complexity and structural integrity. Powders with low fusion or sintering properties can be mixed with a sacrificial binder material for laser sintering to create a “green” part. The binder material can be removed later via debinding process in a controlled furnace environment [74]. Another advantage of SLS is that it allows for efficient use of its material since the non-fused powder can be recycled multiple times without any significant changes in material properties. It is suggested that the temperature and the time at which the residual powder was exposed show the biggest impact on the recyclability of the powder [75]. There are also numerous methods and apparatuses proposed to improve and utilize the recycled powders allowing for improved production with minimal waste [76–78].

The main drawback of SLS technique is that it results in poor surface quality, dimensional accuracy, and weakened material properties. To combat these drawbacks, post-processing treatments, such as polishing, robotic finishing, coating, painting, heat-treatment, and furnace-infiltration are commonly used [64,79].

2.3. Multi Jet Fusion (MJF)

Jet fusion 3D printing (JF3D) or MJF is a recently developed AM method [80]. This new method is similar to SLS, it also uses powdered polymers. However, instead of using laser to sinter or melt the material, MJF uses a fusing agent and detailing agent to bond the powders by IR radiation. MJF consists of two main components, a recoating carriage and printing/fusing carriage. The recoating carriage deposits the build material while the printing/fusing carriage deposits the fusing agent and detailing agent from the HP Thermal Inkjet array. The separation of these two processes allows for optimized performance and efficiency. The build process begins by the recoating carriage laying down a thin layer of material across the build area; this carriage moves from top to bottom. Then, the printing/fusing carriage scans across the initial layer from left to right. The fusing carriage employs a heat energy source that precedes the HP Thermal Inkjet array to ensure that the temperature of build material is consistent throughout printing. As the fusing carriage moves laterally across the material, the printheads in the array deposit a thin layer of fusing agents in precise

Multi Jet Fusion technology

Basic elements of the process

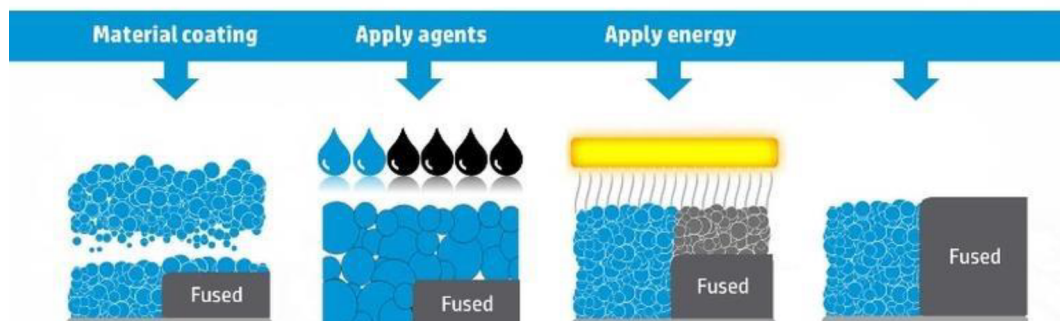


Fig. 9. Schematic showing how a typical MJF machine operates (courtesy of HP).

locations to form the first layer; the detailing agents are also placed to define the specific geometry of the physical part. Lastly, the fusing carriage returns to its original position by moving from right to left and while doing so, it supplies energy to fuse the areas in which the fusing agents were applied. After this layer is completed, a new layer of material at a thickness of 100 µm is applied on top of the previous layer. The recoating carriage moves in the reverse direction for maximum efficiency. Fig. 9 shows the basic elements of the MJF process.

The MJF technology also includes transforming agents which control various properties within the printed part. These properties include but are not limited to electrical and thermal conductivity, translucency, color, and other material properties [80]. A major advantage of this technology is that it allows the user an extreme amount of flexibility by allowing them to place specific properties at desired locations in the fabricated part. Another main advantage of MJF when compared to other powder bed fusion technologies, such as SLS, is that the build time can be greatly reduced by using planar radiation instead of the laser scanning process for SLS [81].

2.4. Stereolithography (SLA)

Stereolithography (SLA) is a commonly used method of 3D printing and was one of the first methods of AM developed. SLA is colloquially used to describe a wider range of Vat Polymerization techniques. Various methods of SLA include digital light processing (DLP), microstereolithography (MSL), digital light synthesis (DLS), and traditional laser SLA. A unique feature of SLA is that it is based on a liquid resin photocuring process where the liquid resin is placed in a tank or reservoir and an ultraviolet (UV) laser or lamp is used to cure the resin. This photopolymerization process converts the resin from liquid to solid via crosslinking. The printing process for traditional laser SLA can be divided into two processes according to the build platform movement and laser location. In the bottom-up process, the reservoir is filled with the liquid resin, then the build platform is initially lowered until only a thin layer of the resin is exposed on the platform surface. The UV laser then fires downward and cures the first thin layer, then the platform moves down, and a roller provides a new coat of uncured liquid resin on top of the previous layer. The second process, the top-down process, places a laser that fires upward at the bottom of the reservoir. Initially, the build platform is lowered into the reservoir until only a thin layer of resin is between the platform and the bottom of the reservoir. This thin layer is cured by the UV laser, then the build platform is lifted to allow the liquid resin to refill the gap between the platform and the reservoir. The top-down process is used more than its counterpart due to several advantages. First, the UV laser is housed below the reservoir, hidden within the machine, preventing the user from being exposed to potentially harmful lasers. Second, the liquid resin is cured in a sealed environment (fully surrounded by uncured liquid resin) which results in better curing. Third, a roller is not needed in the top-down process since gravity automatically refills the liquid resin. Lastly, this process forms smoother part finishes due to complete immersion in liquid resin and full contact to the smooth bottom of the reservoir [82]. Fig. 10 shows a standard SLA format.

SLA photopolymer resins usually consist of the following components: monomers, oligomers/binders, photoinitiators, and various additives. The monomers and oligomers are the primary components of the resin which ultimately crosslink and cause the resin to solidify. When the resin is exposed to UV light the photoinitiators breakdown into radicals which react with the monomer and

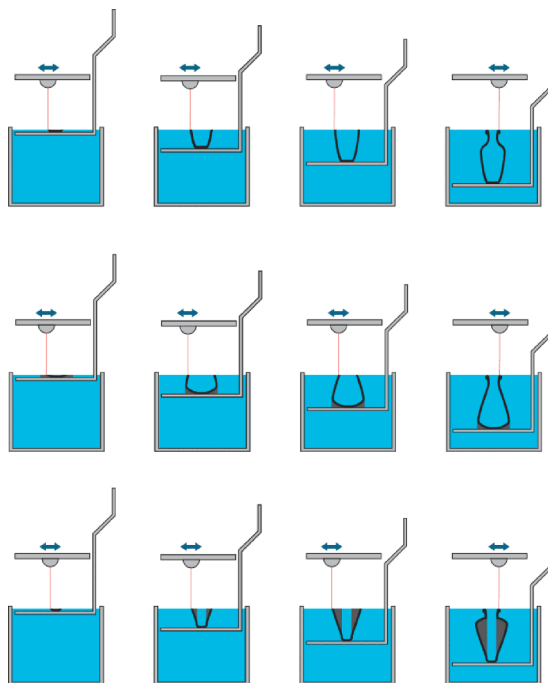


Fig. 10. Schematic showing how a typical SLA (bottom-up process) machine operates [83] (courtesy of Materialise).

oligomers causing them to join and form crosslinks resulting in long polymer chains. The resin additives can be a variety of materials to enhance or visually modify the resin. This includes pigmentation for color and nanomaterials for improved resin performance.

Digital light processing (DLP) is a type of SLA 3D printing. DLP and SLA essentially operate the same way, with the exception of how the light is interfaced with the resin. In SLA the light is projected from a laser to allow for selective exposure to the resin. DLP uses a projector which projects the image of each layer onto the resin, allowing for simultaneous cure of the entire layer compared to point-by-point printing with a laser. The tradeoff is that DLP has a much faster print time at the cost of resolution and surface finish. The gap in print resolution between SLA and DLP is rapidly closing as DLP technology improves. The cost of DLP systems is also often more competitive, making it a strong alternative when 3D printing photopolymer resins.

Carbon's digital light synthesis (DLS), is a method of Vat Polymerization which uses the DLP format to initiate photopolymerization. In addition to using UV digital light processing, Carbon DLS uses a specialized resin system with a secondary thermal step. This secondary thermal step uses epoxies and urethanes, resulting in stronger cures than processes which only use UV. Carbon DLS also utilizes continuous polymerization, reducing some mechanical deficits encountered with layer-by-layer additive manufacturing. Another differentiating feature of Carbon DLS is its use of an oxygen-permeable liquid membrane below the resin. This allows for a constant separation between the resin and the UV source.

Microstereolithography (MSL) include methods of SLA that can be used to achieve a much higher aspect ratio and is capable of printing detailed microstructures. While the process still uses a UV laser to cure photopolymer resins additively, some differences allow for improved resolution and printing at a microscale. The scanning method of MSL uses a galvanometric mirror to focus the UV laser to allow for precision photo-activation of the resin. A second method of MSL is called the dynamic mask process. This process uses a digital mask to selectively allow UV light to pass and interact with the resin. The conformation of the mask changes as each layer is printed. An advantage of the mask method of MSL is that it is faster, allowing for curing of an entire layer as opposed to focused printing which cures the resin of various layers in stages [84]. MSL is an important technology for micro manufacturing, as new resins are developed this tool can potentially be used for printing of microelectronics.

SLA provides the highest printing resolution in comparison to previously mentioned AM methods, such as FFF and SLS. While most commercially available 3D printers print with resolutions of 50–200 μm , SLA machines can print in resolutions of 25 μm or lower. However, despite its extremely high resolution, the main drawback of SLA machines is its slow printing process inherent to curing via laser. Although each layer is formed quickly, there is a significant time interval between the creation of each new layer due to laser scanning and resin cure. The resin must flow to refill the reservoir before a new layer can be made. Therefore, there is a notable time delay between the printing of each layer. Another drawback of SLA is the lack of mechanical performance of the finished part due to limited degree of polymerization and postprocessing is often required.

3. Commercial AM polymers

Although there are many choices of available polymers, a user must carefully consider which materials should be used to manufacture parts because the mechanisms of the four AM technologies discussed above distinctly differ from one another. The FFF material must be available in filament form, SLA material must be available in liquid resin form, and the SLS and JF3D materials must be available in powder form. These physical property requirements require scientists and engineers to evaluate the material mechanical properties to ensure proper compatibility among the AM technologies. To achieve the requirements of many different applications, the materials sometimes must be chemically resistant, flame-retardant, flexible, corrosion-free, have minimum water absorption, or be optically transparent. The ensuing research and rationale for a wide variety of commercially available materials are explained by the various requirements and preferences described above. In this section, the materials that researchers can locate on the internet easily are introduced with their brief descriptions, material properties, and current applications under the category of the four AM technologies.

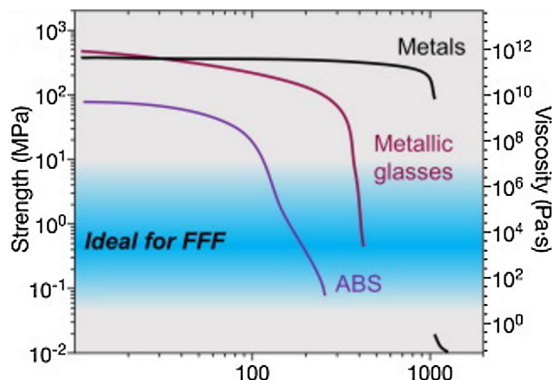


Fig. 11. Typical tensile strength and viscosity range for FFF materials [29]. Copyright 2018, Elsevier.

3.1. FFF Materials

FFF has one of the most versatile materials portfolios among the four AM techniques discussed in this review. All materials are based on thermoplastics which means the polymer will melt or soften at elevated temperatures and re-solidify upon cooling. Fig. 11 illustrates the typical tensile strength and viscosity range for FFF materials. For each specific material, such as ABS, the tensile strength will be affected by factors like temperature and molecular weight and viscosity will decrease as temperature increases. In general, typical tensile strength and viscosity range for FFF printable materials are on the order of 10^{-1} to 10^1 MPa and 10^2 to 10^5 Pa·s, respectively [29].

Gnanasekaran et al. [15] listed the comparison of a spectrum of commonly used polymers for FFF printing (Table 2). The extrudability and printability are somewhat subjectively graded as no supporting data were given, this gives the reader an idea of how each material performs comparatively. It is noted that the printing temperature varies significantly from 120 °C to 450 °C and so is the resulting performance. Because there is no test standard for any AM printed sample, it is difficult to directly compare the properties of each materials. The tensile strength data in Table 2 are values reported in literature.

Since FFF forms 3D parts by extrusion of materials through its heated nozzle from a spool, the materials need to be sufficiently flexible and have their melting temperatures below the system's maximum available heat temperature. The compatibility of the materials is highly affected by their flexibility, stiffness, and viscosity. These properties are more sensitively controlled for high quality printers [85]. Following the popularity of FFF, many materials with various applications have been created and commercialized. Table 3 shows a summary of commercially available polymers for use in FFF.

Acrylonitrile butadiene styrene (ABS) is one of the most common FFF materials with its good printing quality and mechanical properties. Therefore, ABS has been widely used to build functional models for real-scale characterization [86]. Multiple studies have been conducted to research the performance of ABS in terms of FFF printing. Since this 3D printing style is highly directional, ABS printed parts exhibit anisotropic properties. Tensile strength of an ABS printed part can be highly affected by the air gap and raster orientation, while the compressive strength appears to be the least direction-dependent criterion [87].

There are several different kinds of ABS available on market for FFF printing, such as *ABS-ESD7*, *ABSi*, *ABS-M30*, *ABS-M30i*, and *ABSplus*. *ABS-ESD7* is an electrostatic dissipative and durable material that is well fitted for electronic products, jigs, and fixtures for assembly of electronic components and industrial equipment [89]. Due to its unique dissipative properties, it has also been used to make parts that are applied in areas where damage by static charge are likely [90]. It is available with various colors and has good mechanical properties, it has been used to supply automotive tail light lenses [86]. *ABS-M30* is manufactured to be 25 to 70% stronger than normal ABS with excellent tensile, impact, and flexural strength. It is often used to build functional models due to its good mechanical properties and stronger layer bonding [86]. *ABS-M30i* is equivalent to *ABS-M30*, which has better mechanical properties than normal ABS, as a biocompatible material that can be sterilized [91,92]. Lastly, *ABSplus* is an improved ABS in terms of mechanical properties. It has approximately 40% improved nominal tensile strength and 20% increased flexural strength, as well as lower water absorption [93]. It can print tough parts that can be fitted for concept modeling, functional prototyping, and manufacturing tools [94]. *Agilus30* is a distinctive polymer because of its elastomer-like properties [95]. It has been used for compliant components within the bistable element for electronics [96].

Acrylonitrile-styrene-acrylate (ASA) is a terpolymer synthesized with styrene, n-butyl acrylate, and acrylonitrile [97]. It possesses better UV stability and its surface gloss property can be controlled by changing the rubber particle shape, size, and distribution inside the ASA matrix. Blends of ASA with polycarbonate (PC) are also popular and well suited for automobile applications due to the high surface gloss and excellent interfacial properties [98].

High density polyethylene (HDPE) has good strength and stiffness ratio with good chemical inertness. It is excellent in abrasion and

Table 2
Rating of candidate matrix polymers for FFF printing (modified from Table S1 in [15]).

Polymer	Extrudability	Printability	Mechanical properties	Printing temperature (°C)	Ultimate Tensile Strength* (MPa)
PLA	+/-	++	-	190–210	37–46
ABS	++	++	+	210–250	22–37
Nylon	+	+/-	+	235–260	34–68
PS/HIPS	++	+	+/-	240	20–42
PETG	+	++	+/-	230–250	41–53
PBT	+	+	+	220–250	39–60
PBS	+	+/-	+	120–140	19–34
PC	++	+/-	++	275–285	57–72
PMMA	+	-	+	180–250	52–70
HDPE	+	+/-	+	120–150	11–45
PP	+	+/-	+	130–170	9–80
PVC	+/-	+/-	++	200–300	1–59
TPU	+/-	+	+	210–225	6–33
PEI	++	+	++	350–390	69–81
PEEK	++	+	++	360–450	48–265
PPSF	++	+	+/-	350	55
PEKK	++	+	++	350	90–110

* Tensile strength data are collected from multiple sources including materials datasheets and publications.

Table 3

Summary of commercially available polymers for FFF.

Polymer type	Material	Manufacturer	Reference
ABS	Acrylonitrile butadiene styrene (ABS)	Ultimaker, Makerbot, 3dxtech, etc.	[86–88]
	ABS-ESD7	Stratasys	[89,90]
	ABSi	Stratasys	[86,89]
	ABS-M30	Stratasys	[86]
	ABS-M30i	Stratasys	[91,92]
	ABSplus	Stratasys	[93,94]
ASA	Agilus30	Stratasys	[95,96]
	Acrylonitrile-styrene-acrylate (ASA)	Stratasys, 3dxtech, etc.	[97,98]
PE	High density polyethylene (HDPE)	Filaments.ca	[99–101]
PP	Polypropylene	Ultimaker, etc.	[102]
PS	High impact polystyrene (HIPS)	MatterHackers, etc.	[103,104]
Nylon	Nylon 6	Stratasys, 3dxtech etc.	
	Nylon 12	Stratasys	[105–107]
	Nylon 12 CF	Stratasys	[108,109]
PC	Polycarbonate (PC)	Ultimaker, 3dxtech, etc.	
	PC-ABS	Stratasys, 3dxtech, etc.	[110–113]
	PC-ISO	Stratasys	[113,114]
PLA	Polylactic acid (PLA)	Stratasys, Ultimaker, 3dxtech, etc.	[115–117]
PPSF/PPSU	Polyphenylsulfone	Stratasys, 3dxtech, etc.	[118]
TPE	Thermoplastic elastomer (TPE)	MatterHackers	[119,120]
TPU	Thermoplastic polyurethane (TPU)	Stratasys, Ultimaker etc.	[121]
ULTEM™	Polyethylenimine (PEI)	SABIC	[52,122–124]
PEEK	Polyether ether ketone	Solvay, Evonik, Victrex	[125–127]
PEKK	Polyether ketone ketone	Arkema	[128,129]

impact resistance and fatigue behavior. Furthermore, it exhibits a balance of stiffness, creep behavior, and processability. In recent years, PE's good biocompatibility has attracted research attentions in biomedical applications. For example, taking advantage of polyethylene's high wear resistance, Ultra-high-molecular-weight polyethylene (UHMWPE) has been used [130,131] for AM of artificial implants.

High impact polystyrene (HIPS) is usually used as support materials as it dissolves in limonene. It is prepared by dissolving rubber in a styrene monomer followed by polymerization. Because of its 2-phase structure, it creates a non-uniform stress field by initially relaxing the rubber in the matrix when any stress is applied [21]. Flame-retardant HIPS can be made by synthesizing HIPS with red phosphorus and magnesium hydroxide [22].

Nylon 6, nylon 12, and a modified nylon 12 with carbon fiber (nylon 12 CF) are compatible for FFF printing. Nylon 6 usually has different ordered crystalline phases in its matrix resulting in non-crystalline/amorphous regions and a dominant factor of the mechanical property behavior [132,133]. Nylon 12 is also a semi-crystalline polymer and is strongly resistant to chemicals, maintains the lowest water absorption of all polyamides, has high flexibility, and low density. Moreover, it has high fatigue and impact resistance [106]. Nylon 12 CF is a modified polymer that has 35 wt% of dispersed carbon fibers in the nylon 12. The carbon fibers improve the strength and stiffness as well as in-plane properties at room temperature, but lose their effectiveness as ambient temperature increases [109].

Polycarbonate (PC) is an amorphous and transparent polymer with excellent balance of toughness, clarity, and high thermal resistance. Although it is very useful in many applications, the price is relatively expensive compared to other available high-performance polymers. Furthermore, recycling of PC can greatly deteriorate its mechanical properties along with its modulus of elasticity and tensile strength. If PC is reprocessed, its glass transition temperature and initial degradation temperature decrease due to chain break cleavage reactions. Another precaution when using PC is that the material should not be exposed to UV due to photo-degradation, resulting in a yellow color on the surface [134]. Additionally, there are materials that can be formulated by blending PC with other polymers to alter the material so that it can meet the standard of biocompatibility. These materials are *PC-ABS* and *PC-ISO*. *PC-ABS* is a blend of PC and ABS that has improved processability and fracture toughness when a sharp damage episode may occur [111]. It has been popularly used in automotive industry due to its attractive economics, good impact strength, high heat distortion temperature, and low melt viscosity [112]. *PC-ISO* is a commercially available biocompatible material. It can be safely sterilized and, since it is FDA approved, can be used for food packaging [113].

Polylactic acid (PLA) is a linear aliphatic thermoplastic polyester, produced from renewable biodegradable materials, with excellent mechanical properties, thermal stability, processability, and low environment impact [117]. The material is ideal for food packaging and other consumer products. Since it is derived from agricultural feedstock, the usage of PLA provides positive benefit to the agricultural economy. However, it is relatively expensive material compared to other petroleum-based polymers [135]. To enhance the original properties of PLA, research efforts continue to incorporate nanoparticles within PLA. The addition of montmorillonite-layered silicate is expected to provide better barrier properties with increased modulus and decreased toughness, while TiO₂ allows better photo-degradability under UV [136].

Polyphenylsulfone (PPSF or PPSU) was the first FFF high-performance thermoplastic resin for engineering purposes. It has the highest heat and chemical resistance among all the other FFF materials while its mechanical properties are superior to others beside

ULTEM™ 9085. It is resistant to oils, gasoline, chemicals, and acids. Moreover, like the other biocompatible FFF materials, it can be sterilized by steam autoclave, plasma, chemical, and radiation conditions [94].

Thermoplastic elastomer (TPE) is a very flexible printing material [120]. It is similar to a blend of natural rubber and polypropylene that can retain partial flexibility and resilience of thermoplastic elastomers at ambient temperatures. It has been reported that a cross-linked TPE exhibits better tensile strength, Young's modulus, and hardness than non-cross-linked TPE [137].

Thermoplastic polyurethane (TPU) is a polymer that has excellent mechanical properties with good bio-compatibility. It is used as a coating material to provide biomedical products, such as breast implants, catheters, and prosthetic heart valve leaflets. However, proper designs are required due to TPU hydrolytic, oxidative, and enzymatic degradation [138]. According to a study that examined the ideal 3D printing parameter of TPU, it was reported that the TPU printed parts under the setting of 45° orientation with 215 °C had the least internal stress and good thermal bonding among layers [121].

Two different polyetherimide (PEI) products, ULTEM™ 1010 and ULTEM™ 9085, have been commercialized for FFF printing. ULTEM™ 1010 is a thermoplastic amorphous PEI with very little water absorption which can be prepared as a medical-grade polymer [139]. In contrast, ULTEM™ 9085 is suitable for aerospace and aviation applications due to its high mechanical strength, high heat deflection temperature, and flame retardancy. A study that examined the best 3D printing style for ULTEM™ 9085 resulted in the finding that sparse build appeared to be better than solid build because the former can reduce the cost and minimize thermal expansion mismatch between the intended design and the manufactured composite part. Nonetheless, since the sparse build has significantly lower effective strength and modulus compared to the other 3D printing methods, a proper structural design is recommended to withstand higher thermo-mechanical stress that occurs during the curing cycle time [122]. In another study, Chuang et al. used commercial ULTEM™ 9085 and carbon fiber filled ULTEM™ 1000 to print test parts for aircraft engine components [52].

Both Polyether ether ketone (PEEK) & Polyether ketone ketone (PEKK) belongs to the Polyaryletherketone (PAEK) family which contains alternative ketone and ether groups in their backbone. Both are semi-crystalline materials that have high thermal stability, chemical resistance, and mechanical properties. PEEK also has good biocompatibility which makes it a good candidate for medical applications, such as orthopedic implants. Both PEEK and PEKK exhibit excellent fire resistance, thus have been used as aircraft and automotive components.

3.2. SLS Materials

Since the SLS method sinters or melts the material layer by layer, a powdered material is used. Commonly used material on SLS machines are polyamides (PAs) or nylon, specifically polyamide 11 (PA11) and PA12. Although these two materials are widely used, a plethora of variations of these materials exist from the preparation of varying nanocomposites with different nanoparticles; these variations result in enhanced durability, heat resistance, and chemical resistance. Importantly, only semi-crystalline polymers are capable of being used for SLS due to its process melting behavior. PA materials are generally used because they are a very versatile material due to their strong yet flexible properties; therefore, they are ideal for general purpose use. Furthermore, development of polymer nanocomposites using PA as the base material has been moderately successful and many heat and chemical resistant PA materials, such as polymer nanocomposites (PNCs) are already commercially available. Lastly, PA can easily be dyed different colors, therefore, it offers users great control on the color of their finished print. Due to the versatility of PA, SLS has been gaining more interest. Along with its versatility, the low cost of PA powder has made it even more attractive to consumers. Table 4 shows a summary of commercially available polymers for used in SLS.

As it was previously mentioned, PA11 is one of the most common materials used in SLS. PA11, also commonly called nylon 11, naturally offers high elongation and impact strength which results in good toughness. Although PA11 bestows many advantageous properties, two different modified nylon 11 materials exist: *nylon 11 EX* and *nylon 11 FR*. Nylon 11 EX improved the impact resistance and is characterized by excellent toughness similar to molded ABS or polypropylene. This material also provides accurate and precise manufacturability, allowing users to create reproducible and identical parts. Lastly, due to its improved impact resistance and toughness, nylon 11 EX is suited for snap-fit designs and thin-walled components. Nylon 11 FR is flame-retardant version of nylon 11. This material provides nylon 11 flame retardancy as well as improved elongation at break. However, other physical properties of

Table 4
Summary of commercially available polymers for SLS AM.

Polymer type	Material	Manufacturer
Nylon	Nylon 11	Stratasys
	Nylon 11 EX	Stratasys
	Nylon 11 FR	Stratasys
	Nylon 12 AF	Stratasys
	Nylon 12 CF	Stratasys
	Nylon 12 GF	Stratasys
	Nylon 12 GSL	Stratasys
	Nylon 12 HST	Stratasys
	PA2241 FR	EOS GmbH
	Alumide	EOS GmbH
PAEK	PEEK	EOS GmbH
	PEKK	Stratasys

nylon 11 FR are similar to nylon 11 EX. Since this material supplies flame retardancy, it encounters applications in aerospace parts, vehicle under hood components, and other parts that require flame retardancy. Despite the discussed properties, it is worth to notice that the nylon 11 FR contains halogenated FR which has caused rising health concerns in recent years.

Nylon 12 is another common material used in SLS. Like nylon 11, many modified nylon 12 materials are currently commercially available. *Nylon 12 AF* is an aluminum filled composite of nylon 12 which results in strong and rigid products. This material produces a grey metallic appearance on the finished parts. It also has improved tensile and flexural modulus as well as good abrasion resistance. Due to its good abrasion resistance, Nylon 12 AF gains use in various industries, such as aerospace, automotive, packaging, electronics, consumer products, and industrial products.

Nylon 12 CF is a carbon fiber reinforced nylon 12 which provides resistance to extreme temperature and abrasion. The carbon fiber additive also results in high product detail, high stiffness, and improved tensile strength. The carbon fiber filling further allows this material to be electrostatically dissipative. Because of its extreme temperature and abrasion resistance, Nylon 12 CF is generally used in vehicle under hood components as well as other applications that require high strength to weight ratio. *Nylon 12 GF* is like nylon 12 AF and nylon 12 CF in that it has glass fiber additive in its base polymer matrix. This glass fiber reinforcement results in excellent material stiffness, improved temperature resistance, and dimensional stability. Nylon 12 GF is commonly used in housings or enclosures and consumer sporting goods [49]. *Nylon 12 GSL* is a lightweight nylon 12 with carbon fiber reinforcement which exhibits high strength to weight ratio. Furthermore, this material displays great surface finish and detail as well as high-temperature resistance. This allows nylon 12 GSL to be applicable in aerospace, athletic equipment, and unmanned aerial vehicle industries. *Nylon 12 HST* is reinforced by mineral fibers resulting in improved temperature resistance, high stiffness, and most notably, insulative properties and radio-frequency (RF) transparency. Due to these notable insulative and RF transparency properties, Nylon 12 HST is most commonly applied in creating structural components and enclosures for construction industries.

PA2241 FR is a flame-retardant PA12 composite that uses a halogen-based flame retardant. This material exhibits high strain at tensile strength and is recyclable. Its recyclability allows this material to be very economical and allows for low-cost part production. This homopolymer material also exhibits high crystallinity and thermal stability. Since this material is flame-retardant, much like nylon 11 FR, it finds applications in aerospace and aviation [46]. Even though halogenated FR is effective in performance, it is considered as a hazardous species and questionable in future use.

Alumide is a filled polymer consisted of 50/50 aluminum and nylon matrix, which is identified as a metal-polymer composite. This material is used to 3D print jewelry with complex shapes and even gemstone insertions because of its semi-metallic physical characteristics and dye compatibility [140]. Because Alumide is non-porous, it can be machined easily and withstand high temperatures. It has been used in tooling industry, to make wind tunnels for the automotive industry, or for parts where safety is a priority [141].

Although PA11 and PA12 are the two most commonly used SLS materials, *polyetheretherketone (PEEK)* is rapidly gaining more attention as a high-performance polymer available for the SLS manufacturing process. As mentioned, PEEK is a high-performance, semi-crystalline thermoplastic polymer and offers very high-temperature and chemical resistance. Furthermore, it also exhibits good strength and stiffness. Lastly, PEEK also displays excellent biocompatibility; therefore, it is suitable to produce parts for medical uses, such as medical implants.

Polyetherketoneketone (PEKK) is another high-performance polymer which displays great strength to weight ratio and a wide operating temperature range. PEKK also offers great chemical resistance, flame retardancy, and low smoke and toxicity. Due to its inherent flame retardancy and wide operating temperature range, PEKK is applicable to the aerospace and motorsports industries.

3.3. MJF Materials

As explained above, MJF technique requires materials to be in a powder form. HP has commercialized three suitable materials, all consisting of PA family: *PA11*, *PA12*, and *PA12 Glass Beads*. Table 5 shows a summary of commercially available polymers for used in MJF AM.

Since PAs are also very common materials for FFF and SLS, their characteristics are equivalent to the ones introduced in the former sections. These PAs have similar features to each other but have specific differences as well. *PA11*, *PA12*, and *PA12 Glass Beads* all have overall good mechanical properties, excellent chemical resistance, enhanced elongation-at-break, and reusability. Both PA11 and PA12 Glass Beads have 70% reusability, while PA12 has better reusability at 80% [142–144]. Additionally, each material has distinct ideal applications; PA11 is preferred to be used in applications of prostheses, insoles, sports goods, snap fits, or living hinges [142]. Since PA12 is certified with its biocompatibility by USP Class I–VI and US FDA guidance for Intact Skin Surface Device, it can be used to print surgical tools or human organ implants as well as housings, enclosures, and watertight products [142,143]. Lastly, PA12 Glass Beads, which is PA12 with enhanced stiffness by the addition of 40% of glass beads, is robust when applied to building enclosures, housings, fixtures, tooling, or proper parts that requires higher stiffness than regular PA11 and PA12 can withstand [144].

Table 5
Summary of commercially available polymers for MJF AM.

Polymer type	Material	Manufacturer	Reference
Nylon	PA11	HP	[142]
	PA12	HP	[143]
	PA12 Glass Beads	HP	[144]

3.4. SLA Materials

SLA is an AM technique that uniquely uses liquid resins to print parts, as mentioned above. SLA resins are formulations that usually contain monomers, oligomers, photoinitiators, and additional additive materials. Research and development of photopolymer resins are constantly expanding the potential of SLA 3D printing. Commonly available SLA resins types include ceramics, dental, castable, flexible, and heat resistant materials.

Table 6 surveys many of the photocurable resins developed for 3D printing. SLA 3D printing is used for a wide range of applications. Resin development has expanded and specialized to enable high quality printing for many applications. Its applications include hobby printing, art, jewelry casting, medical, and industrial. Manufacturers, such as Detax and NextDent produce high quality biocompatible resins for dental and medical applications. Additionally, manufacturers, such as Bucktown Polymers, 3DR-*syns*, and 3D Systems are less specialized, but produce resins for numerous applications.

Three materials named *Accura Amethyst*, *Accura CastPro*, and *Accura Xtreme* where developed to create accurate patterns with good mechanical properties. *Accura Amethyst* is used to manufacture master patterns for jewelry and similar microcasting applications, which require high-resolution. *Accura CastPro* can produce accurate patterns as well as excellent water absorption resistance and fast production speed. *Accura Xtreme* is tough and durable for breakage and suitable for vacuum casting patterns, snap fits, and functional assemblies.

ProtoGen 18120 is an ABS-like photopolymer, which produces accurate parts for general purposes like medical, electronics, aerospace, and automotive applications. It was demonstrated as the first SLA resin utilized to show different material properties in terms of the control of machine exposure. It is also resistant to high temperature and humidity.

SC 1000P is a casting pattern material with a low deformation of shrinkage, durability, humidity resistance, and clarity of MRI image. It possesses transparent yellow-green color that can be customized as well by tints and paints.

Lastly, Somos materials that are respectively developed for each different application are available for SLA technique. The following materials are identified as *Somos Element*, *Somos NeXt*, *Somos PerFORM*, *Somos WaterClear Ultra 10122*, and *Somos WaterShed XC 11122*. *Somos Element* is an antimony-free SLA material which has an improved repeatability of quality 3D printing casting patterns. It can be used to fabricate high-end alloy castings. *Somos NeXt* has superior strength, durability, and toughness, that is suitable for snap-fit designs, packaging, and sporting goods. It can be used in aerospace, automotive, medical, consumer products, and electronics industries. *Somos PerFORM* is strong and stiff as well as heat resistant. Thus, it is suitable for wind tunnel models for aerospace and automotive applications, and rapid tooling for injection molding. *Somos WaterClear Ultra 10122* is transparent and temperature and water resistant. Last of all, *Somos WaterShed XC 11122* is a colorless photopolymer that has a low viscosity. It can print ABS-like parts that are strong, tough, and water resistant.

4. Recent progresses on polymer composites and polymer nanocomposites for AM

As it was discussed in previous sections, the materials spectrum for AM is still somewhat limited due to the specific requirements of each AM techniques. Due to this restriction, traditional AM polymers often are limited for high-performance applications. Thus, it is crucial to develop functional high-performance materials to expand the capability of AM. Such functionalities can be achieved by developing composite materials that are compatible with the AM process.

A composite material is a type of material that is prepared by combining two different materials with different properties. According to ASTM D3878-18, a composite material is “a substance consisting of two or more materials, insoluble in one another, which are combined to form a useful engineering material possessing certain properties not possessed by the constituents” [145]. The early use of composite materials includes straw and mud from ancient brick structures. However, it wasn’t until the 20th century that the field of composite materials saw significant expansion. This is because of the explosive development of fiber-reinforced polymer (FRP) composites. The FRP composite materials have gained popularity due to their extraordinary properties, such as light weight, corrosion resistance, and strength to weight ratio. Fiber-reinforced polymer composites enjoy many applications in automotive and aerospace industry due to its excellent mechanical properties and chemical resistance. Carbon fiber and glass fiber are common reinforcements with AM applications. Numerous studies in printable fiber-reinforced composite have been carried out by both academia and industry [47,146–148]. The main function is usually to improve mechanical performance. Both continuous and chopped or particulate fiber-reinforced composites parts have been studied [47,149,150]. Although the short or chopped fiber-reinforced composites are easier to process, the continuous fiber-reinforced composites usually exhibit better tensile properties in the printing direction. Recent review papers by Goh et al. [151], Brenken et al. [44], Parandoush et al. [152], and Wang et al. [153] describe this research area comprehensively. To prevent duplication of efforts, this review will mainly focus on recent progress in polymer nanocomposite and other novel composite materials for AM.

Polymer nanocomposites (PNCs) are materials with nanofillers dispersed in the polymer matrix. These nanofillers with at least one dimension in the nanometer range are used as reinforcements or as functional additives in the polymer matrix. Polymer nanocomposites have attracted considerable research interest because of the so called “nano-effect”. It is well recognized that enhancement in properties, such as mechanical, thermal, electrical or chemical are achieved by small loadings of nanofillers [154,155]. Compared to continuous fiber-reinforced composites, PNCs are less prone to anisotropy issues where interlaminar strength is weak due to the lack to fiber reinforcement. When used for AM, the PNCs can be processed the same way as neat polymers without any modification of the machine. Various types of PNCs using different nano-additives or nano-filler have been developed for AM applications. The main effect of reinforcements in PNCs include improvement in mechanical and electrical properties. For example, nanoclay-based nanocomposites are widely used to improve elastic modulus [156–159] and CNT- and graphene-based

Table 6
Summary of commercially available polymers for SLA AM.

Material	Resin Properties	Manufacturer
3D Printing Resin	General use	Wanhao
3D Rapid Resin	Low energy curing	Monocure 3D
3D Standard Resin	General use	Monocure 3D
ABS like Resin	General use	Phrozen
Accura Amethyst	Casting	3D Systems
Accura CastPro	Casting	3D Systems
Accura Phoenix	High temperature	3D Systems
Accura Xtreme	Tough	3D Systems
Adhesive HM	Adhesive	3DRsyns
AMD-6 DLP	Modeling	Ameralabs
Basic Resin	General use	HARZ Lab
B9R Emerald	Casting	B9Creations
B9R Red	Prototyping	B9Creations
Castable Blend	Casting	Fun To Do
Castalite	Casting	Tethon3D
Cast Resin	Casting	HARZ Lab
CD Clear	Casting	Bluecast
Clear and Tough	Tough/transparent	3DRsyns
Clear Resin	General use/transparent	Formlabs
CR UHTR	Tough/chemical resistant	3DRsyns
Dental Resin	Biocompatible	HARZ Lab
Dental SG	Biocompatible	Formlabs
Durable Resin	Tough	Formlabs
EP200-V420	General use	Bucktown Polymers
Electrically Conductive Resins	Electrically conductive	Bucktown Polymers
Ferrolite	Iron polymer composite	Tethon3D
Flex100	Flexible/low energy	Monocure 3D
Flexilalite	Flexible	Tethon3D
Freeprint Resins	Medical/biocompatible	Detax
Genesis	Developmental	Tethon3D
Grey Pro Resin	Prototyping/general use	Formlabs
HE	Tough/Elastic	3DRsyns
HDT1	High temperature/tough	3DRsyns
High Temp Resin	Engineering	Formlabs
HTR UHT	High temperature/tough	3DRsyns
Industrial Blend	Tough	Fun To Do
IPR-10 SLA	Tough/prototyping	Ameralabs
IR	Tough/transparent	3DRsyns
KeyPrint 3D Resins	Dental/biocompatible	Keystone
LS Low Shrink	Casting	Bluecast
Luxaprint Resins	Medical/modeling	Detax
Medicalprint	Biocompatible	Detax
Model Resin	Modeling	HARZ Lab
Peopoly Model Resin	Modeling	Peopoly
PlasGRAY	Modeling/prototyping	Asiga
Porcelite	Ceramic	Tethon3D
ProtoGen 18120	General purpose	DSM
PS100-V420	Rapid cure/polyester	Bucktown Polymers
PS102-V420	General use/rapid cure	Bucktown Polymers
Rigid Resin	Tough	Formlabs
Rinse Out Resin	Casting	Bucktown Polymers
SC 1000P	Casting	Stratasys
SF	Tough	Makerjuice
SF	Soft/flexible	3DRsyns
NextDent Resins	Biocompatible	NextDent
OD-Clear MF “monomer free”	Biocompatible/dental	3DRsyns
SFUT MF “monomer free”	Tough/rapid cure	3DRsyns
SMM Castable	Casting	Phrozen
Somos Bioclear	Medical	DSM
Somos Element	Casting	DSM
Somos GP Plus 14122	Prototyping	DSM
Somos NeXt	Tough	DSM
Somos PERFORM	Tough/high temperature	DSM
Somos ProtoTherm	Tough/high temperature	DSM
Somo Taurus	Tough/high temperature	DSM
Somos WaterClear Ultra 10122	Transparent	DSM
Somos WaterShed XC 11122	Tough	DSM
SpeedCast Resin	Casting	Full Spectrum Laser

(continued on next page)

Table 6 (continued)

Material	Resin Properties	Manufacturer
Spot-e	Flexible	Spot-A Materials
Spot-gp	General use	Spot-A Materials
SR	Soft	3DResyns
Standard	General use	Makerjuice
Standard Blend	General use	Fun To Do
Super Tough Flexible v2	Flexible	Full Spectrum Laser
Thermally Conductive Resins	Thermally conductive	Bucktown Polymers
Type D Dental	Modeling	Druckwege
Type D Pro	General use	Druckwege
Type D Pro Flex	Flexible	Druckwege
UHF	Tough/flexible	3DResyns
Universal Resin	General use	Full Spectrum Laser
UV Flexible Resin	Flexible	Photocentric Group
UV High Tensile	Tough	Photocentric Group
UV Resin	Modeling	Anycubic
UV Tough	Tough	Photocentric Group
Vitrolite	Ceramic/glass	Tethon3D
Water Washable Clear Resin	Casting	Full Spectrum Laser
Waxcast	Casting	Makerjuice
Waxy	Casting	3DResyns
WC Clear BIO	Biocompatible	3DResyns
ZVE200-V470	Tough/low energy curing	Bucktown Polymers
ZVE500-V420	Tough/rapid cure	Bucktown Polymers

nanocomposite are used to develop various electronic devices of benefit to its greatly improved electrical conductivity [11,16,160–170]. Some studies have also focused on material properties, such as thermal and flame-retardant properties [124,171,172].

Although nanoparticles are very effective in improving many materials properties, one of the drawbacks is the decrease in ductility or elongation at break in many nanocomposites [157,158]. Two main factors contribute to this phenomenon, first is the poor interfacial adhesion and the second factor is the agglomeration of nanoparticles acting as stress concentrating defects. For PNCs to provide its best performance, proper dispersion of the nanofillers is a crucial step. To ensure homogeneous dispersion, a high shear processing method, such as twin-screw extrusion is needed. Many researchers use a two-step method to fabricate the filament materials. The first step involves an intensified mixing method usually to include twin-screw extrusion or sonication in a solution. After obtaining well dispersed samples, a second extrusion is implemented to obtain filaments with well controlled diameters and uniform dispersibility.

The mechanical reinforcement effect observed for nanoparticles is as follows: typically increase elastic modulus and decrease elongation or strain at break [156,173]. The large deformation from the printer head induces a certain degree of filler orientation which leads to anisotropy of the printed parts [174].

Key features of PNCs in AM can be summarized as follows:

1. Orientation effects. The mechanical properties of 3D printed samples appear to be strongly dependent on the printing orientation. Such anisotropy in mechanical properties is widely reported [37,87,175–177]. It has been reported that the tensile strength of FFF printed samples printed in the XYZ direction can be 5 times higher than those printed vertically. Depending on the application, it can be viewed with mixed results. The alignment of nanofillers in the printing direction may assist improved thermal conductivity in the aligned direction [174]. Reports have shown that with tailored materials properties using polymer blend, it is possible to lower the mechanical anisotropy [37].
2. Filament uniformity is also an important factor for determining part quality. Numerous factors will affect the output diameter of the filament (e.g., temperature, coefficient of thermal expansion, heat transfer coefficient, specific heat, ambient temperature, feed rate, etc.) [178]. The incorporation of small amounts of nanofiller can dramatically alter the rheological behaviors which is crucial in the filament extrusion process.
3. Loading of the nanoparticles is equally important. Nanofillers or nanoparticles can significantly affect the rheology of the polymer in the molten state and is a dominant factor influencing the printability. This is because nanoparticles tend to restrict the polymer chain mobility [156]. Moreover, nanoparticles tend to aggregate at high loadings (usually above 5 wt%) due to high surface energy. This will further reduce material's printability. It has been reported at a high graphene loading (7.4 wt%), aggregated graphene sheets could obstruct the printer's nozzle, resulting in the 3D printing failure [11].

4.1. Polymer nanocomposite materials for FFF

The most commonly used thermoplastics for FFF include acrylonitrile butadiene styrene (ABS) and polylactic acid (PLA), with typical bulk strengths between 30 and 100 MPa and elastic moduli in the range of 1.3–3.6 GPa. Mechanical properties of 3D printed parts, however, can deviate significantly from the material bulk properties due to the detailed methods of how a structure is formed

on the meso-scale during printing [47]. Nanoparticles will typically increase elastic modulus and decrease elongation or strain at break [156,173]. The large deformation from the printer head induces a certain degree of filler orientation which leads to anisotropy of the printed parts [174].

Due to the novelty of AM, many researchers have compared the performance of the printed parts with conventionally molded (compression and injection molded) samples [166,170,174]. It is generally recognized that FFF printed parts often have lower mechanical performance compared to injection molded parts due to porosity and poor interlayer bonding [156,157].

This section intends to provide an overview of the progress in recent developments in novel printable FFF materials for mechanical, thermal, electrical, and flame-retardant applications. The focus of the following discussion is on recent progresses of high-performance polymer nanocomposites for AM. The majority of the reviewed research articles were published during the last 5 years. In this section, the term FFF and FDM will be used interchangeably to reflect the author's choice. Table 8 summarizes the results discussed in this section.

4.1.1. Clay nanocomposites

Although nanoparticles are very effective in improving many materials properties, one of the drawbacks is the decrease in ductility or elongation at break in many resulting polymer nanocomposites [157,158]. Weng et al. [157] studied the mechanical and thermal properties of ABS/montmorillonite nanocomposites for FDM. Various loadings (1, 3, and 5 wt%) of benzylidimethylhexadecylammonium chloride (HDBAC) modified montmorillonite clay was melt compounded with ABS using a twin-screw extruder. Intercalation of the MMT clay platelets were confirmed by XRD and TEM results (Fig. 12a). They initially compared the tensile properties of the printed parts with injection molded samples. Due to the nature of the extrusion-based printing technique, it is difficult to eliminate voids formed in between extruded filament as shown in Fig. 12b. Compared to injection molded samples, high void content and low level of polymer chain entanglement of the printed parts results in lower values of mechanical properties. However, with 5 wt% of nanoclay loading, the gap between the two processing methods was reduced. For the printed parts, both tensile and flexural properties were enhanced with increasing amount of nanoclay (Fig. 12c and d). In addition, lower linear thermal expansion ratio, higher thermal stability, and T_g were observed for the ABS/OMMT nanocomposite samples.

Francis et al. [159] coated ABS filament with solution blended ABS/OMMT nanocomposite for AM of microwave and radio frequency (RF) components. The OMMT loading was 3 wt%. The coated filament was treated in microwave environment to achieve better adhesion between the core and the nanocomposite shell. Polarization at both the polymer/OMMT interface and the free ions in between clay platelets caused significant increase in relative permittivity and loss tangent. Increase in tensile modulus and hardness

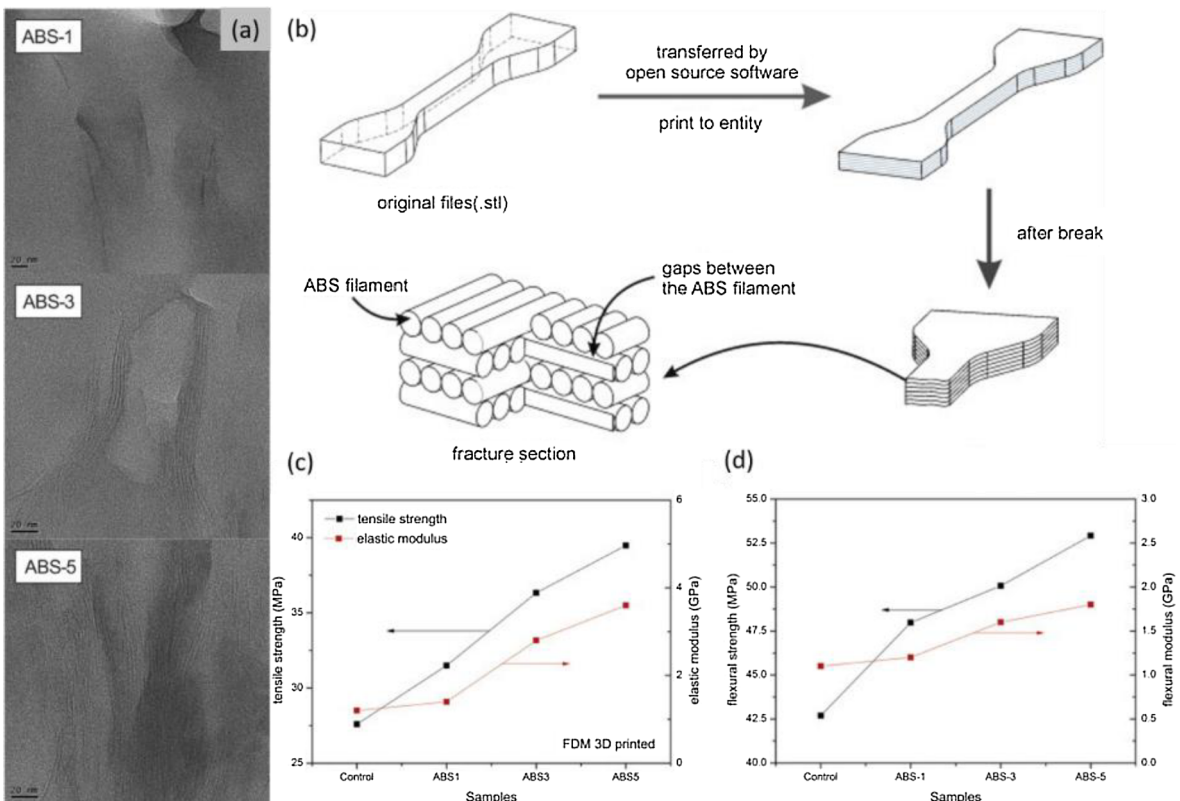


Fig. 12. (a) TEM images of ABS/OMMT nanocomposite; (b) illustration of fracture surface or printed parts; (c) tensile and (d) flexural properties of printed ABS/OMMT nanocomposites. Reprinted with permission from Ref. [157]. Copyright 2016, Elsevier.

of the AM parts was reported.

In another study, Coppola et al. [158] compared the properties of neat PLA and PLA nanocomposite filaments with 4 wt% of Cloisite 30B nanoclay. The addition of nanoclay increased the degree of crystallinity of PLA in both filament and printed forms. Similar to previous studies, an increase in storage and elastic modulus as well as thermal stability were observed for the nanocomposite samples. It was also reported that the nanocomposite printed parts exhibited better shape stability.

Meng et al. [156] compared the properties of ABS nanocomposite reinforced by four different types of inorganic nanofillers: montmorillonite (MMT), multiwalled carbon nanotubes (MWCNTs), calcium carbonate (CaCO_3), and silica (SiO_2). The materials were processed by twin-screw extrusion and the concentration of all nanofillers were fixed at 1 wt%. All nanocomposite printed parts exhibited better tensile strength, flexural modulus, and strength than the neat ABS. Among all the nanocomposites, ABS/MMT showed the highest tensile and flexural strength while the flexural modulus is comparable with ABS/MWCNT and ABS/ CaCO_3 . It is interesting to note that the addition of CaCO_3 improved the elongation at break of neat ABS by about 50%. This is unusual since most inorganic nanoparticles appear to adversely affect material ductility. The reason for this phenomenon was not discussed by Meng et al. The authors also compared the mechanical properties of parts printed in horizontal (XYZ) and vertical directions (ZXY) (Fig. 13). Ductile failure and higher values of tensile properties were observed on horizontally printed parts whereas brittle failure occurs for all vertically printed samples. This difference in material anisotropy was reduced when nanoparticles were introduced into the ABS. The most effective nanofiller for improving anisotropy is CaCO_3 .

4.1.2. Carbon nanotube and carbon nanofiber nanocomposites

Compared with traditional fabrication processes, AM enables the fabrication of many electronic devices in a simplified process at lower cost and with greater design flexibility. To achieve this benefit, material development is a key ingredient. Compared to conventional conductive fillers, such as carbon black [179], only low concentrations of nanofillers are required.

Dispersion of the CNT is critical not only for optimum polymer performance but also to avoid poorly dispersed CNT agglomerates that can obstruct the printer nozzle and significantly affect the printing process [160]. Because of the high electrical conductivity of

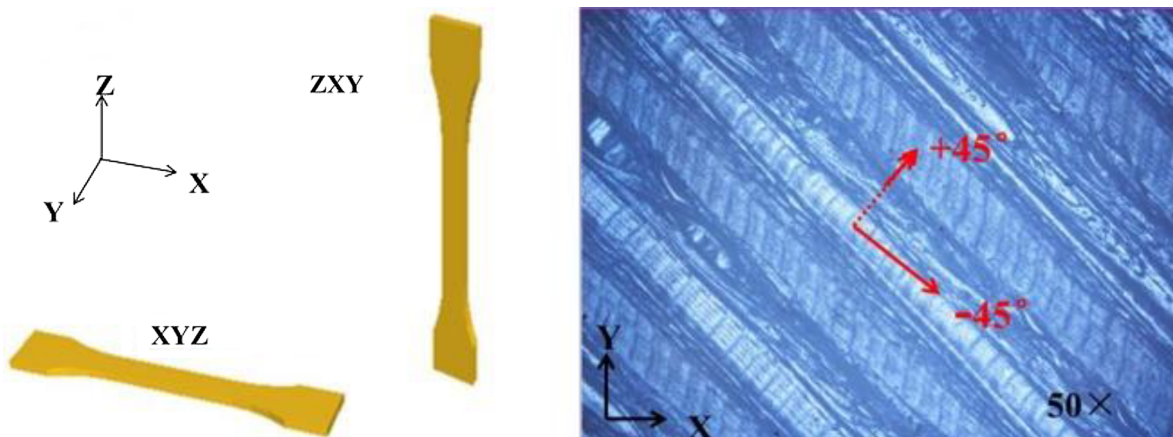


Fig. 13. Building orientations and raster angle patterns of the tensile specimens. (a) TS and (b) EL values for specimens printed in the xyz and zxy build orientations. Reprinted with permission from Ref.[156]. Copyright 2016, John Wiley and Sons.

CNT and graphene, the development of printable CNT nanocomposite AM materials has attracted tremendous research interest in electronic applications, such as wearable electronics [161], flexible circuits [162], force [16], strain [160], and liquid sensors [163].

Shofner et al. [164] were among first to report the use of carbon-based nanocomposite filaments for FFF. 10 wt% of vapor grown carbon fiber (VGCF) was melt mixed with ABS to produce the filament. Increase in tensile strength, elastic and storage modulus, and decrease in ductility were reported for the nanocomposite samples.

Dorigato et al. [165] compounded ABS/MWCNT filament by diluting commercially available ABS/MWCNT masterbatch with neat ABS using twin-screw extrusion. To gain a better understanding of the materials behavior, a series of samples with various CNT loadings (1–15 wt%) were compression molded and tested. The Melt Flow Index (MFI) as well as the electrical resistivity of the molded parts decreases dramatically as the CNT loading increases. Moreover, rapid heating of the nanocomposite under applied voltage was observed as shown in Fig. 14. Similar to clay nanocomposites, addition of CNTs enhanced the elastic modulus and yield strength but in the meantime drastically reduced the elongation at break. The authors also compared the effect of printing orientation on mechanical and electrical properties of the printed parts. Finally, the nanocomposite samples exhibited lower specific heat and higher thermal conductivity and diffusivity.

Dul et al. [166] conducted a thorough study on properties of ABS/MWCNT nanocomposites and the printed parts. The authors first modified the processing method by direct melt compounding ABS with MWCNTs instead of using masterbatch. A total of six filaments with various CNT loadings (0, 1, 2, 4, 6, and 8 wt%) were produced. Similar results in melt flow behavior as well as mechanical and electrical properties were reported by Dorigato et al. [165]. At 6 wt% CNT loading, the elastic modulus and tensile strength at break of the nanocomposite filament were increased by 20% and 33% when compared to the neat ABS filament. In addition, it was reported that filaments with higher CNT loading possessed less die-swell. The mechanical properties and electrical resistivity of the printed parts are dependent on the printing direction which influences the CNT alignment. The optimum CNT loading was found to be at 6 wt%.

With the goal to develop flexible high strain sensors, TPU/MWCNT nanocomposite filaments were compounded by Christ et al. [160]. A masterbatch with 5 wt% CNT loading was first compounded by twin-screw extrusion after which it was diluted by the second extrusion process to obtain lower concentration samples (1–4 wt%). The printed samples exhibited good interlayer adhesion as shown in Fig. 15. As the CNT loading increases linearly from 1 to 5 wt%, the elastic modulus of both filament and printed coupons increased almost linearly. The electrical conductivity was significantly improved from 1 to 2 wt% and the increase continued to 5 wt %. Both through layer and interlayer conductivity exhibit similar behavior and are very similar to each other (Fig. 16). Cyclic piezoresistivity results show consistent responses. Under cyclic strains of 100%, strain softening, and non-monotonic piezoresistivity behavior were observed on TPU nanocomposite printed parts. Christ et al. also demonstrated that the sensitivity can be tuned by changing CNT loadings.

Hohimer et al. [167] have examined the mechanical properties of TPU/MWCNT printed parts. TPU with 1 and 2 wt% of MWCNTs were twin-screw extruded into filament and printed in two directions. MWCNTs improved modulus but decreased ultimate tensile strength, with a slight decrease in elongation at break. Axial printed samples exhibit higher tensile strength than transverse printed counterparts due to the lack of interfacial adhesion between extruded layers.

Kim et al. [168,180] studied the piezoelectrical properties of poly(vinylidene fluoride) (PVDF) with MWCNT and barium titanate (BT) ceramic nanoparticles for energy harvesting and pressure sensor applications. In this nanocomposite system, PVDF and BT serve as the main components for piezoelectrical properties whereas the MWCNT was added to facilitate the electron as well as stress transfer properties. Adding MWCNT results in higher concentrations of β phase within PVDF which enhances the piezoelectric conversion efficiency. The electrical output can be augmented with increasing amount of MWCNT and BT. The highest piezoelectric coefficient was found to be 129 pC/N at 0.4 wt%-MWCNTs and 18 wt%-BT loading.

The distinct advantage of TPU's high flexibility and CNT's high electrical conductivity allowed Kim et al. [16] to print multiaxial force sensors that can detect forces in three orthogonal axes with TPU/MWCNT nanocomposites. Filament with 4 wt% of MWCNTs were melt compounded for this application and the average electrical resistivity of the filament was $0.143 \pm 0.036 \Omega \cdot m$. By using a

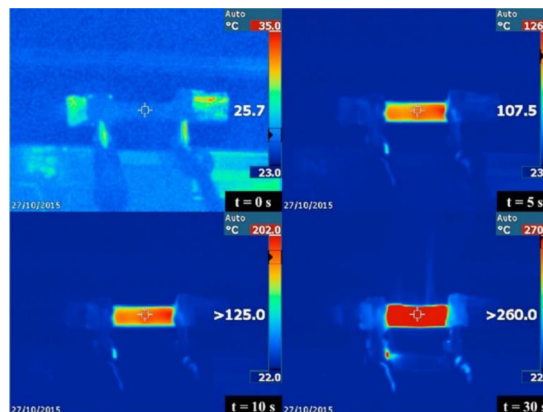


Fig. 14. Infrared thermal imaging of ABS-CNT-06 nanocomposite samples under an applied voltage of 24 V [165]. Copyright 2017, Elsevier.

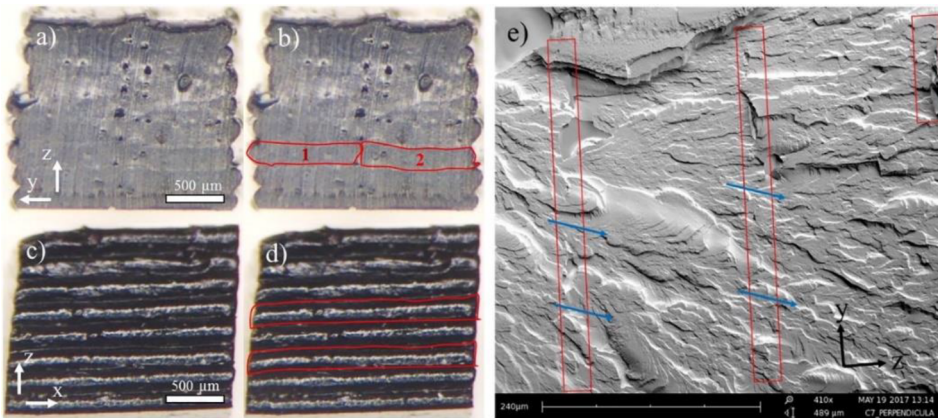


Fig. 15. Structure of TPU/3 wt% MWCNT: (a) cross-section, and (b) cross-section with highlighted extrudate layers in y-direction. The cross section of each layer in 200 μm by 800 μm . (c) Layer profile, and (d) profile with two highlighted extrudate layers. The layers were printed in the x-y plane, along x direction, and stacked along z-axis. (e) SEM micrograph showing y-z view of the interlayer bonds. The red rectangles show the interlayer areas and the blue arrows indicate the regions where the failure flows across the interlayer regions [160]. Copyright 2017, Elsevier. (For interpretation of the references to color in this figure legend, the reader is referred to the web version of this article.)

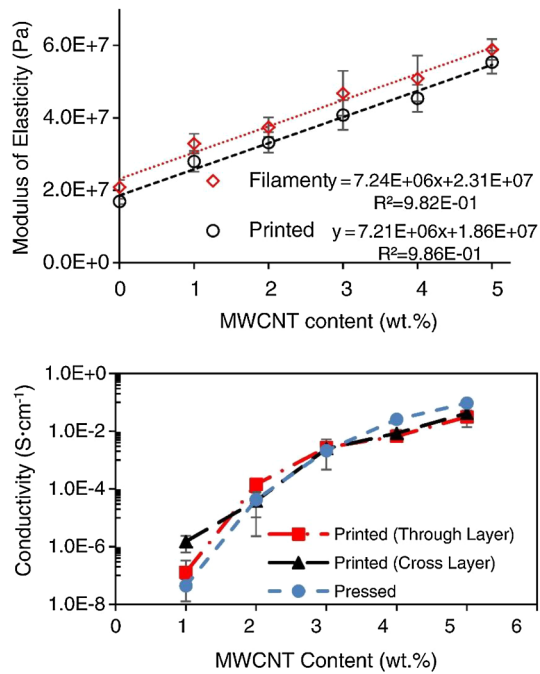


Fig. 16. Elastic modulus and electrical conductivity of the pressed and FDM 3D printed TPU/MWCNT nanocomposites as a function of MWCNT content [160]. Copyright 2017, Elsevier.

dual head printer shown in Fig. 17, the authors were able to print the structural part and the sensing part concurrently which largely simplifies the sensor manufacturing process.

One of the commonly encountered drawbacks of the FFF process is the poor mechanical strength in the vertical Z direction due to the lack of interlayer adhesion [173]. To solve this problem, Sweeney et al. [169] applied electromagnetic radiation to MWCNT nanocomposite coated core-shell PLA filaments. Taking advantage of CNT's local heating properties, the team developed locally induced RF (LIRF) welding to reinforce the FFF printed parts. The LIRF welding facilitates interfacial polymer diffusion for improving mechanical properties (Fig. 18). To optimize the CNT concentration, a loading study was carried out on hot pressed PLA nanocomposite films. PLA nanocomposite films with various CNT loadings from 0.5 to 20 wt% were prepared by solution mixing and casting. Compared to neat PLA printed samples, fracture strength of the LIRF welded nanocomposite with 10 wt% of CNTs increased by 275% (Fig. 19).

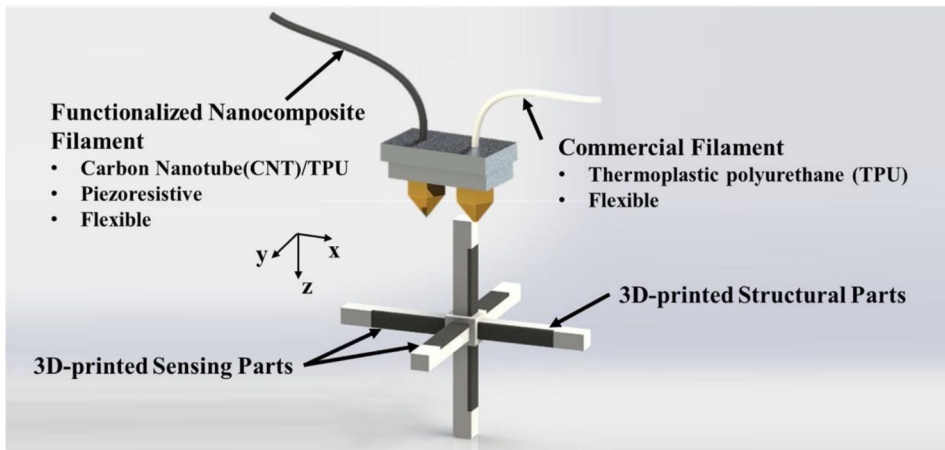


Fig. 17. Schematic of the dual head printer for multiaxial force sensor application [16]. Copyright 2017, Elsevier.

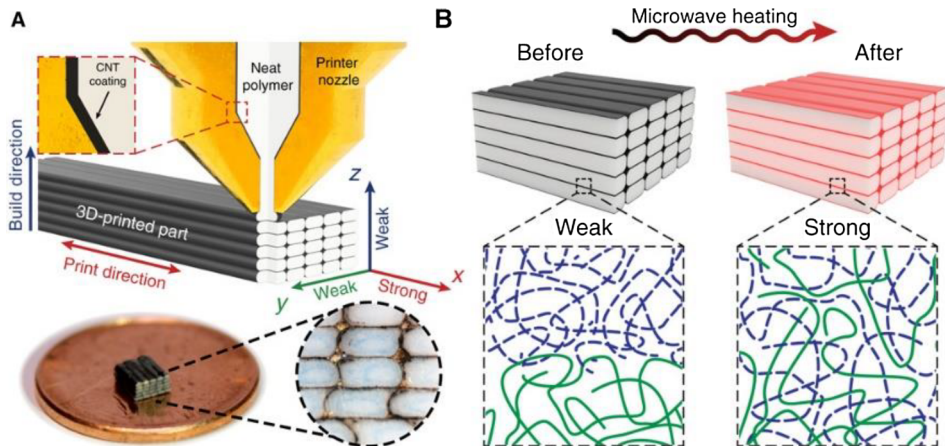


Fig. 18. (A) 3D-printed parts tend to display weak tensile properties in the y and z directions due to poor interlayer welding. To address this, the authors coated thermoplastic filament with a CNT-rich layer; the resulting 3D-printed part contains RF-sensitive nanofillers localized at the interface. (B) When a microwave field is applied, the interface is locally heated to allow for polymer diffusion and increased fracture strength [169]. Copyright 2017, American Association for the Advancement of Science.

4.1.3. Graphene nanocomposites

Graphene nanoplatelets (GnP) are ultra-thin particles consisting of short stacks of graphene sheets. This kind of nanofiller has been used as multifunctional reinforcement, because it possesses 2D graphene stacked structures resulting in superior mechanical, electrical, and thermal properties. Therefore, for thermoplastic nanocomposite filled with graphene nanoplatelets, dramatic enhancement of mechanical properties and thermal stability are reported [170]. To avoid phase separation and aggregation of the graphene platelets, some researchers used graphene oxide (GO) which contains oxygen containing functional groups on the surface.

Using chemically reduced graphene oxide (rGO), Wei et al. [11] were among the first to develop a graphene reinforced ABS composite material for extrusion-based AM (Fig. 20). Compared to neat graphene, the oxygen-containing functional groups on the GO enables better dispersion. ABS and GO were solution mixed as the rGO was obtained by reacting with hydrazine. A loading study on the electrical conductivity indicated that, the conductivity of the ABS/rGO nanocomposite increases from 1.78×10^{-7} S/m to 1.05×10^{-3} S/m as the rGO loading increases from 0.4 to 5.6 wt%.

Zhang et al. [162] fabricated PLA/rGO nanocomposite for flexible circuits applications. The synthesized GO was first chemically reduced followed by thermal reduction at 1050 °C for 1 h in argon. The resulting rGO was melt compounded using twin-screw extrusion followed by filament extrusion using single-screw extrusion. The experimental process is shown in Fig. 21. The electrical conductivity showed a significant increase when the rGO content changed from 4 to 6 wt%. Based on this observation, it was suggested that the percolation threshold is between 4 and 8 wt%. They also found that the electrical conductivity will increase after each melt extrusion process which is believed to be caused by the improvement in rGO alignment. At 6 wt% rGO loading, the electrical conductivity of the printed fibrous nanocomposite filament approached 476 S/m. Various applications were explored using the developed nanocomposite materials (Figs. 22 and 23).

Chen et al. [173] blended flexible TPU with rigid PLA in 7:3 ratio to create a material with robust mechanical properties. Various

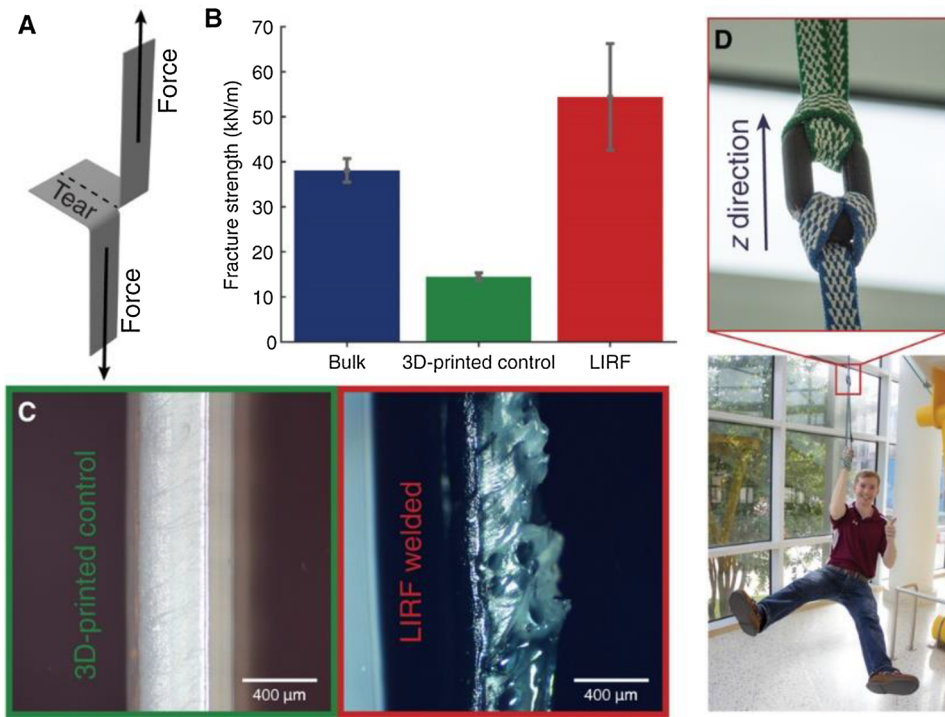


Fig. 19. (A) Tear tests are used to determine that (B) the fracture strength of 3D-printed PLA coupons is increased by 275% when CNT coatings and LIRF welding are applied. (C) Optical micrographs of the fracture surfaces reveal significant necking and crazing in the LIRF-welded sample, whereas the smooth surface of the 3D-printed control sample indicates a brittle fracture. (D) A nanotube-coated, LIRF-welded PLA chain link printed in the z direction is able to support the weight of C.B.S. [169]. Copyright 2017, American Association for the Advancement of Science.



Fig. 20. (a) Picture of graphite flakes. (b and c) Dispersions of GO and ABS in NMP solvent. (d and e) Pictures showing a homogeneous mixture of GO-ABS in NMP before and after chemical reduction by hydrazine hydrate at 95 °C for 1 h. Brownish GO-ABS turned into black G-ABS suspension during chemical reduction. (f) G-ABS coagulations obtained after isolation (e) with water. (g) G-ABS composite powder after washing and drying. (h) Schematic illustration of fused deposition modeling 3D printing process. Inset is the graphene-based filament winding on a roller. The filament was deposited through a nozzle onto a heated building plated, whose temperature was set at 80 °C. (i) A typical 3D printed model using 3.8 wt% G-ABS composite filament, scale bar: 1 cm [11]. Copyright 2015, Springer Nature.

amounts of synthesized GO(0.5, 2, and 5 wt%) was added to the polymer blend to examine compression and tensile properties. From compression test results, anisotropic behavior of the parts printed in different directions was reported. At 0.5 wt% GO loading, elastic modulus and tensile strength of the coupons printed in the V direction (for printing direction, refer to Fig. 26) were improved by 75.5% and 69.2% respectively. In addition, the 0.5 wt% TPU/PLA/GO sample also shows the best biocompatibility to support cell growth as shown in Fig. 24).

Dul et al. [170] produced ABS/graphene nanocomposite filament using non-solvent method by first compounding with an internal mixer followed by twin-screw filament extrusion. Optimization of the graphene concentration was done by examining the tensile and melt flow behavior of compression molded samples with graphene content at 2, 4, and 8 wt% (Fig. 25). As the graphene loading increases, the ultimate tensile strength and the MFI decreases whereas the elastic modulus increases. Dul et al. attribute the

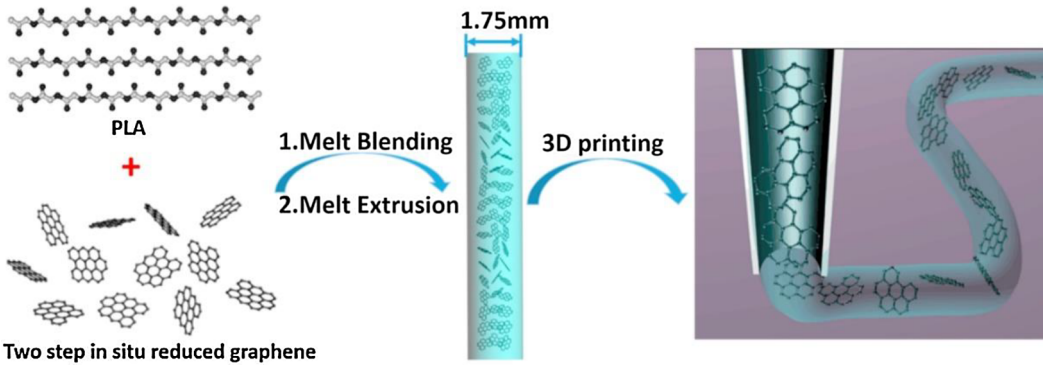


Fig. 21. Schematics depicting the process of graphene-based 3D printing using the technique of FFF [162]. Copyright 2016, Elsevier.

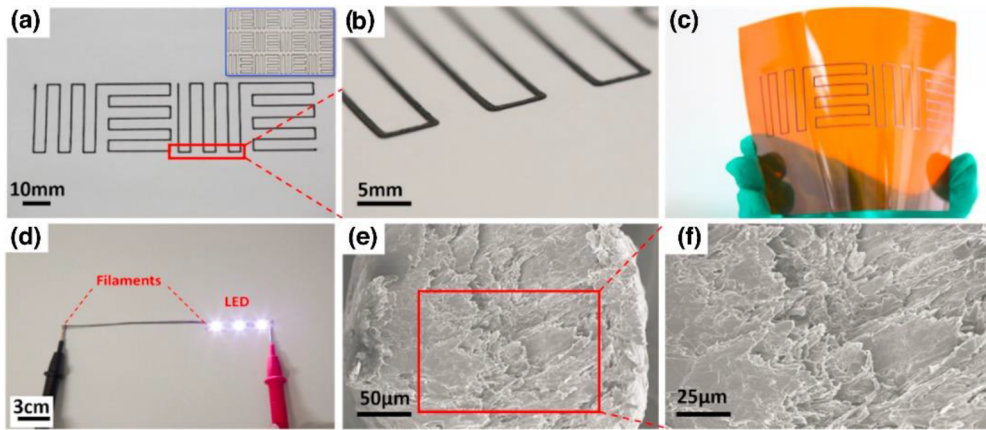


Fig. 22. (a) Two units of 3D printed paper-based flexible circuits pattern and the inset is an A4 paper with twelve units, (b) enlarged drawing of the selected part of (a), (c) 3D printed PI-based flexible circuits pattern, (d) LED circuit with many 3D printed filaments, (e) SEM cross section image of the filament from the 3D printer, and (f) enlarged drawing of the selected part of (e) [162]. Copyright 2016, Elsevier.

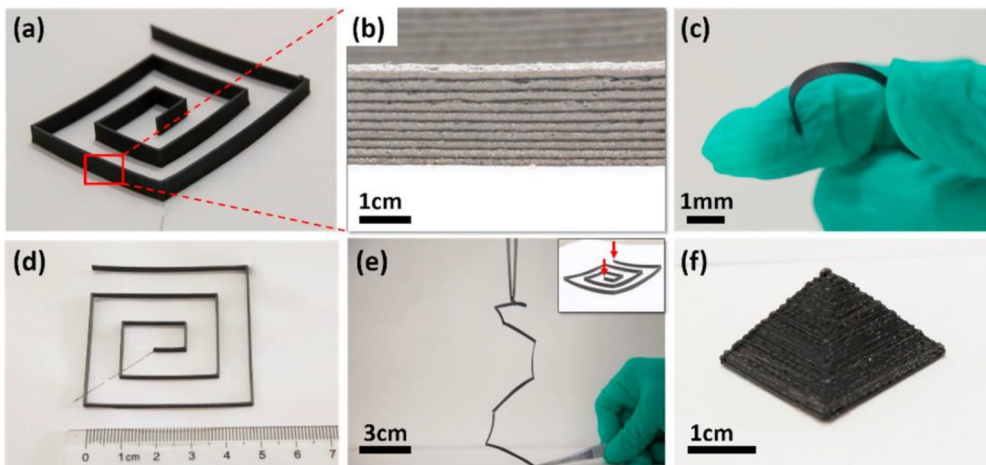


Fig. 23. (a) 3D printed flexible circuits, (b) enlarged drawing of the selected part of (a), (c) the bend of part of the 3D flexible circuits, (d) vertical view picture of the 3D flexible circuits and the measuring ruler, (e) fore and aft stretch (vertical direction) of the 3D flexible circuits, the inset are the schematic drawing for the places of clamps, (d) 3D printed mini pyramid [162]. Copyright 2016, Elsevier.

decrease in tensile strength due to the poor adhesion between graphene and polymer. No characterization on the dispersion of the graphene was performed in this study. The formulation with 4 wt% graphene was chosen for printing based on balance between tensile and rheological properties. Print quality in three different directions were examined by SEM as shown in Fig. 26.

Gnanasekaran et al. [15] selected polybutylene terephthalate (PBT) as the polymer matrix and prepared CNT and graphene

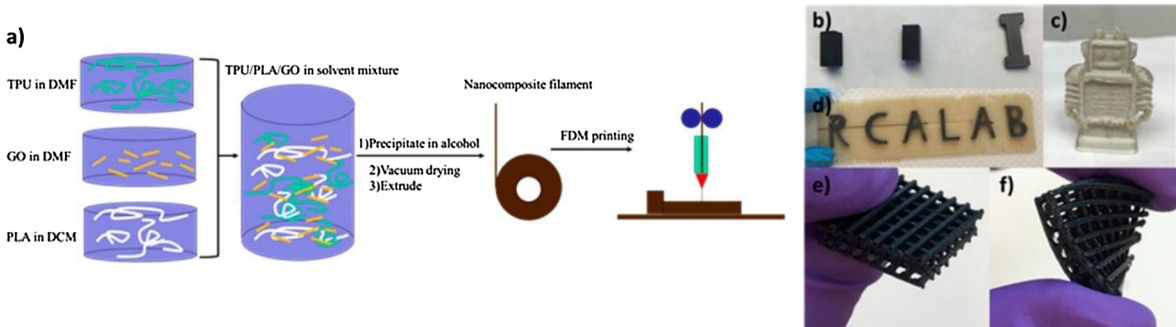


Fig. 24. (a) TPU/PLA/GO nanocomposites filament preparation and FDM printing process. (b–f) Photos of FDM printed TPU/PLA/GO nanocomposites. (b) 3D printed cuboid specimen and dumbbell specimen for mechanical testing (0.5 wt% of GO). (c) 3D printed Ultimaker robot (0 wt% of GO). (d) 3D printed “RCA Lab” (black: 2 wt% of GO; yellow: 0 wt% of GO). (e) 3D printed microlattice (5 wt% of GO). (f) 3D printed microlattice under bending (5 wt% of GO) [173]. Copyright 2016, American Chemical Society. (For interpretation of the references to color in this figure legend, the reader is referred to the web version of this article.)

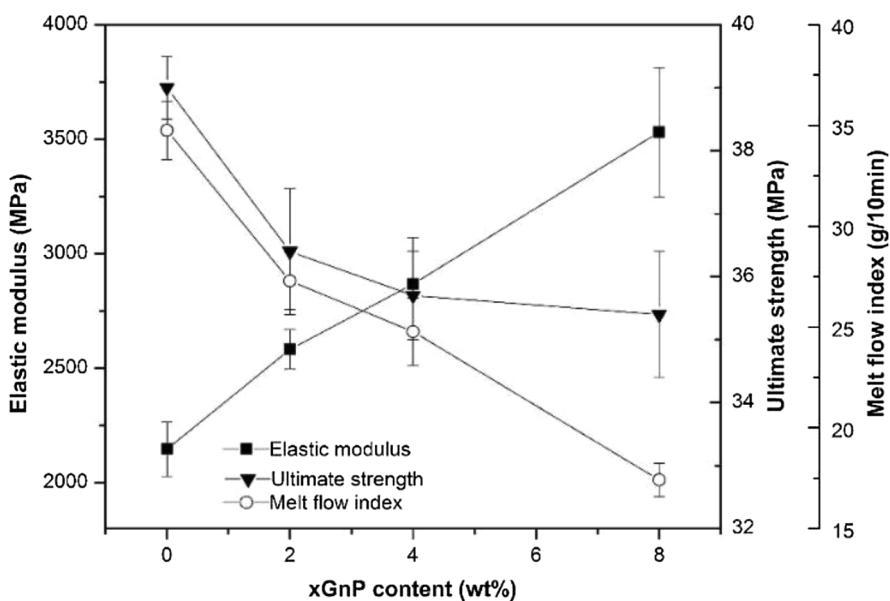


Fig. 25. Tensile modulus, tensile strength, and melt flow index values for compression molded neat ABS and ABS-xGnP nanocomposites [170]. Copyright 2016, Elsevier.

nanocomposites by solution mixing followed by extrusion process. To better preserve the electrical conductivity, non-functionalized CNT and graphene were used. Compared to the CNT nanocomposites, the graphene-based filaments and printed monolayers have rough surface and brittle behavior as shown in Fig. 27. The authors attributed this phenomenon to the void formation caused by the evaporation of moisture from thermally expanded graphene platelets. The calculated percolation threshold for electrical conductivity of PBT was ~0.49 wt% (~0.31 vol%) of CNT and ~5.2 wt% (~3.3 vol%) of graphene, respectively. This correlates well with the experimental results shown in Fig. 28. It was also noted by Gnanasekaran et al. that a significant amount of nozzle wear occurred after prolonged printing of nanocomposites containing abrasive additives, such as CNTs and graphene (Fig. 29).

To integrate the functions of printable materials, some researchers investigated the feasibility of printing functional materials on various substrates instead of printing free standing parts. One of these applications is smart textiles. Compared to conventional smart textile printing methods, direct printing of functional parts using AM would allow significant cost savings by eliminating the excessive use of water and hazardous chemicals with improved productivity.

Sanatgar et al. [181] studied the adhesion properties of FFF printing on textile substrates. Two types of filaments, such as PLA and nylon were used to print on PLA and PA66 substrates. Both printing temperature and printing speed facilitate the important role in determining the bond strength. The 5 wt% carbon black filled PLA (PLA/CB) filament show lower break strength than the 2 wt% CNT filled nanocomposite filament which had the same electrical conductivity as the PLA/CB.

Yamamoto et al. [178] reported enhanced mechanical properties of ABS at very low loadings of graphene oxide (0.02, 0.04, and 0.06 wt%). To ensure proper GO dispersion, solution mixing and sonication was performed prior to filament extrusion. The solution mixing process resulted in a reduction in elongation at break and toughness, but the strength and stiffness were improved unlike

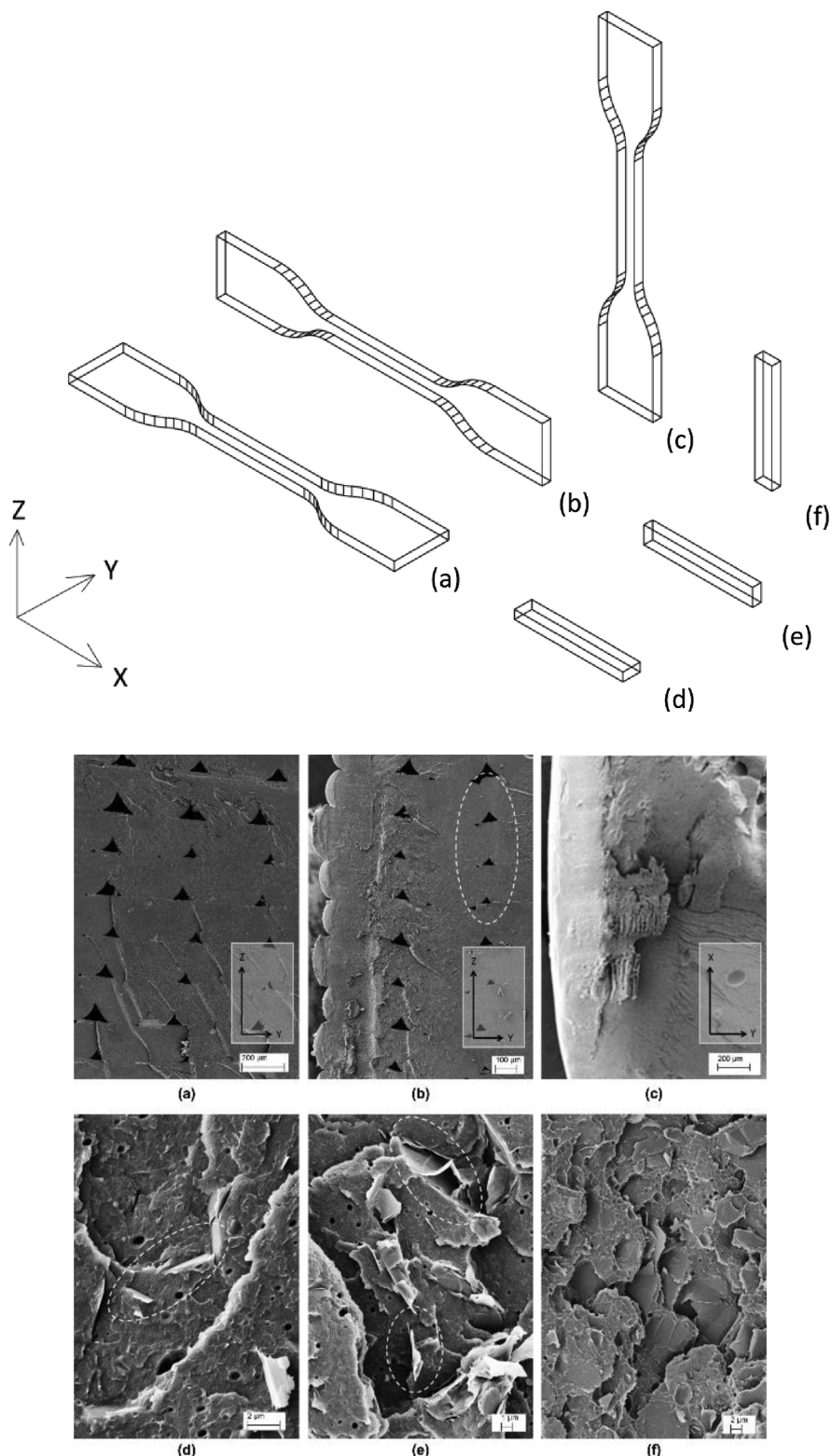


Fig. 26. SEM micrographs of 3D-printed dumbbell specimens printed from neat ABS, H (a), V (b), and P (c); and from graphene nanocomposites, 4-H (d), 4-V (e) and 4-P (f) [170]. Copyright 2016, Elsevier.

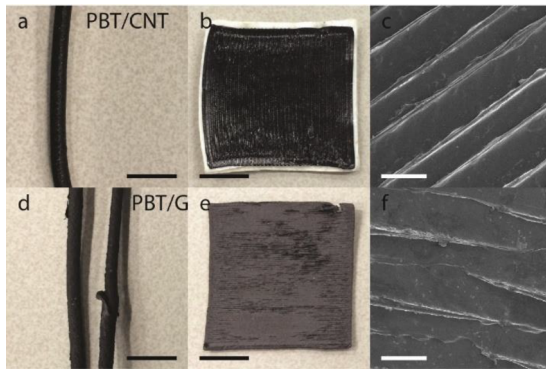


Fig. 27. (a) Extruded PBT/CNT composite filament. (b) 3D printed monolayer of PBT/CNT composite. (c) SEM image of the PBT/CNT monolayer illustrating the ridges. (d) Extruded PBT/G composite filament. (e) 3D printed monolayer of PBT/G composite. (f) SEM image of the PBT/G monolayer illustrating the ridges. Black scale bars are 1 cm and white scale bars are 500 nm [15]. Copyright 2017, Elsevier.

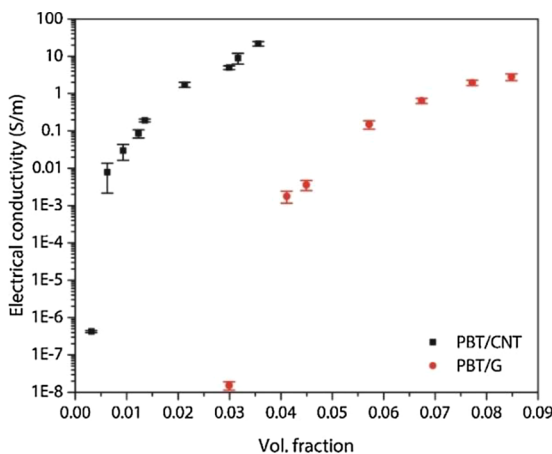


Fig. 28. Electrical conductivity plotted as a function of CNT and graphene volume fraction for 3D printed polymer nanocomposites. Note that the electrical conductivity of pure PBT is $\sim 1 \times 10^{-15}$ S/cm and of the pure CNT/graphene is $\sim 1 \times 10^5$ S/cm [15]. Copyright 2017, Elsevier.

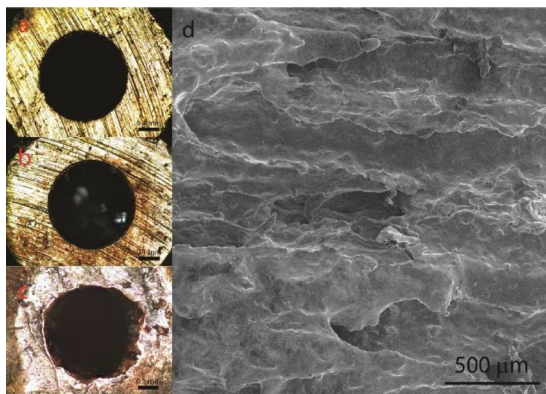


Fig. 29. Optical micrographs showing the surface of a 3D printing nozzle before and after printing. (a) Unused nozzle. (b) Nozzle after printing ~ 10 cm of PBT/G. (c) Nozzle after printing ~ 1.5 m of PBT/CNT. (d) SEM image of PBT/G composite printed with an abraded nozzle [15]. Copyright 2017, Elsevier.

many other reported results. Although all printed samples exhibit brittle failure, the increase in GO content led to increase in ductility and toughness. The increase in fracture toughness was explained by interfacial covalent bonding and the “microcrack mechanism” where more energy is needed to initiate and propagate the microcracks through the GO reinforced polymer matrix. When printed in the P direction (Fig. 26), samples with 0.06 wt% GO exhibit 29% improvement in elongation at break and 55% improvement in toughness.

Zhu et al. [174] studied thermal and mechanical properties of printable polyamide 12 (PA12)/graphene nanocomposites. Zhu et al. indicated that the GNP agglomerates are hard to avoid at the selected loading levels (2, 4, 6, 8, and 10 wt%) and result in deficient mechanical properties. Due to restricted chain mobility, the nanocomposite samples also exhibit lower crystallinity and better thermal stability than the neat PA12. The optimal GNP concentration of 6 wt% was selected for printing parts based on thermal, tensile, and processability results. With the optimal GNP loading, the compression molded nanocomposite sample shows 43.4% improvement in elastic modulus and a factor of 3.4 increase in thermal conductivity (λ) (Fig. 30). Because of the preferential alignment of the GNP platelets, the λ of AM produced samples printed parallel to the through plane direction (Type B in Fig. 31) is 51.4% greater than the compression molded counterparts and 2.6 times higher than the ones printed perpendicular to the through plane direction (Type A in Fig. 31). Tensile properties of parts printed in three different raster angles were also compared. Moreover, the high melt viscosity of the nanocomposites reduced the coalescence rate during printing which explains the higher degree of anisotropy of the printed nanocomposite parts.

4.1.4. Other novel AM materials for FFF

Gantenbein et al. [14] recently examined aromatic thermotropic polyester liquid crystal polymers (LCP) for improved mechanical performances. During the printing process, the nematic domains are aligned with one another creating the hierarchical structure by shear and extensional flow field (Fig. 32). Upon cooling, core-shell structure was generated due to the difference in cooling rate. The printed filament surface cools more rapidly which locks in the alignment in nematic domains whereas the interior experienced slower cooling thus allows for the re-orientation of the nematic domains. Gantenbein et al. found that decreasing nozzle diameter, layer height as well as printing temperature leads to increase in Young's modulus and ultimate tensile strength. In addition, the printed layers of the LCP can be further crosslinked by annealing.

Wang et al. [183] developed FFF printable foam materials using thermally expandable microspheres in low melt temperature "polywax" to reduce the porosity and improve the mechanical properties of printed parts. With 2 wt% of the microspheres, heat treatment increased the tensile and compressive strength by 25.4% and 52.2%, respectively. However, the low foaming temperature of the microsphere at 120 °C limits its application in more commonly used polymers, such as ABS and PLA which require extrusion temperature above 190 °C.

To mitigate the problem in mechanical anisotropy, an extensive study on print quality and fracture behavior of six types of ABS composite and four types of ABS polymer blends (Table 7) were examined by Torrado et al. [37]. Anisotropy was studied by comparing tensile properties of parts printed in two different directions shown in Fig. 33. While no samples show improvement in Ultimate Tensile Strength (UTS), the binary blend with 20 wt% of SEBS elastomer significantly improved ductility in XYZ direction and the ternary blend containing 25 wt% SEBS and 10 wt% UHMWPE exhibit lowest level of anisotropy in UTS.

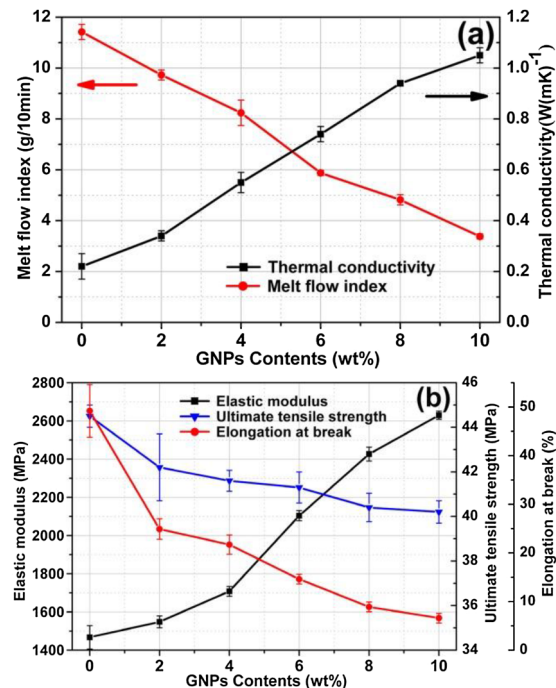


Fig. 30. (a) The MFI values, thermal conductivity (λ), and (b) tensile test results of pure PA12 and PA12/GNPs nanocomposites and its CM specimens, respectively [174]. Copyright 2017, John Wiley & Sons.

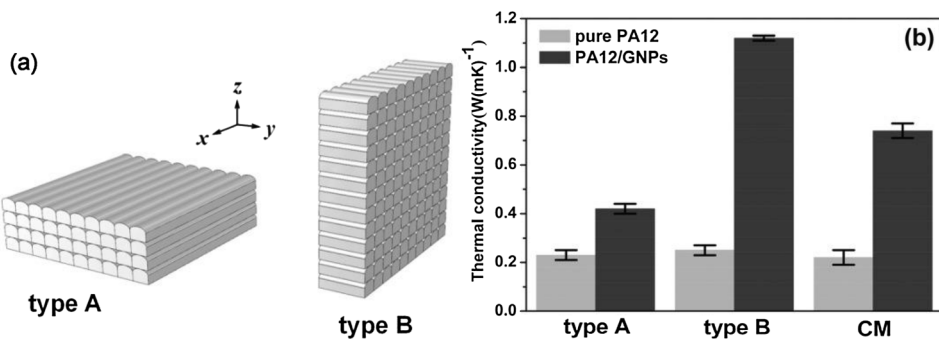


Fig. 31. (a) Schematic illustration of three-dimensional printed LFA specimens ($10\text{ mm} \times 10\text{ mm} \times 1.5\text{ mm}$, type A: printing direction perpendicular to through-plane direction, type B: printing direction parallel to through-plane direction); (b) thermal conductivity (λ) of PA12 and PA12/GNPs as measured on type A, type B, and compression molded specimens [174]. Copyright 2017, John Wiley & Sons.

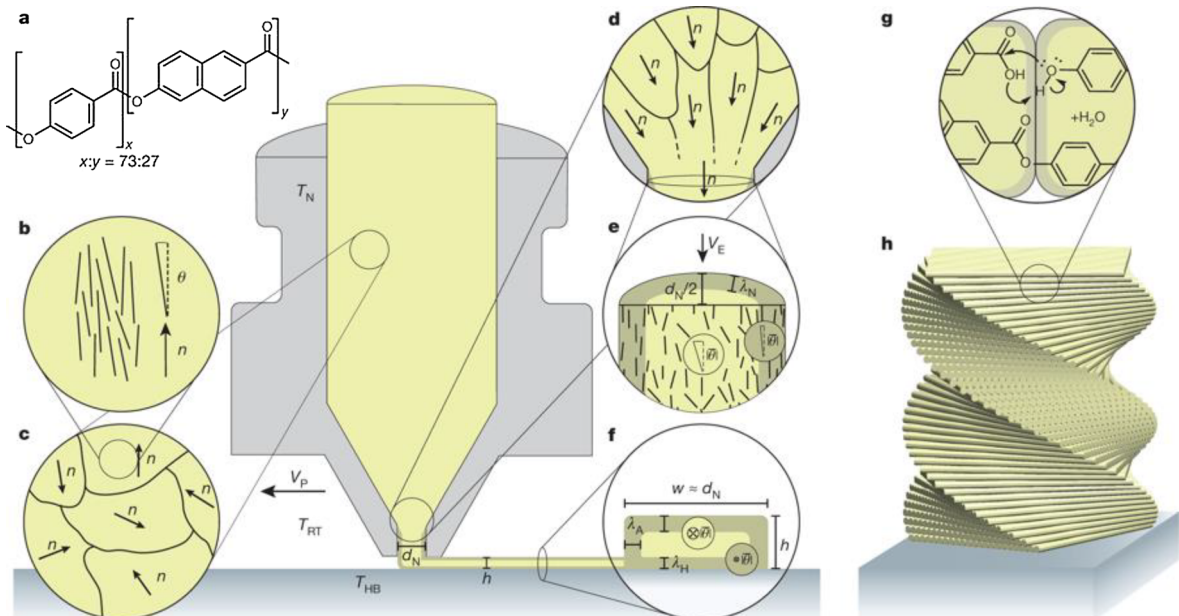


Fig. 32. Printing hierarchical, thermotropic LCPs using fused deposition modeling [14]. Copyright 2018, Springer Nature.(This schematic may not be accurate representation of the actual kinematics of flow as this area is still under active investigation [182].)

Table 7
Material formulations studied in [37].

ABS (wt%)	Additive (wt%)
<i>ABS matrix composites</i>	
100	-
95	JUTE
98	MAYACROM® Blue
95	TiO ₂
98	ZnO
95	SrTiO ₃
95	Al ₂ O ₃
<i>ABS blends (weight ratio)</i>	
ABS:SEBS	
95:05	
80:20	
ABS:UHMWPE:SEBS	
75:25:10	
90:10:10	

Table 8
Summary of reviewed materials for FFF.

Polymer type	Type of nanofillers	Surface functionalization	Concentration	Mixing method	Filament structure	Printer used	Enhancement in properties	Ref.
ABS	MMT	HDBAC	1, 3, and 5 wt%	Homogeneous	Creator, Flashforge	Tensile strength, elastic modulus, Flexural strength and modulus, Thermal stability, T_g , linear thermal expansion ratio	[157]	
ABS	MMT	surfactant unspecified	3 wt%	Core-shell nanocomposite shell with neat ABS core.	Creator Pro, Flashforge	Relative permittivity, loss tangent, tensile modulus, hardness	[159]	
PLA	MMT	MT2EtOH (Cloisite® 30B)	4 wt%	Homogeneous	Sharebot NG (Sharebot S.r.l., Italy)	Crystallinity, storage modulus, elastic modulus, Thermal stability	[158]	
ABS	Carbon nanofiber		10 wt%	Homogeneous	Stratasys FDM 1600 Modeler	Electrical conductivity, elastic modulus and yield strength, thermal conductivity and diffusivity	[164]	
ABS	MWCNTs,	Non	6 wt%	Homogeneous	Sharebot Next Generation	Elastic modulus	[165]	
ABS	MWCNTs		1, 2, 4, 6, and 8 wt%.	Homogeneous	Sharebot HT Next Generation	Electrical conductivity	[166]	
TPU	MWCNT		1 and 2 wt%	Homogeneous	Custom made	Elastic modulus	[167]	
TPU	MWCNT		4 wt%	Homogeneous	Unspecified commercial dual head printer Lulzbot® Taz 5	Electrical conductivity	[16]	
PVDF	MWCNT and barium titanate (BT) nanoparticles	MWCNT (0–0.4 wt %) BT(0–18 wt%)	Homogeneous				[168,180]	
ABS	MMT	Non	1 wt%	Homogeneous	SI-B, Guoguang Instruments Co., Ltd., China	Tensile strength, flexural strength and modulus, Vicat softening temperatures, T_g	[156]	
ABS	MWCNT	Non	1 wt%	Homogeneous	SI-B, Guoguang Instruments Co., Ltd., China	Tensile strength, flexural strength and modulus, Vicat softening temperatures, T_g	[156]	
ABS	CaCO ₃	Non	1 wt%	Homogeneous	SI-B, Guoguang Instruments Co., Ltd., China	Tensile strength, flexural strength and modulus, Elongation at break, Mechanical anisotropy, Vicat softening temperatures, T_g	[156]	
ABS	SiO ₂	Non	1 wt%	Homogeneous	SI-B, Guoguang Instruments Co., Ltd., China	Tensile strength, flexural strength and modulus, Vicat softening temperatures, T_g	[156]	
PBT	MWCNT	Non	0.6–3 vol%	Homogeneous	Ultimaker 2	Electrical conductivity	[15]	
PBT	graphene	Non	4–6 vol%	Homogeneous	Ultimaker 2	Electrical conductivity	[15]	
Polypropylene	Carbon black	N/A	~15–~30 wt%	Homogeneous	Makerbot Dual and Flashforge Creator	Electrical conductivity	[161]	
PLA			2, 4, 6, and 8 wt%	Homogeneous			[162]	

(continued on next page)

Table 8 (continued)

Polymer type	Type of nanofillers	Surface functionalization	Concentration	Mixing method	Filament structure	Printer used	Enhancement in properties	Ref.
TPU	reduced graphene oxide (r-GO)	chemical reduced by 4-iodoaniline; thermally reduced at 1050°C in Ar	1–5 wt%	Homogeneous	Core-shell nanocomposite shell with neat PLA core.	MakerBot Replicator 2, MakerBot Industries, LLC, Brooklyn, New York	Electrical conductivity, tensile strength, elastic modulus	[160]
	MWCNT	Non	0.5–20 wt%				Electrical conductivity	
PLA	MWCNT	Non	0.5–20 wt%	Homogeneous	Interlayer fracture strength, electrical conductivity	MakerBot Replicator 2×, MakerBot Industries, LLC, Brooklyn, New York	[169]	
	Graphene	Non	2, 4 and 8 wt%					
ABS	Reduced graphene oxide (rGO)	hydrazine hydrate	0.4, 0.8, 1.6, 2.3, 3.8, 5.6, and 7.4 wt %	Homogeneous	Elastic modulus, thermal and creep stability	Sharebot Next Generation (Sharebot NG, Italy)	Electrical conductivity, T_g	[170]
	Graphene oxide	Non	0.5, 2, 5 wt%				Electrical conductivity, T_g	
TPU/PLA blend (7:3)	Graphene oxide	Non	0.02, 0.04, and 0.06 wt%	Solution mixing	Homogeneous	Baoyan Automation Co., LTD, China	Elastic modulus yield tensile strength, thermal stability	[173]
	Graphene oxide	Non	2, 4, 6, 8, and 10 wt %				Elastic modulus, thermal stability, thermal conductivity	
PA12	Graphene	Non	2, 4, 6, 8, and 10 wt %	Twin screw extrusion	Homogeneous	HUEWAY 3D-304, Shenzhen Hueway Technology Co., Ltd. China	[174]	

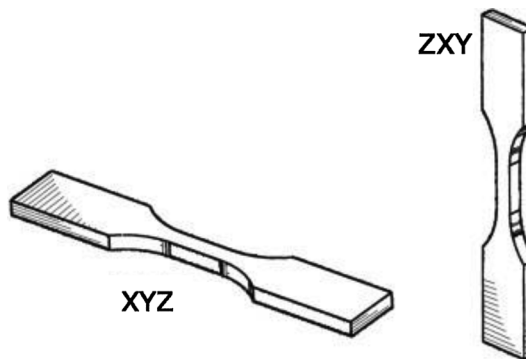


Fig. 33. Representation of XYZ and ZXY printing directions and actual raster orientations after printing (hash marks) [37]. Copyright 2015, Elsevier.

4.2. Polymer nanocomposite materials for SLS

SLS possesses the capability to produce multi-layer nanocomposites because of the layer-by-layer fabrication method with highly localized heating. SLS-processed parts normally exhibit enhanced mechanical properties with smaller particle size of processing powder [65]. A recent review by Yuan et al. [184] provides a comprehensive summary of powder preparation methods and the applications for powder-based AM systems. With the introduction of nanoparticles, physical and mechanical properties of the parts can be further tailored to be used for specific applications. Extensive studies have been conducted on the creation of various nanomaterial-incorporated polymers for the development of new materials due to the unique mechanical, electrical, and thermal properties of nanomaterials. Commonly used nanomaterials in SLS process include MWCNT, carbon nanofiber, Al₂O₃ nanoparticles, silica nanoparticles, clay nanoparticles, Cu nanoparticles, Ag nanoparticles, and TiO₂ nanoparticles. Table 9 lists the property improvement of various polymer nanocomposites with addition of nanomaterials.

Numerous research studies have been conducted by incorporating carbon nanomaterials, including nanoparticles and nanofibers into SLS-compatible polymers. Athreya et al. proposed carbon black-filled electrically conductive nylon 12 nanocomposite produced with SLS process, which showed slightly reduced flexural modulus possibly due to the weak polymer-filler interface bonding. However, five orders of magnitude of improvement in electrical conductivity with lower percolation threshold was also observed. SLS-processed PA12/MWCNTs nanocomposite showed improvement in tensile strength by 10% with a reduction in elongation by up to 11% compared to PA12 [186,187]. Goodridge et al. studied the incorporation of carbon nanofibers into PA12, which showed 22% increase in the storage modulus compared to the original material. However, the production of powder with suitable size and morphology for SLS process still presents a challenge [188]. Extensive studies have been reported by Koo et al. on the incorporation of MMT nanoclay, CNF, and MWCNTs on PA11 and PA12 for SLS process, which showed enhanced properties in thermal stability, flame retardancy, strength, toughness, modulus, and elongation. Fig. 34 shows the SLS-process 3D parts with full density and complex geometry made from CNF-based PA11 polymer [190]. Reduced flammability properties, namely heat release rate, carbon monoxide emission, and smoke extinction were observed with the addition of nanoclays and carbon nanofibers [189,190,195,196].

Metal oxide-based polymer nanocomposites are also shown to be suitable for the SLS process. Material solidification and mechanical properties can be improved with increasing nanomaterial content. Nano Al₂O₃ polyamide composites processed by SLS showed a nearly linear increase of tensile strength with increasing nano-filler content [191]. Polystyrene-coated Al₂O₃ nanoparticles processed via SLS exhibited a dense structure with 300% increase in tensile strength and 50% increase in notched impact strength [192]. Kim et al. compared the mechanical properties for SLS-processed specimens made of neat PA12, PA12/TiO₂, and PA12/functionalized graphite nanoplatelet where the nanocomposite polymers showed improved ultimate strength and tensile modulus with some decrease in ductility. Stress-strain curves of different PA12 nanocomposites are compared in Fig. 35 [193]. Nanosilica/PA12 composite powder processed by SLS showed enhancement in mechanical and thermal properties, including higher thermal stability, tensile strength (by 20.9%), tensile modulus (by 39.4%), and impact strength (by 9.54%) with decreased elongation at break (by 3.65%). Heterogeneous nucleation effect of nanosilica on PA12 was also observed [194].

Table 9
Properties improvement of SLS-processed polymer nanocomposites.

Nanomaterials	Properties Improvement	Ref.
Carbon black/PA12	Enhanced electrical conductivity with lower percolation threshold	[185]
MWCNT/PA12	Improved tensile strength with reduced elongation at break	[186]
CNF/PA11&PA12	Improved storage modulus, tensile yield strength, and flammability properties	[187–190]
Nanoclay/PA12	Improved modulus with reduced elongation at break, and improved flammability properties	[190]
Al ₂ O ₃ /Polyamide	Improved tensile strength with reduced elongation at break	[191]
Al ₂ O ₃ /Polystyrene	Improved tensile strength and notched impact strength	[192]
TiO ₂ /PA12	Improved ultimate strength and tensile modulus with reduced elongation at break	[193]
Nanosilica/PA12	Improved tensile strength, tensile modulus, impact strength, and thermal stability	[194]



Fig. 34. SLS parts made from CNF-based PA11 polymers [190].

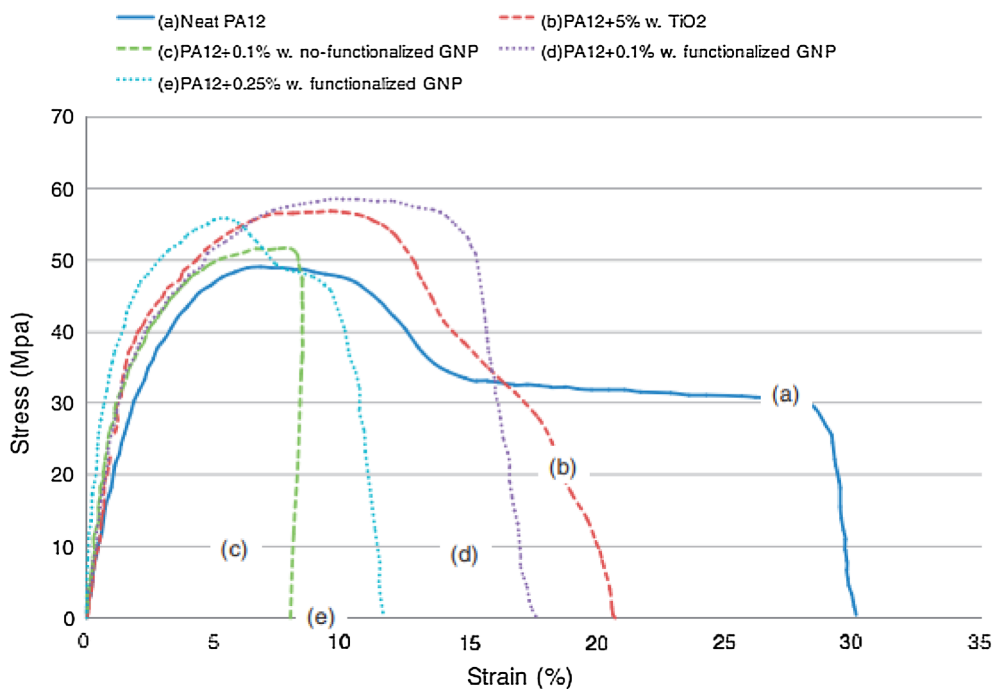


Fig. 35. Stress-strain curves of PA12 nanocomposites [193]. Copyright 2013, SAGE Publications.

SLS of nanoparticles on polymer substrate has generated considerable interest for electronics applications due to the low annealing temperature, fast processing speed with significant oxidation suppression even in air environment. These novel SLS processes enable a low temperature, environmentally friendly, and cost-effective manufacturing of flexible electronics on polymer substrates. Fig. 36 shows the schematics of the SLS of metal nanoparticles on a plastic substrate. The nanoparticles are initially deposited on the plastic substrate by spin coating or inkjet printing. This thin layer is selectively sintered by focused laser beam, and then, the non-sintered nanoparticles are removed by organic solvent. The result is a patterned metal structure on the substrate [197]. Ming et al. reported SLS of TiO₂ nanoparticles film on plastic conductive substrates for the production of high-efficiency flexible solar cells. The SLS-processed films showed significant improvement in short-circuit current density, fill factor, and solar conversion efficiency (4.5–5.7%). The films also showed a great potential to be integrated into roll-to-roll manufacturing processes [198]. Low-temperature SLS of Cu nanoparticles on a polymer substrate was achieved by Kwon et al. for the production of flexible touch panel applications. The laser sintered Cu films demonstrated excellent electrical properties with reduced oxidation compared to conventional thermal heating process. It also ensures the compatibility of Cu nanoparticle films with plastic substrate for Cu-based flexible electronics applications [199,200]. Different laser sources were investigated by Theodorakos et al. to achieve the SLS of Ag nanoparticles for flexible electronics applications [201].

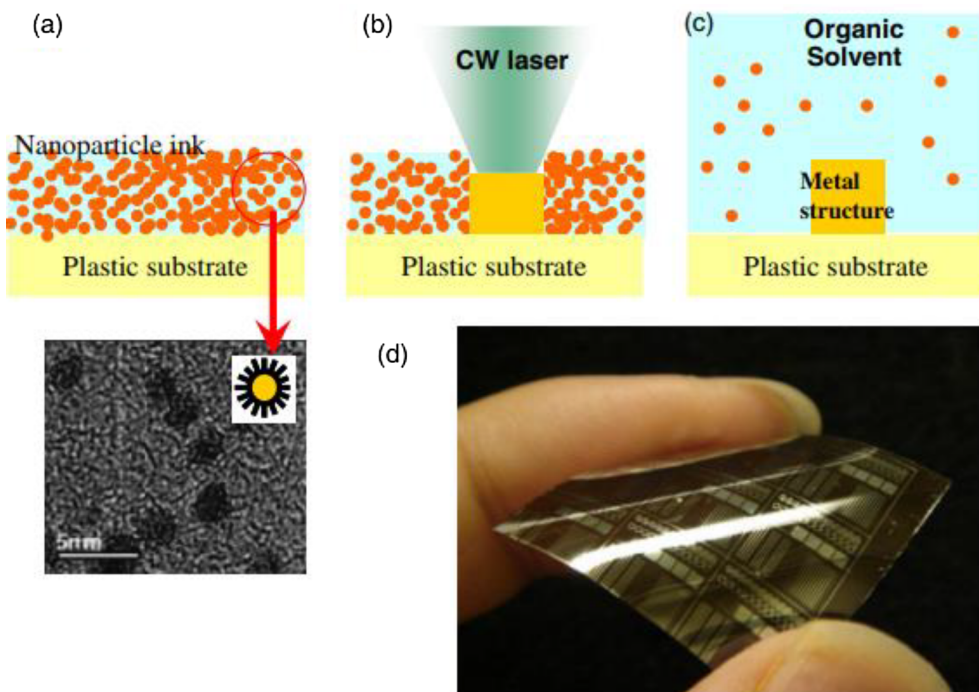


Fig. 36. Schematics of the SLS of metal nanoparticles on the plastic substrate [197]. Copyright 2010, The Japan Society of Applied Physics.

4.3. Polymer nanocomposite materials for SLA

Nanocomposite resins offer potential for improved properties such as thermal, mechanical, conductivity, magnetism, biocompatibility, and processing [82]. The introduction of nanomaterials into resin systems for 3D printing can be complicated by many factors. An important detail for printable resin is its viscosity. Small amounts of additives can have a large impact on resin viscosity, if the viscosity is too high the resin can become difficult to work with and require increased cure times. Dispersion is often another challenge. Many nanomaterials can prove incompatible with resins even at small loadings. It is often effective to treat nanomaterials to add surface functionalization to the particles. While surface functionalization can be used to improve dispersion, the method of mixing also has a large impact. Nanocomposite resins are primarily mixed mechanically through sheer mixing, sonication, or a combination of the two. Another complication that can occur is caused by the absorption of UV radiation by some nanomaterials. Higher loadings of these nanomaterials can result in decreased resin cure speed. Using lower loadings of nanomaterials can be a solution to high viscosity, poor dispersion, and UV absorption. Table 10 surveys nanocomposite photoresin research and is discussed in the following sections.

4.3.1. Clay nanocomposite resins

The addition of clay nanomaterials in photopolymer resins has both improved resin reactivity and improved its mechanical properties [212,213]. Corcione et al. studied the compatibility and effect on reactivity of organically modified Dellite 43B montmorillonite clay with UV 6105 photoresin [212]. The nanoresins reactivity to UV curing was measured using Photo Differential Scanning Calorimetry (pDSC). The pDSC data shown in Fig. 37 demonstrates an improved reactivity of 15% with the addition of 0.3 wt% clay. Higher loadings of the nanoclay, 1.0 wt%, showed the reversal of this trend with a decrease in reactivity of over 60%. At lower loadings the clay may act as a diffusion-aid for photopolymerization leading to an increase in cure rate whereas at higher loadings the nanoclay begins to interfere with the photopolymerization process [212]. It is possible that the higher loadings result in decreased dispersion with larger aggregates of nanoclays. These intercalated clumps of nanoclays could interfere with UV absorption by the photoinitiators and result in a decreased cure rate. This effect of decreased cure rate was noted by Weng et al. whom demonstrated that a loading of 10 wt% of montmorillonite and attapulgite nanoclays increased the gel phase of the photopolymerization process.

Weng et al., investigated montmorillonite and attapulgite nanoclay photoresin composites [213]. The results of the study, summarized in Table 11, demonstrated an improvement in elastic modulus with both types of clay, with the montmorillonite also showing improved tensile strength, especially at lower loadings. Both types of clay were however outperformed by nano silica, which maintained elongation at break while improving modulus and tensile strength.

4.3.2. CNT nanocomposite resins

Carbon nanotubes (CNTs) are an extensively studied material in the field of material science and polymer composite development.

Table 10
Properties improvements for SLA-processed nanocomposites.

Base resin	Photoinitiator	Nanofiller	Surface functionalization	Concentration (wt %)	Printer used	Enhancement in properties	Ref.
Acrylate mixture	Irgacure 784 (T784)	Silica dioxide	Vinyl	9, 7, 17, and 30	Perfactory Multilets	Modulus, shrinkage reduction, more accurate prints, reduced EASO, light transmittance not reduced in silica concentration up to 17 wt%	[202]
Acrylate mixture	T184	Zirconia oxide	Vinyl	≤30	–	Increased conversion rate	[203]
Acrylic epoxy-acrylate mixture	T784	Magnetic Cellulose nanocrystals	–	25	Custom MSL	Greatly enhanced storage modulus	[204]
PIC100	TMPO	Hydroxyl	–	1–5	3D Systems VIPER si	Improved tensile and elongation	[205]
Acrylic ester	–	Single layer graphene oxide	–	0.2	MSL	Improved reflection loss and absorption	[206]
Acrylate mixture	–	MWNT	–	0.5–1.5	Micraft digital light processing-based SLA	–	[207]
Acrylate mixture	T784	Silica dioxide	–	0.5–1	–	Improved tensile, hardness, dimensional stability, degradation temperature, manufacture time	[208]
Acrylic	Tianjin Jiuri 369 and isopropyl thioanthonone (ITX)	Silica dioxide	KH570	0.3, 0.7	–	Increased Tg, improved tensile and impact strength, improved flexural modulus	[209]
Methacrylate	Lucirin TPO	Hydroxyapatite	–	20, 40	SLA technique	Flexibility maintained, improved compressive elastic modulus	[210]
Formlabs-Grey Resin	–	Graphene oxide	–	0.1, 0.5, 1.0	Not specified	Improved tensile strength and modulus, improved thermal stability	[211]
UV 6105	UVI 6976	Clay	–	0–1.0	SLA 250–50	Potential for dual curing mechanism using cationic and radical, improved reactivity	[212]
Acrylate mixture	TPO	Silicon dioxide	Alkene	1, 3, 5, 10	Homemade 405 nm SLA	Improved tensile and modulus strength, increased curing speed	[213]
Acrylate mixture	TPO	Clay	Alkene	1, 3, 5, 10	Homemade 405 nm SLA	Improved modulus strength, decreased curing speed	[213]
Acrylate mixture	TPO	Attapulgite	Alkene	1, 3, 5, 10	Homemade 405 nm SLA	Improved modulus strength, decreased curing speed	[213]
Acrylate mixture	BAPO	MWNT	–	0.1, 0.3, 0.5	Freeform Pico Plus 49	Improved modulus and conductivity	[214]
Methacrylate	–	Cellulose nanocrystals	lignin	0.1, 0.5, 1	Form 1 +	Improved modulus and tensile strength, improved thermal stability	[215]
FLGPCL02	–	Boron nitride nanoplates	–	0.5, 1	Form 1 +	Enhanced damping properties	[216]

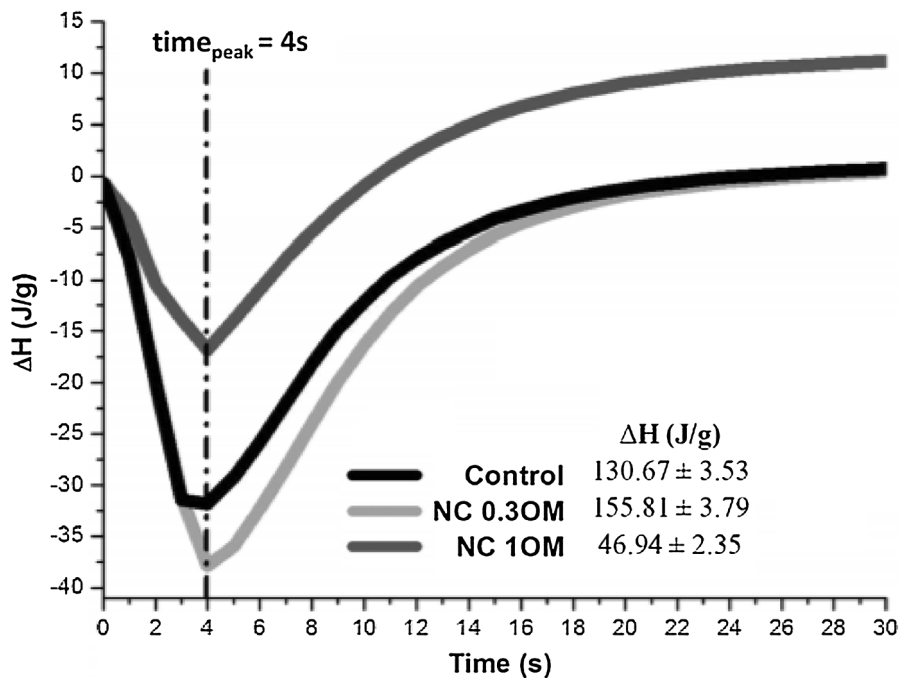


Fig. 37. pDSC showing nanoclays impact on resin reactivity [212]. Copyright 2014, John Wiley & Sons.

Table 11

Mechanical properties of various nano resin composites (table reproduced from [213]).

Samples	Tensile strength (MPa)	Elastic modulus (GPa)	Elongation at break (%)
Control	44.7	1.7	5.1
SiO_2 1% w/w	46.1	1.7	5.1
SiO_2 3% w/w	50.0	2.0	4.2
SiO_2 5% w/w	54.0	2.7	2.6
OMMT 1% w/w	47.2	2.1	4.4
OMMT 3% w/w	44.4	2.4	2.3
OMMT 5% w/w	46.7	2.8	1.9
ATP 1% w/w	40.8	2.0	2.6
ATP 3% w/w	38.4	2.2	2.1
ATP 5% w/w	36.6	2.4	1.7

CNTs are cylindrical nanomaterials with a large surface area, and high aspect ratio. They are known for their exceptional thermal, mechanical, and electrical properties.

Zhang et al. studied the effects of CNT on photoresin composites for the purpose of 3D printable radar absorbing materials [207]. CNTs utilize polarization at interfaces and multiple scattering as a primary electromagnetic wave absorbing mechanism allowing them to be potential candidates for radar absorption [207]. They studied acrylic ester photopolymer nanocomposites with the 0.5, 1.0, and 1.5 wt% of CNTs. The study examined the effect of CNTs on printability, microwave absorption, and electromagnetic parameters [207]. SEM microimaging was used to check CNT dispersion within the resin. As expected, the higher loadings had poorer dispersion with more frequent aggregate formations. It was also found that higher concentrations of CNT decreased UV transmission depth through the resin, probably a direct result of the CNTs absorptive properties. Fig. 38 shows the results of free space time domain reflectivity analysis for the CNT composites.

Measurements at three different frequencies and with three different print thicknesses were taken. The composites reflectivity generally decreased with increased thickness and CNT loadings. The highest thickness, 9 mm, performed worse than the 6 mm at the highest frequency of 12–16 GHz. The highest recorded absorption was about 16 dB for the 9 mm composite with 1.5 wt% CNT [207]. The radar absorbing potential of CNTs are promising but also limited to the CNTs dispersion in the resin system with improved dispersion allowing for better printability and higher loadings.

Gonzalez et al. studied the effect of CNTs on electrical and mechanical properties with PEGDA:PEGMEMA photoresin [214]. The study examined CNT with loadings up to 1.5 wt%. Increases in CNT resulted in decreases in photopolymerization due to high UV absorptivity of the CNT filler. Higher loadings of photoinitiator were used to mitigate this effect. 3D printing was performed for loadings up to 0.5 wt% CNT, with higher loadings showing limited resolution and printability. Higher loadings could potentially be printed with increased UV intensity or further additions of photoinitiator.

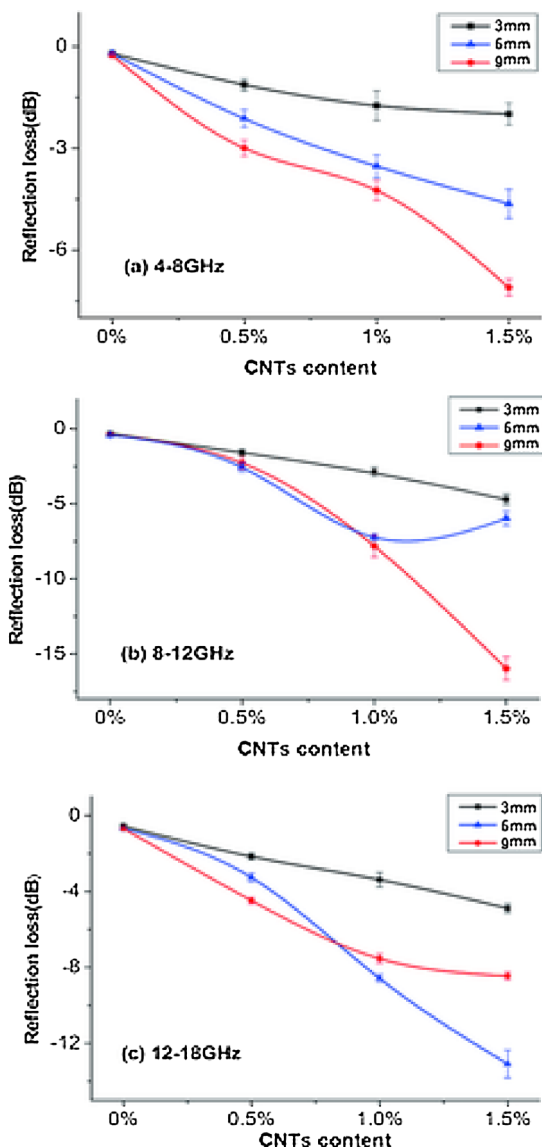


Fig. 38. Reflectivity of CNT composites at various frequencies [207]. Copyright 2016, Society of Plastics Engineers.

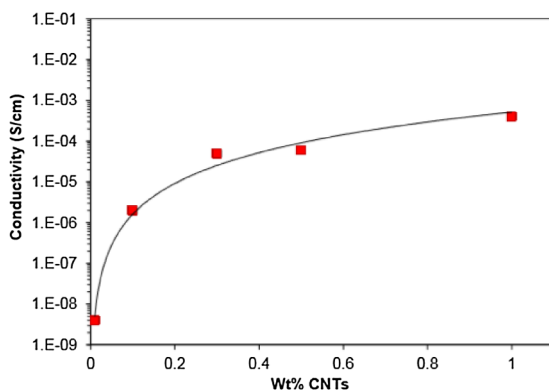


Fig. 39. Conductivity of CNT composites [214]. Copyright 2016, Elsevier.

A two-point measurement using a Keithley 4200-SCS Semiconductor Characterization System was used to test electrical conductivity. Fig. 39 shows the results of the conductivity testing, with the neat resin having a conductivity of 2.00×10^{-9} S/cm compared to the 0.5 wt% CNT composite with a conductivity of 2.00×10^{-5} S/cm. In addition, DSC and tensile testing was done to investigate the mechanical and T_g of select CNT composites, these results are summarized in Table 12. The tensile test results show the best improvement in modulus at the lowest loadings with the 0.1 wt% CNT composite having a modulus of 13.2 MPa compared to 9.6 MPa for the neat resin. Additionally, loadings beyond 0.3 wt% CNT were shown to have a negative impact on the modulus. Lastly, the DSC results show a decrease in glass transition temperature with the neat resin having a T_g of 59.5 °C compared to 42.8 °C for 0.5 wt% CNT composite.

4.3.3. Graphene nanocomposite resins

Manapat et al. used Formlabs Grey resin with nano graphene oxide (GO) to create a nano resin for SLA 3D printing. After the 3D printing process, the samples were annealed at 50 °C and 100 °C for 12 h before testing [211]. TGA and tensile test results show improved tensile strength, tensile modulus, and thermal stability with the higher annealing temperatures. Fig. 40 shows the tensile strength of the composites under two annealing conditions and a control with no annealing. Annealing at 100 °C produced considerably better tensile strength with a 674% improvement with 1 wt% GO. The improved mechanical properties from annealing was attributed to the metastable structure of GO, polymer-GO crosslinking, and removal of intercalated water [211].

Lin et al. studied the use of single-layer graphene oxide (SLGO) as reinforcement for complex 3D printed structures [206]. The authors prepared two SLGO nanocomposite resin blends using 0.2 and 0.5 wt% SLGO. The resins were 3D printed using mask projection based stereolithography. Test samples were printed for tensile testing and for compression testing. Prior to testing, some tensile test samples were heat treated at 60 and 110 °C for 6 h each, respectively. Results of tensile testing shown in Fig. 41 demonstrate that small amounts of SLGO, 0.2 wt%, resulted in improvements in tensile strength of 62.2% and improvements in elongation of 12.8% when compared to the neat resin.

The authors investigated the strengthening mechanism of the 3D printed structure in terms of tensile strength and modulus found that the increase in ductility is related to increases in crystallinity of the reinforced polymer composites [206]. TEM results revealed that the nanomaterials aligned randomly in the resin matrix.

4.3.4. Silica nanocomposite resins

One widely studied nano additive for photopolymer resin is silica. Silica consistently improves resin composites with near uniform dispersion even at high loadings above 10 wt%. It also offers improved cure rate, print accuracy, and improvement to mechanical and thermal properties [202,208,209,213].

Gurr et al. studied the potential of nano silica photopolymers for use in structural light modulation [202]. The study investigated the upper limits of silica loadings that can be used without reduction of light transmittance, loadings up to 17 wt% had minimal on transmittance as shown in Fig. 42. TEM results verified that loadings of up to 17 wt% maintained excellent dispersion and as a result did not reduce the light transmittance of the photoresin. Additionally, the use of nano silica improved the dimensional stability and physical properties of printed materials.

Several studies have examined the effect of nano silica on the mechanical properties of photopolymer resin systems. Gurr et al. found an increase in modulus from 1290 to 1700 MPa with the addition of 30 wt% n-silica [202]. Fig. 43 shows the effects of multiple weight loadings of nano silica on the composites fracture toughness and modulus. In addition to this study, Zhang et al. and Weng et al. also look at the effects of nano silica on photoresin mechanical properties. Table 11 summarizes Weng et al.'s work on the mechanical properties of their silica nanocomposites. The study found an improvement in tensile strength and modulus with only a small detriment to the elongation at break. Nano silica loadings of 1, 3, and 5% were examined. The 5 wt% saw an improvement in tensile strength from 45 to 54 MPa and an increase in elastic modulus from 1.7 to 2.7 GPa [213]. Zhang et al. studied silica nanocomposite resins with low silica loadings up to 0.7 wt%. Lower loadings allowed them to maximize dispersion for greater silica interaction within the resin matrix. They found that the addition of 0.3 wt% silica improved tensile strength by 47% and impact strength by 165% [209]. Fig. 44 shows the changes in impact strength and elongation at break with the various loadings. Compared to the neat resin system, Zhang et al. were able to improve the flexural strength and strain at break from 32 MPa and 1.4% to 108 and 2.3% [209]. Silica loadings of 0.7 wt% improved the flexural modulus from 1.7 to 8.0 GPa compared to the neat resin.

Chiu & Wu, and Zhang et al. characterized thermal properties with their respective silica nanocomposite resin studies [208,209]. Zhang et al. used DSC analysis to study the effect of silica loading on the glass transition temperature of the resin. The authors processed the nanocomposite photoresin using a three-roll mill and ultrasonication. A film was produced by application of resin onto a glass surface before exposure to UV light. Data analysis show an increase in T_g from 67.2 °C with the neat resin system to 71.7 °C and

Table 12

Properties characterization of CNT composites (table reproduced from [214]).

Sample	T_g (°C)	Young's modulus (MPa)	Conductivity (S/cm)
0 wt% CNTS	59.5	9.6	2.00E-09
0.1 wt% CNTS	53.4	13.2	1.00E-07
0.3 wt% CNTS	45.8	10.3	8.00E-06
0.5 wt% CNTS	42.8	4.4	2.00E-05

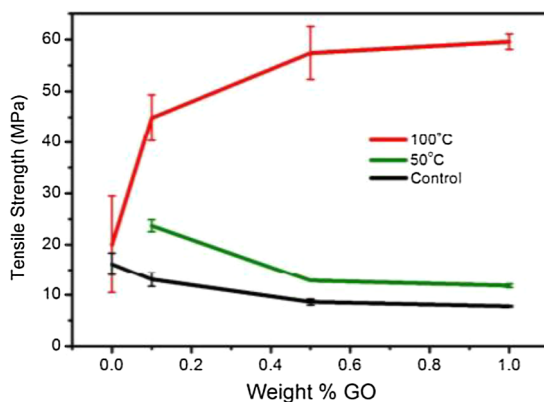


Fig. 40. Tensile results for GO composites [211]. Copyright 2017, American Chemical Society.

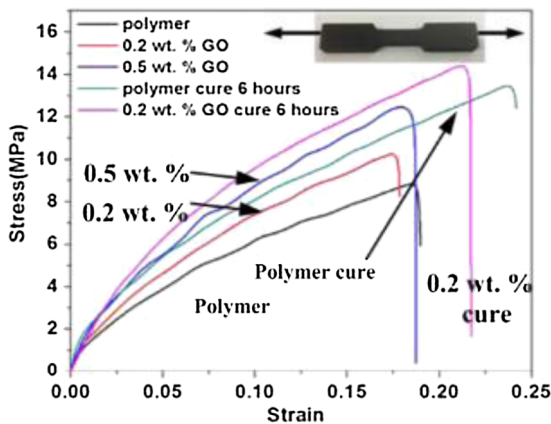


Fig. 41. Tensile results for SLGO composites [206]. Copyright 2015, IOP Publishing Ltd.

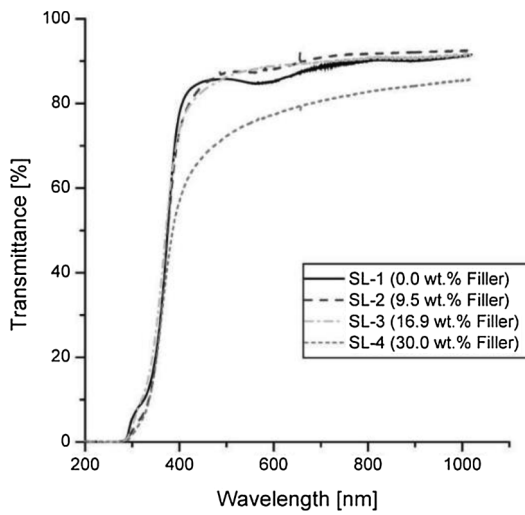


Fig. 42. Transmittance of n-silica composites [202]. Copyright 2008, John Wiley and Sons.

80.1 °C with the addition of 0.3 and 0.7 wt%, respectively [209]. DSC data did not show any significant changes to thermal stability. Chiu & Wu studied TPA/HDDA nano resin composites using nano silica. They used TGA to analyze the degradation and thermal stability of the composites. The neat resin had an onset degradation temperature of 268 °C and a complete degradation temperature of 489 °C. Composites using 0.5 wt% silica saw an improvement in onset and complete degradation temperatures with 335 °C and 507 °C, respectively. Composites with 1.0 wt% silica had onset and complete degradation temperatures at 324 °C and 557 °C [208].

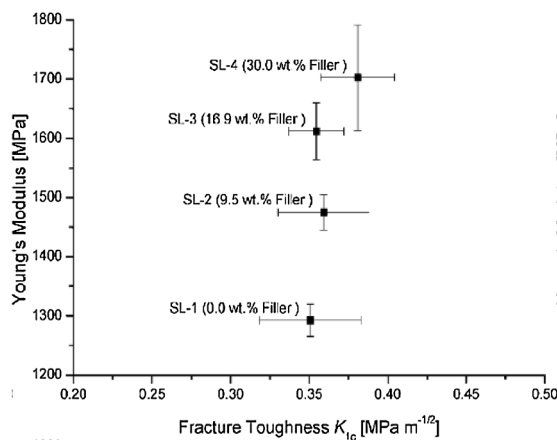


Fig. 43. Modulus and fracture toughness for n-silica composites [202]. Copyright 2008, John Wiley and Sons.

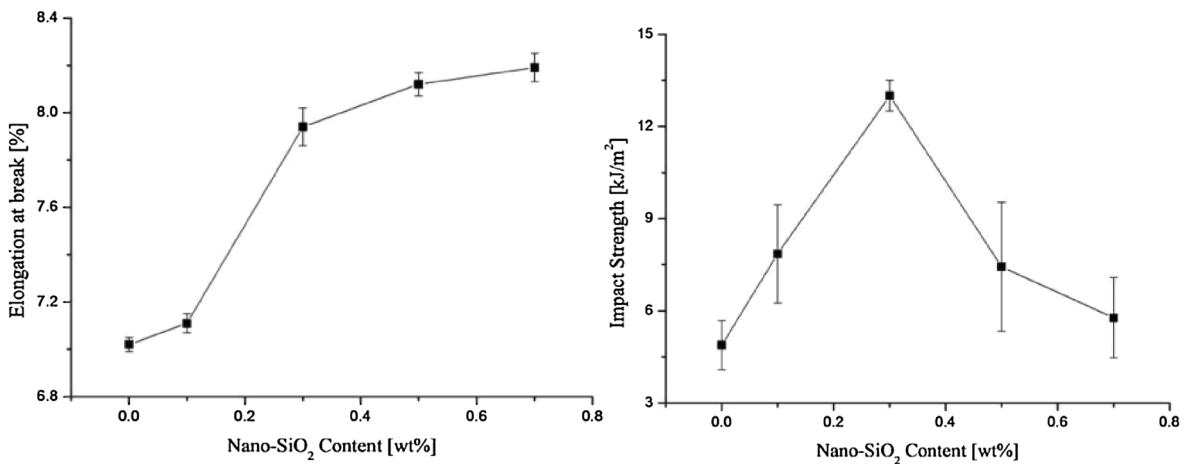


Fig. 44. Tensile (left) and impact strength (right) of silica resin composites [209]. Copyright 2015, John Wiley and Sons.

Both loadings had significant improvements to thermal properties of the studied resin.

4.3.5. Crystalline nanocellulose (CNC) nanocomposite resins

Kumar, Sandeep, et al. studied stereolithography resin composites with crystalline nanocellulose (CNC) [205]. The team studied CNC composites at 0.5, 1.0, 2.0, and 5.0 wt%, the authors found that these loadings had very little impact on processability of the resin with the use of a commercially available SL printer. The study examined the impact of the CNC on the resin mechanical properties. The addition of CNC was found to have a significant improvement of resin mechanical properties. Table 13 shows the results of mechanical testing, an improvement in storage modulus of 166, 233, and 587% with 0.5, 1.0, and 5.0 wt% CNC when compared to the neat resin. Other mechanical properties examined also saw improvements with additions of CNC, however tensile strength saw a peak in improvement at 2 wt% with 82 MPa compared to a tensile strength of 69 MPa in the neat resin. When tested at loadings of 5 wt% CNC, a detrimental effect was noted with a decrease the tensile strength to 65 MPa. A similar trend was noticed with flexural modulus, with a peak value of 3.3 GPa at 2 wt%, however even 5 wt% saw an improvement at 3.1 GPa compared to 2.6

Table 13

Mechanical and thermal properties of CNC nanocomposites (table reproduced from [205]).

Property	Neat resin	0.5% w/w CNC	1.0% w/w CNC	2.0% w/w CNC	5.0% w/w CNC
Tensile strength (MPa)	69	74	77	82	65
Young's modulus (GPa)	3.1	3.4	3.6	3.9	4.1
Elongation at break (%)	3.8	3.7	2.8	2.6	1.6
Flexural modulus (GPa)	2.7	3.0	3.2	3.3	3.1
Storage modulus at 25 °C (GPa)	2.6	3.2	3.8	n.a	4.3
Storage modulus at 120 °C (GPa)	0.033	0.088	0.11	n.a	0.23
T _g (°C)	95	98	104	n.a	107

GPa for the neat resin.

Feng, Xinhao, et al. investigated Ligin coated CNC (L-CNC) dispersed with methacrylate resin [215]. Composites with 0, 0.1, 0.5, and 1.0 wt% CNC were processed with mixing and ultrasonication. The composites were manufactured with SL Form 1 + 3D printer. Half of the printed samples were post cured in an oven at 120 °C for 40 min. The study was comprehensive, examining many properties including thermal and mechanical. The mechanical study demonstrated that a post cure improves the tensile strength and modulus compared to samples that were not post cured. At 0.5 wt% CNC the post cured samples had a tensile strength and modulus of about 69 MPa and 1.18 GPa compared to 66 MPa and 1.15 GPa with the samples that were not post cured. for the neat resins which were also cured. Results of TGA showed an improvement of thermal stability, $T_{5\%}$ and T_{max} , with the addition of CNC.

4.3.6. Boron nitride nanoflakes nanocomposite resins

Bustillos, Jennifer, et al. processed and examined PSP resin composites using 0, 0.5, and 1.0 wt% of boron nitride nanoflakes (BNNP) [216]. Composites were printed using a Form 1 + SLA 3D printed. Table 14 summarizes the thermal and mechanical properties analyses conducted on the nanocomposites. Hardness of the composites were also examined. The 1 wt% BNNP composite saw a significant ~42% drop off in hardness, yet examination of the composites failed to reveal signs of porosity. On the contrary, the density of the 1 wt% BNNP was essentially the same as the neat resin, 1.183 compared to 1.180 g/cm³. This anomaly was attributed to incomplete curing of the higher loading composite, probably caused by absorption of UV radiation by the BNNP particles. Fig. 45 shows the fractures resulting from the compression tests. Results of this testing show the neat resin to have a higher compressive strength of 44.9 MPa compared to the 0.5 and 1.0 wt% composites at 37.2 and 40.2 MPa respectively. Images a–c of Fig. 45 show the worsening of stress fractures as the amount of BNNP in the composites increase. This is again attributed to incomplete curing with increasing presence of BNNP particles. DSC tested was used to analyze the T_g of the composites and the neat PSP resin systems. Neat PSP had a T_g of 45.2 °C compared to values of 49.8 and 50.3 °C, respectively with the 0.5 and 1.0 wt% BNNP composites.

This study highlights the significance of UV absorption by resin fillers. Additions of materials with high interference can lead to decreases in the composite's properties. Lower loadings of these fillers, or otherwise the use of more photoinitiators, may result in more complete resin crosslinking.

5. Challenges and opportunities in future AM developments

This review attempts to provide a comprehensive summary of the commercially available polymers as well as recent progress in novel polymer composites development especially polymer nanocomposites for four AM methods namely, FFF, SLS, MJF, and SLA. The development of polymer nanocomposites for AM provides a way of expanding the material performance portfolio, enabling the production of multifunctional parts with more design flexibilities. The role of AM should not be to completely replace the conventional manufacturing processes, but rather to complement and make it more robust. To take full advantage of AM, designers need to come up with new design methodologies. This can be beneficial to a number of industries including but not limited to aerospace, automotive, medical, and oil & gas industries. The following concluding remarks are made summarizing research areas related to polymeric materials development for AM:

1. Materials portfolio for AM needs to keep expanding. Current AM materials are based on a few polymer types, such as ABS and nylon. Compatibility of undocumented or novel polymers with different AM methods need to be explored. In addition, new polymer composites and polymer nanocomposites and their *processing-structure-performance* relationship in AM context will facilitate the discovery of lightweight, stronger, and multi-functional materials further expanding the capability of AM. Combining polymer nanocomposites with continuous fiber reinforcement could yield strong AM parts with improved interlaminar strength.
2. Test standards that are specifically tailored to AM processing need to be established. As Popescu et al. [50] pointed out, it is difficult to compare mechanical properties of FFF parts without considering printing conditions. As discussed in this review, the performance of an AM part is affected by many factors which varies among different types of AM technologies. The new test standards need to take into account of the complexity of AM processing.
3. Scale up challenge. One of the major obstacles to scale up AM processes is the lack of speed [217]. For example, heat transfer is a limiting factor in increasing the manufacturing rate of FFF [218,219]; it is also a critical parameter for powder-based AM to prevent residual stress induced print failure. New development in large area AM methods, such as Big Area Additive Manufacturing (BAAM) overcomes this challenge by replacing FFF's filament heating mechanism with a large diameter feeding screw. The large nozzle diameter drives output rate up to 50 kg/hour [220]. However, the tradeoff for BAMM is the resolution, therefore surface finish of the printed parts are often necessary.
4. Reliable modeling prediction and optimization of AM part performance is also needed. As the print quality is governed by a

Table 14

Mechanical and thermal properties of BNNP nanocomposites [216].

Sample	T_g (°C)	Density (g/cm ³)	Hardness (MPa)	Compressive modulus (MPa)	Compressive yield strength (MPa)	Compressive strength (MPa)
0 wt% BNNP	45.2	1.180	135.6 ± 4.0	549	29.8	44.9
0.5 wt% BNNP	49.8	1.181	135.6 ± 4.0	421	18.7	37.2
1 wt% BNNP	50.3	1.183	78.5 ± 6.2	439	23.2	40.2

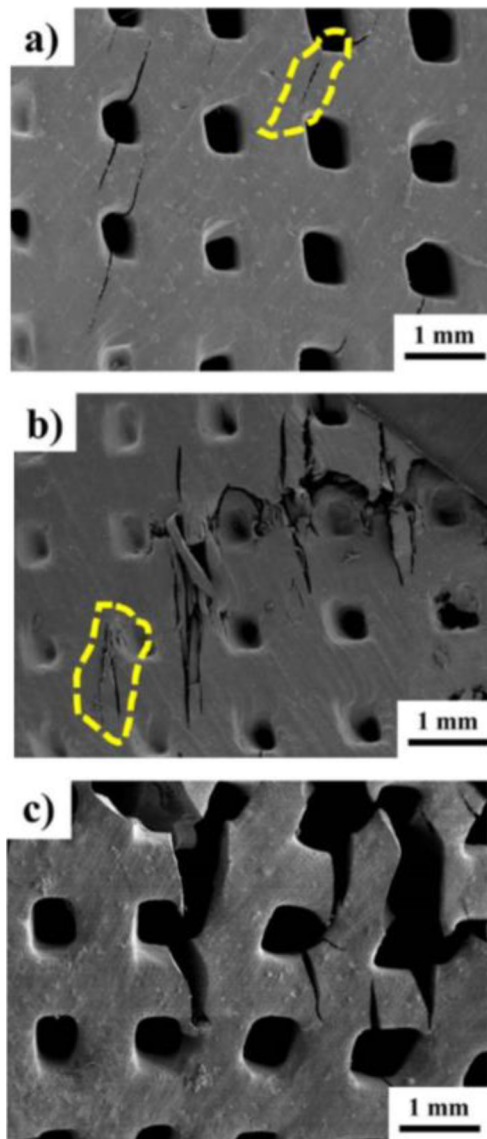


Fig. 45. BNNP nanocomposite structures after compression testing [216]. Copyright 2017, Society of Plastics Engineers.

multitude of parameters, oversimplified simulation methods without considering enough key parameters will not be able to predict part performance consistently. Process optimization is critical to improve interlayer bonding and to reduce porosity and residual stress of any given material. AM parts should also be optimized based on their applications. For example, in order for AM parts to be used in structural applications, fatigue properties under cyclic loading conditions needs to be optimized.

5. Reduce manufacturing cost. For low volume (< 100) application (Fig. 3), AM produced parts are often a more economical option than conventional manufacturing methods due to no need in tooling cost. However, the feedstock materials for AM are generally more expensive to produce. For example, filaments for FFF and powders for SLS and MJF need to have high size tolerance to maintain good print quality. Due to limited printing resolutions, post processing is often needed for the final product. In addition, the long processing times of AM relative to processes like injection molding also drives up energy consumption and more importantly time cost which goes back to point 3 [221].
6. Reduce materials waste and increase recyclability. As more low-cost AM machines become readily available on market, excessive consumption of materials for production of low value parts should be avoided. From materials development perspective, this can be achieved by reducing waste materials, such as support materials and reducing the use of toxic chemical compounds. One advantage of thermoplastics is its recyclability. As more and more AM parts are produced, their recyclability should also be explored to alleviate environmental burden of plastic pollution.

Because the AM techniques are relatively new compared to other conventional manufacturing methods, many issues need to be

investigated. For example, the lack of Z directional strength due to part anisotropy. Nonetheless, it is believed that more breakthroughs in both materials development as well as process optimization are likely to emerge as the AM field is rapidly expanding and wide applications of AM in our daily life can be expected in the foreseeable future.

Declaration of Competing Interest

The authors declare that they have no known competing financial interests or personal relationships that could have appeared to influence the work reported in this paper.

References

- [1] Wohlers T. *Wohlers report 2016*. Wohlers Associates Inc; 2016.
- [2] Coykendall J, Cotteler M, Holdowsky J, Mahto M. 3D opportunity in aerospace and defense: Additive manufacturing takes flight. A Deloitte series on additive manufacturing. 2014;1.
- [3] Stansbury JW, Idacavage MJ. 3D printing with polymers: Challenges among expanding options and opportunities. *Dent Mater* 2016;32:54–64.
- [4] Tack P, Victor J, Gummel P, Annemans L. 3D-printing techniques in a medical setting: a systematic literature review. *Biomed Eng Online* 2016;15:115.
- [5] Vries Cd. Volkswagen Autoeuropa: Maximizing production efficiency with 3D printed tools, jigs, and fixtures. ultimaker.com: Ultimaker B.V.; 2017.
- [6] Klocke F, Klink A, Veselovac D, Aspinwall DK, Soo SL, Schmidt M, et al. Turbomachinery component manufacture by application of electrochemical, electro-physical and photonic processes. *CIRP Ann* 2014;63:703–26.
- [7] Rosochowski A, Matuszak A. Rapid tooling: the state of the art. *J Mater Process Technol* 2000;106:191–8.
- [8] Hiemenz J. Production floor trends, justifying additive manufacturing through jigs & fixtures. stratasys.com: Stratasys; 2016.
- [9] Thompson MK, Moroni G, Vaneker T, Fadel G, Campbell RI, Gibson I, et al. Design for additive manufacturing: trends, opportunities, considerations, and constraints. *CIRP Ann* 2016;65:737–60.
- [10] ASTM. Standard terminology for additive manufacturing - general principles – terminology. ASTM ISO/ASTM52900-15. West Conshohocken (PA); 2015.
- [11] Wei X, Li D, Jiang W, Gu Z, Wang X, Zhang Z, et al. 3D printable graphene composite. *Sci Rep* 2015;5:11181.
- [12] Quinlan HE, Hasan T, Jaddou J, Hart AJ. Industrial and consumer uses of additive manufacturing: a discussion of capabilities, trajectories, and challenges. *J Ind Ecol* 2017;21:S15–20.
- [13] Küpper D, Heising W, Corman G, Wolfgang M, Knizek C, Lukic V. Get ready for industrialized additive manufacturing. Digital, BCG, Boston Consulting Group; 2017.
- [14] Gantzenbein S, Masania K, Woigk W, Sesseg JPW, Tervoort TA, Studart AR. Three-dimensional printing of hierarchical liquid-crystal-polymer structures. *Nature* 2018;561:226–30.
- [15] Gnanasekaran K, Heijmans T, van Bennekom S, Woldhuis H, Wijnia S, de With G, et al. 3D printing of CNT- and graphene-based conductive polymer nanocomposites by fused deposition modeling. *Appl Mater Today* 2017;9:21–8.
- [16] Kim K, Park J, Suh J-h, Kim M, Jeong Y, Park I. 3D printing of multiaxial force sensors using carbon nanotube (CNT)/thermoplastic polyurethane (TPU) filaments. *Sens Actuators, A* 2017;263:493–500.
- [17] Gao W, Zhang Y, Ramanujan D, Ramani K, Chen Y, Williams CB, et al. The status, challenges, and future of additive manufacturing in engineering. *Comput Aided Des* 2015;69:65–89.
- [18] Huang X, Xie M. Evolutionary topology optimization of continuum structures: methods and applications. John Wiley & Sons; 2010.
- [19] Simpson TW, Williams CB, Hripko M. Preparing industry for additive manufacturing and its applications: summary & recommendations from a National Science Foundation workshop. *Addit Manuf* 2017;13:166–78.
- [20] ASTM. Additive manufacturing technology standards. <https://www.astm.org/2019>.
- [21] ASTM. The global leader in additive manufacturing standards. ASTM International; 2017. <https://www.astm.org/>.
- [22] Waller JM, Parker BH, Hodges KL, Burke ER, Walker JL. Nondestructive evaluation of additive manufacturing state-of-the-discipline report; 2014.
- [23] Möhring HC, Kersting P, Carmignato S, Yagüe-Fabra JA, Maestro M, Jiménez R, et al. A testpart for interdisciplinary analyses in micro production engineering. *Procedia CIRP* 2015;28:106–12.
- [24] Migler KD, Ricker RE. Measurement science roadmap for polymer-based additive manufacturing. *Adv Manuf Ser NIST* 2016.
- [25] Everton SK, Hirsch M, Stravroulakis P, Leach RK, Clare AT. Review of in-situ process monitoring and in-situ metrology for metal additive manufacturing. *Mater Des* 2016;95:431–45.
- [26] Coogan TJ, Kazmer DO. In-line rheological monitoring of fused deposition modeling. *J Rheol* 2019;63:141–55.
- [27] Kurfess T, Cass WJ. Rethinking additive manufacturing and intellectual property protection. *Res-Techol Manage* 2014;57:35–42.
- [28] Kietzmann J, Pitt L, Berthon P. Disruptions, decisions, and destinations: Enter the age of 3-D printing and additive manufacturing. *Bus Horiz* 2015;58:209–15.
- [29] Gibson MA, Mykulowycz NM, Shim J, Fontana R, Schmitt P, Roberts A, et al. 3D printing metals like thermoplastics: fused filament fabrication of metallic glasses. *Mater Today* 2018;21:697–702.
- [30] Warrier N, Kate KH. Fused filament fabrication 3D printing with low-melt alloys. *Prog Addit Manuf* 2018;3:51–63.
- [31] Frazier WE. Metal additive manufacturing: a review. *J Mater Eng Perform* 2014;23:1917–28.
- [32] Lewandowski JJ, Seifi M. Metal additive manufacturing: a review of mechanical properties. *Annu Rev Mater Res* 2016;46:151–86.
- [33] Tapia G, Elwany A. A review on process monitoring and control in metal-based additive manufacturing. *J Manuf Sci Eng* 2014;136:060801.
- [34] Crump SS. Apparatus and method for creating three-dimensional objects. Google Patents 1992.
- [35] Crump SS, Comb JW, Priedeman Jr. WR, Zinniel RL. Process of support removal for fused deposition modeling. Google Patents 1996.
- [36] Akande SO, Dalgarno K, Munguia J. Process control testing for fused filament fabrication. *Rapid Prototyp J* 2017;23:246–56.
- [37] Torrado AR, Shemelya CM, English JD, Lin Y, Wicker RB, Roberson DA. Characterizing the effect of additives to ABS on the mechanical property anisotropy of specimens fabricated by material extrusion 3D printing. *Addit Manuf* 2015;6:16–29.
- [38] Nardone MJ. A feasibility study of fused filament fabrication for improving industrial manufacturing. San Antonio: The University of Texas; 2017.
- [39] Jiang J, Xu X, Stringer J. Support structures for additive manufacturing: a review. *J Manuf Mater Process* 2018;2:64.
- [40] Sood AK, Ohdar RK, Mahapatra SS. Experimental investigation and empirical modelling of FDM process for compressive strength improvement. *J Adv Res* 2012;3:81–90.
- [41] Tymrak BM, Kreiger M, Pearce JM. Mechanical properties of components fabricated with open-source 3-D printers under realistic environmental conditions. *Mater Des* 2014;58:242–6.
- [42] Sood AK, Ohdar RK, Mahapatra SS. Parametric appraisal of mechanical property of fused deposition modelling processed parts. *Mater Des* 2010;31:287–95.
- [43] Goh GD, Yap YL, Tan HKJ, Sing SL, Goh GL, Yeong WY. Process–structure–properties in polymer additive manufacturing via material extrusion: a review. *Crit Rev Solid State Mater Sci* 2019;1:21–.
- [44] Brenken B, Barocci E, Favoloro A, Kunc V, Pipes RB. Fused filament fabrication of fiber-reinforced polymers: a review. *Addit Manuf* 2018;21:1–16.
- [45] Mohamed OA, Masood SH, Bhowmik JL. Optimization of fused deposition modeling process parameters: a review of current research and future prospects. *Adv Manuf* 2015;3:42–53.
- [46] Ertay DS, Yuen A, Altintas Y. Synchronized material deposition rate control with path velocity on fused filament fabrication machines. *Addit Manuf* 2018;19:205–13.

- [47] Blok LG, Longana ML, Yu H, Woods BKS. An investigation into 3D printing of fibre reinforced thermoplastic composites. *Addit Manuf* 2018;22:176–86.
- [48] Dikshit V, Nagalingam AP, Yap YL, Sing SL, Yeong WY, Wei J. Crack monitoring and failure investigation on inkjet printed sandwich structures under quasi-static indentation test. *Mater Des* 2018;137:140–51.
- [49] Turner BN, Strong R, Gold SA. A review of melt extrusion additive manufacturing processes: I. Process design and modeling. *Rapid Prototyp J*. 2014;20:192–204.
- [50] Popescu D, Zapciu A, Amza C, Baciu F, Marinescu R. FDM process parameters influence over the mechanical properties of polymer specimens: a review. *Polym Test* 2018;69:157–66.
- [51] Jiang J, Lou J, Hu G. Effect of support on printed properties in fused deposition modelling processes. *Virtual Phys Prototyp* 2019;14:308–15.
- [52] Chuang CK, Grady JE, Draper RD, Shin E-SE, Patterson C, Santelle TD. Additive manufacturing and characterization of ultem polymers and composites. Dallas (TX): CAMX; 2015.
- [53] Torrado AR, Roberson DA. Failure analysis and anisotropy evaluation of 3D-printed tensile test specimens of different geometries and print raster patterns. *J Fail Anal Prev* 2016;16:154–64.
- [54] Perez ART, Roberson DA, Wicker RB. Fracture surface analysis of 3D-printed tensile specimens of novel ABS-based materials. *J Fail Anal Prev* 2014;14:343–53.
- [55] Davis CS, Hillgartner KE, Han SH, Seppala JE. Mechanical strength of welding zones produced by polymer extrusion additive manufacturing. *Addit Manuf* 2017;16:162–6.
- [56] Shaffer S, Yang K, Vargas J, Di Prima MA, Voit W. On reducing anisotropy in 3D printed polymers via ionizing radiation. *Polymer* 2014;55:5969–79.
- [57] Stratasys. Stratasys technical information; 2019. www.stratasys.com.
- [58] Mansour S, Gilbert M, Hague R. A study of the impact of short-term ageing on the mechanical properties of a stereolithography resin. *Mater Sci Eng, A* 2007;447:277–84.
- [59] Ni R, Qian B, Liu C, Liu X, Qiu J. A cross-linking strategy with moderated pre-polymerization of resin for stereolithography. *RSC Adv* 2018;8:29583–8.
- [60] Polymeric Paesano A. Additive manufacturing: present status and future trends of materials and processes. *Boeing Tech J* 2016;1:12.
- [61] Deckard CR. Method and apparatus for producing parts by selective sintering. Google Patents 1989.
- [62] Beaman JJ, Deckard CR. Selective laser sintering with assisted powder handling. Google Patents 1990.
- [63] Schmidt M, Pohle D, Rechtenwald T. Selective laser sintering of PEEK. *CIRP Ann* 2007;56:205–8.
- [64] Olakanmi EO, Cochrane RF, Dalgarno KW. A review on selective laser sintering/melting (SLS/SLM) of aluminium alloy powders: processing, microstructure, and properties. *Prog Mater Sci* 2015;74:401–77.
- [65] Kruth JP, Mercelis P, Van Vaerenbergh J, Froyen L, Rombouts M. Binding mechanisms in selective laser sintering and selective laser melting. *Rapid Prototyp J* 2005;11:26–36.
- [66] Laoui T, Froyen L, Kruth J-P. Effect of mechanical alloying on selective laser sintering of WC-9Co powder. *Powder Metall* 1999;42:203–5.
- [67] O'Neill W, Sutcliffe CJ, Morgan R, Lansborough A, Hon KKB. Investigation on multi-layer direct metal laser sintering of 316L stainless steel powder beds. *CIRP Ann* 1999;48:151–4.
- [68] Li L. The advances and characteristics of high-power diode laser materials processing. *Opt Lasers Eng* 2000;34:231–53.
- [69] Manzur T, Roychoudhuri C, Marcus H. SFF using diode lasers. In: 1996 International solid freeform fabrication symposium; 1996.
- [70] Tolochko NK, Khlopov YV, Mozzharov SE, Ignatiev MB, Laoui T, Titov VI. Absorptance of powder materials suitable for laser sintering. *Rapid Prototyp J* 2000;6:155–61.
- [71] Nelson JC, Vail NK, Barlow JW, Beaman JJ, Bourell DL, Marcus HL. Selective laser sintering of polymer-coated silicon carbide powders. *Ind Eng Chem Res* 1995;34:1641–51.
- [72] Marcus H, Barlow J, Beaman J, Bourell D, Agarwala M. Direct selective laser sintering of metals. *Rapid Prototyp J* 1995;1:26–36.
- [73] Froyen L, Kruth JP, Laoui T, Wang X. Lasers and materials in selective laser sintering. *Assembly Autom* 2003;23:357–71.
- [74] Kruth JP. Lasers and materials in selective laser sintering. *Assembly Autom* 2003;23:357–71.
- [75] Dotchev K. Recycling of polyamide 12 based powders in the laser sintering process. *Rapid Prototyp J* 2009;15:192–203.
- [76] Cox BD. Selective laser sintering powder recycle system. Google Patents 2011.
- [77] Monsheimer S, Grebe M, Baumann F-E, Christoph W, Schiffer T, Scholten H. Laser sintering powder with improved recycling properties, process for its production, and use of the laser sintering powder. Google Patents 2004.
- [78] Laser Cox B. sintering powder recycle system. Google Patents 2006.
- [79] Shi D, Gibson I. Improving surface quality of selective laser sintered rapid prototype parts using robotic finishing. *Proc Instit Mech Engineers, Part B: J Eng Manuf* 2000;214:197–203.
- [80] HP Development Company LP. HP multi jet fusion technology; 2017. p. 2–7.
- [81] O'Connor HJ, Dickson AN, Dowling DP. Evaluation of the mechanical performance of polymer parts fabricated using a production scale multi jet fusion printing process. *Addit Manuf* 2018;22:381–7.
- [82] Manapat JZ, Chen Q, Ye P, Advincula RC. 3D Printing of Polymer Nanocomposites via Stereolithography. *Macromol Mater Eng* 2017;302:1600553.
- [83] Materialise. Stereolithography. 3D printing technologies; 2019. i.materialise.com.
- [84] Limaye AS. Multi-objective process planning method for mask projection stereolithography. Georgia Institute of Technology; 2007.
- [85] Masood SH, Song WQ. Development of new metal/polymer materials for rapid tooling using Fused deposition modelling. *Mater Des* 2004;25:587–94.
- [86] Novakova-Marcincinova L, Novak-Marcincin J. Testing of the ABS materials for application in fused deposition modeling technology. *Appl Mech Mater* 2013;309:133–40.
- [87] Ahn SH, Montero M, Odell D, Roundy S, Wright PK. Anisotropic material properties of fused deposition modeling ABS. *Rapid Prototyp J* 2002;8:248–57.
- [88] Arivazhagan A, Masood S. Dynamis mechanical properties of ABS material processed by fused deposition modelling. *Int J Eng Res Appl*. 2012;2:2009–14.
- [89] Novakova-Marcincinova L, Novak-Marcincin J. Applications of rapid prototyping fused deposition modeling materials. In: Annals of DAAAM for 2012 & proceedings of the 23rd international DAAAM symposium; 2012. p. 2304–82.
- [90] Perez M, Block M, Espalin D, Winker R, Hoppe T, Medina F, et al. Sterilization of FDM-manufactured parts. In: Proceedings of the 2012 annual international solid freeform fabrication symposium, Austin, TX; Aug 2012. p. 6–8.
- [91] Manikandan S, Kumar AS, Sharma C, Raja VP, Adhiyamaan A. Investigation on the effect of fused deposition modeling process parameters on flexural and surface roughness properties of PC-ABS blend. *Int J Recent Technol Mech Electr Eng* 2015;2:41–7.
- [92] McCarthy K. Improving rapid prototyping through the installment of 3D printers in automotive companies; 2012.
- [93] Vairis A, Petousis M, Vidakis N, Savvakis K. On the strain rate sensitivity of ABS and ABS plus fused deposition modeling parts. *J Mater Eng Perform* 2016;25:3558–65.
- [94] Fischer F. Thermoplastics: the best choice for 3D printing White Paper Edn Prairie (MN): Stratasys Inc; 2011.
- [95] Chen T, Shea K. An autonomous programmable actuator and shape reconfigurable structures using bistability and shape memory polymers. arXiv e-prints; 2017.
- [96] Chen T, Bilal OR, Shea K, Daraio C. Harnessing bistability for directional propulsion of soft, untethered robots. *Proc Natl Acad Sci* 2018;115:5698–702.
- [97] Tolute S, Moghboli MR, Ghafelebashi SM. Preparation of ASA (acrylonitrile-styrene-acrylate) structural latexes via seeded emulsion polymerization. *Eur Polym J* 2009;45:714–20.
- [98] Seo YS, Kim JH, Kim CK, Lee R, Keum JK. Polycarbonate/acrylonitrile-styrene-acrylic elastomer terpolymer blends with enhanced interfacial adhesion and surface gloss. *J Appl Polym Sci* 2005;96:2097–104.
- [99] Filaments.ca. HDPE Filament – Natural – 1.75 mm; 2019. <https://filaments.ca/products/hdpe-filament-natural-1-75mm>.
- [100] Muñoz-Rojas PA, Kühl A, Mendonça PD, Benvenuti IJ, Creus GJ. Modeling nonlinear viscoelastic behavior of High Density Polyethylene (HDPE): application of stress-time equivalence versus interpolation of rheological properties. III International symposium on solid mechanics. 2011.
- [101] Wu S, Zhang J, Xu X. Studies on high density polyethylene (HDPE) functionalized by ultraviolet irradiation and its application. *Polym Int* 2003;52:1527–30.

- [102] Ultimaker. Ultimaker PP; 2019. <https://ultimaker.com/materials/pp>.
- [103] MatterHackers. High Impact Polystyrene (HIPS) dissolvable filament – 1.75mm (1kg); 2019. <https://www.matterhackers.com/store/3d-printer-filament/hips-175mm-1kg>.
- [104] Silberberg J, Han CD. The effect of rubber particle size on the mechanical properties of high-impact polystyrene. *J Appl Polym Sci* 1978;22:599–609.
- [105] Stratasys. FDM Nylon 12; 2019. <https://www.stratasys.com/materials/search/fdm-nylon-12>.
- [106] Knoop F, Schoeppner V, Knoop F, Schoeppner V. Mechanical and thermal properties of FDM parts manufactured with polyamide 12. In: Proceedings of the 26th annual international solid freeform fabrication symposium—An additive manufacturing conference, Austin, TX, USA; 2015. p. 10–2.
- [107] Arbaoui Y, Laur V, Maalouf A, Queffelec P. 3D printing for microwave: Materials characterization and application in the field of absorbers. In: 2015 IEEE MTT-S international microwave symposium; 2015. p. 1–3.
- [108] Stratasys. Carbon fiber material: FDM NYLON 12CF; 2019. <https://www.stratasys.com/materials/search/fdm-nylon-12cf>.
- [109] Türk D-A, Brenni F, Zogg M, Meboldt M. Mechanical characterization of 3D printed polymers for fiber reinforced polymers processing. *Mater Des* 2017;118:256–65.
- [110] Stratasys. PC-ABS; 2019. <https://www.stratasys.com/materials/search/pc-abs>.
- [111] Wildes G, Keskkula H, Paul DR. Fracture characterization of PC/ABS blends: effect of reactive compatibilization, ABS type and rubber concentration. *Polymer* 1999;40:7089–107.
- [112] Lombardo BS, Keskkula H, Paul DR. Influence of ABS type on morphology and mechanical properties of PC/ABS blends. *J Appl Polym Sci* 1994;54:1697–720.
- [113] Cunha JAM, Mellis K, Sethi R, Siauw T, Sudhyadhom A, Garg A, et al. Evaluation of PC-ISO for customized, 3D printed, gynecologic HDR brachytherapy applicators. *J Appl Clin Med Phys* 2015;16:246–53.
- [114] Stratasys. PC-ISO; 2019. <https://www.stratasys.com/materials/search/pc-iso>.
- [115] Stratasys. PLA; 2019. <https://www.stratasys.com/materials/search/pla>.
- [116] Ultimaker. Ultimaker PLA; 2019. <https://ultimaker.com/materials/pla>.
- [117] Carrasco F, Pagès P, Gámez-Pérez J, Santana OO, MasPOCH ML. Processing of poly(lactic acid): characterization of chemical structure, thermal stability and mechanical properties. *Polym Degrad Stab* 2010;95:116–25.
- [118] Stratasys. PPSU; 2019. <https://www.stratasys.com/materials/search/ppsf-ppsu>.
- [119] MatterHackers. Black PRO Series Flex – 1.75mm Flexible TPE (0.5kg); 2019. <https://www.matterhackers.com/store/3d-printer-filament/proflex-black-tpe-filament-175-05kg>.
- [120] Korger M, Bergschneider J, Lutz M, Mahltig B, Finsterbusch K, Rabe M. Possible applications of 3D printing technology on textile substrates. *IOP Conf Ser: Mater Sci Eng* 2016;141:012011.
- [121] Xiao J, Gao Y. The manufacture of 3D printing of medical grade TPU. *Progr Addit Manuf* 2017;2:117–23.
- [122] Li H, Taylor G, Bheemreddy V, Iyibilgin O, Leu M, Chandrashekara K. Modeling and characterization of fused deposition modeling tooling for vacuum assisted resin transfer molding process. *Addit Manuf* 2015;7:64–72.
- [123] Schöppner V, KTP KP. Mechanical properties of fused deposition modeling parts manufactured with Ultem® 9085. In: Proceedings of 69th annual technical conference of the society of plastics engineers (ANTEC11); 2011. p. 1294–8.
- [124] Wu H, Sulkis M, Driver J, Saade-Castillo A, Thompson A, Koo JH. Multi-functional ULTEM™1010 composite filaments for additive manufacturing using Fused Filament Fabrication (FFF). *Addit Manuf* 2018;24:298–306.
- [125] Solvay. KetaSpire® PEEK; 2019. <https://www.solvay.com/en/brands/ketaspire-peek>.
- [126] Evonik. Evonik develops the world's first PEEK filament in implant-grade quality for 3D printing; 2018. <https://industrial.vestakeep.com/product/peek-industrial/en/pages/article.aspx?articleId=100227>.
- [127] VICTREX. VICTREX™ PEEK POLYMERS; 2019. <https://www.victrex.com/en/victrex-peek>.
- [128] Arkema. Kepstan®; 2019. <https://www.arkema.com/en/products/product-finder/range-viewer/Kepstan/2019>.
- [129] Kishore V, Ajinjeru C, Duty CE, Hassen AA, Lindahl JM, Liu P, et al. Rheological characteristics of fiber reinforced poly(ether ketone ketone) (PEKK) for melt extrusion additive manufacturing. Oak Ridge (TN, United States): Oak Ridge National Lab (ORNL); 2017.
- [130] Ramli M, Wahab M, Ahmad M, Bala A. FDM preparation of bio-compatible UHMWPE polymer for artificial implant. *Int J Adv Manuf Technol* 2016;11:5473–80.
- [131] Ansari MHBM, Ibrahim MHIB. Thermal characteristic of waste-derived hydroxyapatite (HA) reinforced ultra high molecular weight polyethylene (UHMWPE) composites for fused deposition modeling (FDM) process. *IOP Conf Ser: Mater Sci Eng: IOP Publish* 2017;012014.
- [132] Hoashi K, Andrews RD. Morphological changes in nylon 6 and effect on mechanical properties. II. Dynamic mechanical properties. *J Polym Sci Part C: Polym Symp* 1972;38:387–404.
- [133] Wu H. Flame retardant nylon 6 nanocomposite fibers: processing and characterization. The University of Texas at Austin; 2016.
- [134] Pérez JM, Vilas JL, Laza JM, Arnáiz S, Mijangos F, Bilbao E, et al. Effect of reprocessing and accelerated ageing on thermal and mechanical polycarbonate properties. *J Mater Process Technol* 2010;210:727–33.
- [135] Lim LT, Cink K, Vanyo T. Poly(lactic acid): synthesis, structures, properties, processing, and applications; 2010.
- [136] Jamshidian M, Tehrany EA, Imran M, Jacquot M, Desobry S. Poly-lactic acid: production, applications, nanocomposites, and release studies. *Compr Rev Food Sci Food Saf* 2010;9:552–71.
- [137] Passador FR, Alzate Rojas GJ, Pessan LA. Thermoplastic elastomers based on natural rubber/polypropylene blends: effect of blend ratios and dynamic vulcanization on rheological, thermal, mechanical, and morphological properties. *J Macromol Sci, Part B* 2013;52:1142–57.
- [138] Chen R, Morsi Y, Patel S, Ke Q-f, Mo X-m. A novel approach via combination of electrospinning and FDM for tri-leaflet heart valve scaffold fabrication. *Front Mater Sci Chin* 2009;3:359–66.
- [139] Richardson RR, Miller JA, Reichert WM. Polyimides as biomaterials: preliminary biocompatibility testing. *Biomaterials* 1993;14:627–35.
- [140] De Beer D, Becker L, van der Walt P, Mauchline D, Campbell R, Dean L. Additive manufacturing of alumide jewellery; 2012.
- [141] De Beer D, Booyens G. Rapid tooling using Alumide®. In: Proceedings of the 2nd international conference on advanced research and rapid prototyping, Leiria, Portugal; 2005. p. 387–94.
- [142] HP Development Company LP. HP 3D High Reusability PA 11; 2019.
- [143] HP Development Company LP. HP 3D High Reusability PA 12; 2019.
- [144] HP Development Company LP. HP 3D High Reusability PA 12 Glass Beads. 2019.
- [145] ASTM. Standard terminology for composite materials. West Conshohocken (PA): ASTM D3878-18; 2018.
- [146] Zhong W, Li F, Zhang Z, Song L, Li Z. Short fiber reinforced composites for fused deposition modeling. *Mater Sci Eng, A* 2001;301:125–30.
- [147] Tekinalp HL, Kunc V, Vélez-García GM, Duty CE, Love LJ, Naskar AK, et al. Highly oriented carbon fiber-polymer composites via additive manufacturing. *Compos Sci Technol* 2014;105:144–50.
- [148] Ning F, Cong W, Qiu J, Wei J, Wang S. Additive manufacturing of carbon fiber reinforced thermoplastic composites using fused deposition modeling. *Compos B Eng* 2015;80:369–78.
- [149] Matsuzaki R, Ueda M, Namiki M, Jeong T-K, Asahara H, Horiguchi K, et al. Three-dimensional printing of continuous-fiber composites by in-nozzle impregnation. *Sci Rep* 2016;6:23058.
- [150] Dickson AN, Ross K-A, Dowling DP. Additive manufacturing of woven carbon fibre polymer composites. *Compos Struct* 2018;206:637–43.
- [151] Goh GD, Yap YL, Agarwala S, Yeong WY. Recent progress in additive manufacturing of fiber reinforced polymer composite. *Adv Mater Technol* 2019;4:1800271.
- [152] Parandoush P, Lin D. A review on additive manufacturing of polymer-fiber composites. *Compos Struct* 2017;182:36–53.
- [153] Wang X, Jiang M, Zhou Z, Gou J, Hui D. 3D printing of polymer matrix composites: a review and prospective. *Compos B Eng* 2017;110:442–58.
- [154] Bourbigot S, Duquesne S, Jama C. Polymer nanocomposites: how to reach low flammability? *Macromol Symp* 2006;233:180–90.
- [155] Paul DR, Robeson LM. Polymer nanotechnology: nanocomposites. *Polymer* 2008;49:3187–204.

- [156] Meng S, He H, Jia Y, Yu P, Huang B, Chen J. Effect of nanoparticles on the mechanical properties of acrylonitrile–butadiene–styrene specimens fabricated by fused deposition modeling. *J Appl Polym Sci* 2017;134.
- [157] Weng Z, Wang J, Senthil T, Wu L. Mechanical and thermal properties of ABS/montmorillonite nanocomposites for fused deposition modeling 3D printing. *Mater Des* 2016;102:276–83.
- [158] Coppola B, Cappetti N, Maio LD, Scarfato P, Incarnato L. Layered silicate reinforced polylactic acid filaments for 3D printing of polymer nanocomposites. In: 2017 IEEE 3rd international forum on research and technologies for society and industry (RTS); 2017. p. 1–4.
- [159] Francis V, Jain PK. Achieving improved dielectric, mechanical, and thermal properties of additive manufactured parts via filament modification using OMMT-based nanocomposite. *Progr Addit Manuf* 2017;2:109–15.
- [160] Christ JF, Aliheidari N, Ameli A, Pötschke P. 3D printed highly elastic strain sensors of multiwalled carbon nanotube/thermoplastic polyurethane nanocomposites. *Mater Des* 2017;131:394–401.
- [161] Kwok SW, Goh KHH, Tan ZD, Tan STM, Tjiu WW, Soh JY, et al. Electrically conductive filament for 3D-printed circuits and sensors. *Appl Mater Today* 2017;9:167–75.
- [162] Zhang D, Chi B, Li B, Gao Z, Du Y, Guo J, et al. Fabrication of highly conductive graphene flexible circuits by 3D printing. *Synth Met* 2016;217:79–86.
- [163] Chizari K, Daoud MA, Ravindran AR, Therriault D. 3D Printing of highly conductive nanocomposites for the functional optimization of liquid sensors. *Small* 2016;12:6076–82.
- [164] Shofner ML, Lozano K, Rodríguez-Macías FJ, Barrera EV. Nanofiber-reinforced polymers prepared by fused deposition modeling. *J Appl Polym Sci* 2003;89:3081–90.
- [165] Dorigato A, Moretti V, Dul S, Unterberger SH, Pegoretti A. Electrically conductive nanocomposites for fused deposition modelling. *Synth Met* 2017;226:7–14.
- [166] Dul S, Fambri L, Pegoretti A. Filaments production and fused deposition modelling of ABS/carbon nanotubes composites. *Nanomaterials* 2018;8:49.
- [167] Hohimer C, Aliheidari N, Mo C, Ameli A. Mechanical behavior of 3D printed multiwalled carbon nanotube/thermoplastic polyurethane. *Nanocomposites* 2017;V001T08A4.
- [168] Kim H, Torres F, Islam MT, Islam MD, Chavez LA, Garcia Rosales CA, et al. Increased piezoelectric response in functional nanocomposites through multiwall carbon nanotube interface and fused-deposition modeling three-dimensional printing. *MRS Commun* 2017;7:960–6.
- [169] Sweeney CB, Lackey BA, Pospisil MJ, Achee TC, Hicks VK, Moran AG, et al. Welding of 3D-printed carbon nanotube–polymer composites by locally induced microwave heating. *Sci Adv* 2017;3:e1700262.
- [170] Dul S, Fambri L, Pegoretti A. Fused deposition modelling with ABS–graphene nanocomposites. *Compos A Appl Sci Manuf* 2016;85:181–91.
- [171] Richardson MJ, Wu H, Wilcox TJ, Broadhurst M, Lin PC, Krifa M, et al. Flame retardant Nylon 6 nanocomposites for fused deposition modelling (FDM) applications. Seattle: SAMPE 2017; 2017.
- [172] Ortiz R, Wu H, Koo JH. Fire-retardant polyamide 11 nanocomposites/elastomer blends for selective laser sintering: further studies. p. 1655.
- [173] Chen Q, Mangadlao JD, Wallat J, De Leon A, Pokorski JK, Advincula RC. 3D printing biocompatible polyurethane/poly(lactic acid)/graphene oxide nanocomposites: anisotropic properties. *ACS Appl Mater Interfaces* 2017;9:4015–23.
- [174] Zhu D, Ren Y, Liao G, Jiang S, Liu F, Guo J, et al. Thermal and mechanical properties of polyamide 12/graphene nanoplatelets nanocomposites and parts fabricated by fused deposition modeling. *J Appl Polym Sci* 2017;134:45332.
- [175] Ahn SH, Baek C, Lee S, Ahn IS. Anisotropic tensile failure model of rapid prototyping parts-fused deposition modeling (FDM). *Int J Mod Phys B* 2003;17:1510–6.
- [176] Domingo-Espín M, Puigoriol-Forcada JM, García-Granada A-A, Llumá J, Borros S, Reyes G. Mechanical property characterization and simulation of fused deposition modeling Polycarbonate parts. *Mater Des* 2015;83:670–7.
- [177] Smith WC, Dean RW. Structural characteristics of fused deposition modeling polycarbonate material. *Polym Test* 2013;32:1306–12.
- [178] Yamamoto BE, Trimble AZ, Minei B, Ghasemi Nejhad MN. Development of multifunctional nanocomposites with 3-D printing additive manufacturing and low graphene loading. *J Thermoplast Compos Mater* 2018;32:383–408.
- [179] Leigh SJ, Bradley RJ, Purcell CP, Billson DR, Hutchins DA. A simple, low-cost conductive composite material for 3D printing of electronic sensors. *PLoS ONE* 2012;7:e49365.
- [180] Kim H, Torres F, Islam T, Islam D, Chavez LA, Garcia Rosales CA, et al. Increased piezoelectric response in functional nanocomposites through multiwall carbon nanotube interface and fused-deposition modeling three-dimensional printing – CORRIGENDUM. *MRS Commun* 2017;7:974.
- [181] Hashemi Sanatgar R, Campagne C, Nierstrasz V. Investigation of the adhesion properties of direct 3D printing of polymers and nanocomposites on textiles: effect of FDM printing process parameters. *Appl Surf Sci* 2017;403:551–63.
- [182] Osswald TA, Puentes J, Kattinger J. Fused filament fabrication melting model. *Addit Manuf* 2018;22:51–9.
- [183] Wang J, Xie H, Weng Z, Senthil T, Wu L. A novel approach to improve mechanical properties of parts fabricated by fused deposition modeling. *Mater Des* 2016;105:152–9.
- [184] Yuan S, Shen F, Chua CK, Zhou K. Polymeric composites for powder-based additive manufacturing: Materials and applications. *Prog Polym Sci* 2019;91:141–68.
- [185] Athreya SR, Kalaitzidou K, Das S. Processing and characterization of a carbon black-filled electrically conductive Nylon-12 nanocomposite produced by selective laser sintering. *Mater Sci Eng, A* 2010;527:2637–42.
- [186] Salmoria GV, Paggi RA, Lago A, Beal VE. Microstructural and mechanical characterization of PA12/MWCNTs nanocomposite manufactured by selective laser sintering. *Polym Test* 2011;30:611–5.
- [187] Salmoria GV, Leite JL, Vieira LF, Pires ATN, Roesler CRM. Mechanical properties of PA6/PA12 blend specimens prepared by selective laser sintering. *Polym Test* 2012;31:411–6.
- [188] Goodridge RD, Shofner ML, Hague RJM, McClelland M, Schleia MR, Johnson RB, et al. Processing of a Polyamide-12/carbon nanofibre composite by laser sintering. *Polym Test* 2011;30:94–100.
- [189] Koo J, Pilato L, Wissler G, Cheng J, Ho D, Nguyen K, et al. Flammability and mechanical properties of Nylon 11 nanocomposites. Proceedings of the SAMPE 2005 ISSE. SAMPE; 2005. p. 1–14.
- [190] Koo J, Lao S, Ho W, Nguyen K, Cheng J, Pilato L, et al. Polyamide nanocomposites for selective laser sintering. *Proc SFF Symp, Austin*. 2006. p. 392–409.
- [191] Warnakula A, Singamneni S. Selective laser sintering of nano Al₂O₃ infused polyamide. *Materials* 2017;10:864.
- [192] Zheng H, Zhang J, Lu S, Wang G, Xu Z. Effect of core–shell composite particles on the sintering behavior and properties of nano-Al₂O₃/polystyrene composite prepared by SLS. *Mater Lett* 2006;60:1219–23.
- [193] Kim HC, Hahn HT, Yang YS. Synthesis of PA12/functionalized GNP nanocomposite powders for the selective laser sintering process. *J Compos Mater* 2013;47:501–9.
- [194] Chunze Y, Yusheng S, Jinsong Y, Jinhui L. A nanosilica/Nylon-12 composite powder for selective laser sintering. *J Reinf Plast Compos* 2008;28:2889–902.
- [195] Cheng J, Lao S, Nguyen K, Ho W, Cummings A, Koo J. SLS processing studies of Nylon 11 nanocomposites. *Proc SFF Symp, Austin*. 2005. p. 141–9.
- [196] Moore AL, Cummings AT, Jensen JM, Shi L, Koo JH. Thermal conductivity measurements of Nylon 11–carbon nanofiber nanocomposites. *J Heat Transfer* 2009;131:091602–91605.
- [197] Ko SH, Pan H, Lee D, Grigoropoulos CP, Park HK. Nanoparticle selective laser processing for a flexible display fabrication. *Jpn J Appl Phys* 2010;49:05EC3.
- [198] Ming L, Yang H, Zhang W, Zeng X, Xiong D, Xu Z, et al. Selective laser sintering of TiO₂ nanoparticle film on plastic conductive substrate for highly efficient flexible dye-sensitized solar cell application. *J Mater Chem A* 2014;2:4566–73.
- [199] Kwon J, Cho H, Eom H, Lee H, Suh YD, Moon H, et al. Low-temperature oxidation-free selective laser sintering of Cu nanoparticle paste on a polymer substrate for the flexible touch panel applications. *ACS Appl Mater Interfaces* 2016;8:11575–82.
- [200] Suh YD, Kwon J, Lee J, Lee H, Jeong S, Kim D, et al. Maskless fabrication of highly robust, flexible transparent Cu conductor by random crack network assisted Cu nanoparticle patterning and laser sintering. *Adv Electron Mater* 2016;2:1600277.
- [201] Theodorakos I, Zacharatos F, Geremia R, Karnakis D, Zergioti I. Selective laser sintering of Ag nanoparticles ink for applications in flexible electronics. *Appl Surf Sci* 2015;336:157–62.
- [202] Gurr M, Hofmann D, Ehm M, Thomann Y, Kübler R, Mühlaupt R. Acrylic nanocomposite resins for use in stereolithography and structural light modulation

- based rapid prototyping and rapid manufacturing technologies. *Adv Funct Mater* 2008;18:2390–7.
- [203] Check C, Chartoff R, Chang S. Effects of nanoparticles on photopolymerization of acrylate monomers in forming nano-composites. *Eur Polym J* 2015;70:166–72.
- [204] Leigh SJ, Purcell CP, Bowen J, Hutchins DA, Covington JA, Billson DR. A miniature flow sensor fabricated by micro-stereolithography employing a magnetite/acrylic nanocomposite resin. *Sens Actuators, A* 2011;168:66–71.
- [205] Kumar S, Hofmann M, Steinmann B, Foster EJ, Weder C. Reinforcement of stereolithographic resins for rapid prototyping with cellulose nanocrystals. *ACS Appl Mater Interfaces* 2012;4:5399–407.
- [206] Lin D, Jin S, Zhang F, Wang C, Wang Y, Zhou C, et al. 3D stereolithography printing of graphene oxide reinforced complex architectures. *Nanotechnology* 2015;26:434003.
- [207] Zhang Y, Li H, Yang X, Zhang T, Zhu K, Si W, et al. Additive manufacturing of carbon nanotube-photopolymer composite radar absorbing materials. *Polym Compos* 2018;39:E671–6.
- [208] Chiu S-H, Wu D-C. Preparation and physical properties of photopolymer/SiO₂ nanocomposite for rapid prototyping system. *J Appl Polym Sci* 2008;107:3529–34.
- [209] Zhang C, Cui Y, Li J, Jiang D. Nano-SiO₂-reinforced ultraviolet-curing materials for three-dimensional printing. *J Appl Polym Sci* 2015;132.
- [210] Guillaume O, Geven MA, Grijpma DW, Tang TT, Qin L, Lai YX, et al. Poly(trimethylene carbonate) and nano-hydroxyapatite porous scaffolds manufactured by stereolithography. *Polym Adv Technol* 2017;28:1219–25.
- [211] Manapat JZ, Mangadlo JD, Tiu BDB, Tritchler GC, Advincula RC. High-strength stereolithographic 3D printed nanocomposites: graphene oxide metastability. *ACS Appl Mater Interfaces* 2017;9:10085–93.
- [212] Esposito Corcione C, Striani R, Montagna F, Cannoletta D. Organically modified montmorillonite polymer nanocomposites for stereolithography building process. *Polym Adv Technol* 2015;26:92–8.
- [213] Weng Z, Zhou Y, Lin W, Senthil T, Wu L. Structure-property relationship of nano enhanced stereolithography resin for desktop SLA 3D printer. *Compos A Appl Sci Manuf* 2016;88:234–42.
- [214] Gonzalez G, Chiappone A, Roppolo I, Fantino E, Bertana V, Perrucci F, et al. Development of 3D printable formulations containing CNT with enhanced electrical properties. *Polymer* 2017;109:246–53.
- [215] Feng X, Yang Z, Chmely S, Wang Q, Wang S, Xie Y. Lignin-coated cellulose nanocrystal filled methacrylate composites prepared via 3D stereolithography printing: Mechanical reinforcement and thermal stabilization. *Carbohydr Polym* 2017;169:272–81.
- [216] Bustillo J, Montero-Zambrano D, Loganathan A, Boesl B, Agarwal A. Stereolithography-based 3D printed photosensitive polymer/boron nitride nanoplatelets composites. *Polym Compos* 2019;40:379–88.
- [217] Goh GD, Dikshit V, Nagalingam AP, Goh GL, Agarwala S, Sing SL, et al. Characterization of mechanical properties and fracture mode of additively manufactured carbon fiber and glass fiber reinforced thermoplastics. *Mater Des* 2018;137:79–89.
- [218] Go J, Schiffres SN, Stevens AG, Hart AJ. Rate limits of additive manufacturing by fused filament fabrication and guidelines for high-throughput system design. *Addit Manuf* 2017;16:1–11.
- [219] Phan DD, Swain ZR, Mackay ME. Rheological and heat transfer effects in fused filament fabrication. *J Rheol* 2018;62:1097–107.
- [220] Duty ChadE. Structure and mechanical behavior of Big Area Additive Manufacturing (BAAM) materials. *Rapid Prototyp J* 2017;23:181–9.
- [221] Post B, Lloyd PD, Lindahl J, Lind RF, Love LJ, Kunc V. The economics of big area additive manufacturing. Proceedings of the 27th annual international solid freeform fabrication symposium. 2016. p. 8–10.